2016-03-01

The Influence of Pile Shape and Pile Sleeves on Lateral Load Resistance

Dalin Newell Russell
Brigham Young University

The Influence of Pile Shape and Pile Sleeves on Lateral Load Resistance

Dalin Newell Russell

A thesis submitted to the faculty of
Brigham Young University
in partial fulfillment of the requirements for the degree of

Master of Science

Kyle M. Rollins, Chair
Kevin W. Franke
Fernando S. Fonseca

Department of Civil Engineering

Brigham Young University

March 2016

ABSTRACT

The Influence of Pile Shape and Pile Sleeves on Lateral Load Resistance

Dalin Newell Russell
Department of Civil Engineering, BYU
Master of Science

The lateral resistance of pile foundations is typically based on the performance of round piles even though other pile types are used. Due to lack of data there is a certain level of uncertainty when designing pile foundations other than round piles for lateral loading. Theoretical analyses have suggested that square sections will have more lateral resistance due to the increased side shear resistance, no test results have been available to substantiate the contention. Full-scale lateral load tests involving pile shapes such as circular, circular wrapped with high density polyethylene sheeting, square, H, and circular with a corrugated metal sleeve have been performed considering the influence of soil-pile interaction on lateral load resistance. The load test results, which can be summarized as a p-y curve, show higher soil resistance from the H and square sections after accounting for differences in the moment of inertia for the different pile sections. The increased soil resistance can generally be accounted for using a p-multiplier approach with a value of approximately 1.25 for square or 1.2 for H piles relative to circular piles. It has been determined that high density polyethylene sheeting provides little if any reduction in the lateral resistance when wrapped around a circular pile. Circular piles with a corrugated metal sleeve respond to lateral loading with higher values of lateral resistance than independent circular piles in the same soil.

Keywords: laterally loaded piles, shape influence, lateral resistance, full-scale test, LPile, circular pile, H pile, square pile, plastic sleeve, corrugated metal pipe, lateral deflection

ACKNOWLEDGEMENTS

Funding for this study was provided by FHWA pooled fund study TPF-5(272) "Evaluation of Lateral Pile Resistance Near MSE Walls at a Dedicated Wall Site", supported by Departments of Transportation from the states of Florida, Iowa, Kansas, Massachusetts, Minnesota, Montana, New York, Oregon, Texas, Utah and Wisconsin. Utah served as the lead agency with Jason Richins as the project manager. This support is gratefully acknowledged; however, the opinions, conclusions and recommendations in this document do not necessarily represent those of the sponsoring organizations. In addition, significant in-kind contributions from a number of entities made it possible for this project to be undertaken with a scope sufficient to accomplish the project objectives. I gratefully acknowledge the assistance of Chris Ragan at Atlas Tube in donating the circular and square steel piles along with Price Bethel at Spartan Steel in donating the H piles used in this study. Eric Hendricksen at Desert Deep Foundations, Inc. provided pile driving services at cost and Carl Clyde at Geneva Rock, Inc. donated site grading services and the use of their land for the MSE abutment test site.

I would like to give personal thanks to Dr. Kyle M. Rollins for his inspiration and encouragement in this work and in my professional development. To my committee members, Dr. Kevin W. Franke and Dr. Fernando Fonseca, I am grateful for their advice and expertise. This project could not have been completed without the field support of David Anderson and Rodney Mayo during the construction, testing, and data collection processes. I also appreciate the contributions of my colleagues Andrew Luna, Ryan Budd, Jason Besendorfer and Guillermo Bustamante. Lastly, I must mention the support of my wife, Kris, and daughter, Cesillie, for their enduring encouragement, love, support and smiles.

TABLE OF CONTENTS

LIST OF TABLES

LIST OF FIGURES

1 INTRODUCTION

Up until the mid-twentieth century engineers did not know how to evaluate deep foundations for lateral loads. It was generally assumed that deep foundations could only resist axial loads (Coduto, 2001). Since that time, case studies and theoretical models have proven that the same mechanisms that allow a pile to resist vertical loads are also inherent when a pile experiences lateral loads. Although it is still a relatively new field of study, there are various methods available to compute the response of a pile to lateral load. Many of these methods are based on lateral load test experiments performed on circular piles. Pile shapes such as square and H are commonly used in practice but without high regard to shape effect. It is generally considered that the resistance of the square or H pile is equal to that of a comparable circular pile. Site specific tests are sometimes performed on pile shapes to ensure a determined resistance can be met but no case study has been found correlating the data to other pile shapes. Shape factors have been generated based on theoretical assumptions yet lack the backing of full scale test data.

A study performed by Bustamante (2014) was the first of its kind to laterally test round, H, and square piles in similar soil conditions. The tubular steel piles were consistent in material properties, with comparable dimensions and moments of inertia. The study confirmed that, under similar conditions, the square and H piles responded with greater lateral resistance than a round pile after accounting for differences in widths and moments of inertia. Using a pile analysis

program called LPile, models were created to match the observed load verse deflection curves of the load tests. Bustamante suggested that including p-multipliers of 1.2 for square piles and 1.35 for H piles in the LPile model more accurately predicted the lateral resistance of the non-circular piles. More data like this study would be beneficial in verifying the shape effect of laterally loaded piles.

A common scenario where piles are subjected to lateral loading can be seen in the foundation of abutment bridges. Piles that support the abutment are first driven a portion into the native soil before the backfill is placed around the pile to reach the final elevation. As the soil around a pile is compacted, negative stresses can build on the pile face. This phenomenon is called downdrag which can cause settlement issues as negative stresses build up along the entire height of backfill. Various practices can be set in place to mitigate downdrag, two of which are: wrapping the pile with high density polyethylene (HDPE) sheeting to reduce skin friction and covering the pile with a corrugated metal pipe, or corrugated metal sleeve (CMS). These practices, meant to reduce downdrag, introduce a new level of uncertainty in the pile's ability to resist lateral forces. It is believed that a majority of the lateral resistance of a pile comes from the top five to ten pile diameters (Duncan et al., 1994) and it isn't strange for the sleeve to extend beyond that as it matches the abutment height. There is little in the technical literature that can describe the sleeves effect on the lateral resistance of the pile or support the practice of using pile sleeves in lateral conditions. This research will study piles subjected to lateral loads and investigate how pile shape and pile sleeves affect the resistance to such loads.

1.1 Objectives

A primary objective of this research was to measure the reaction of comparable round, H and square piles to lateral loads. In addition to piles of different shape, this research also studied the effect of pile sleeves; namely round piles wrapped with HDPE sheeting as well as round piles with a corrugated metal pipe placed around it like a sleeve. This study determined how pile shape affects the way in which the pile interacts with the soil in terms of lateral displacement, heave, moment verse depth and deflection of the soil at distances from the pile. With this data a method to account for the lateral resistance of piles of different shapes and sleeves was further defined. Procedures similar to the lateral tests and analysis of Bustamante (2014) were used to determine whether the suggested p-multipliers accurately describe the resistance of a square and H pile. The end objective is to develop design recommendations for the lateral resistance of piles with similar geometries and sleeves which will ultimately minimize ambiguity in design.

1.2 Scope

This research is a continuation of the tests performed by Bustamante (2014). Some of the piles tested by Bustamante were re-tested after sufficient recompaction of the soil had ensued with the addition of five feet of backfill material. A square pile and round piles with a CMS constructed in the same area, in a similar manner were also tested. Overall, this research facilitated full scale, lateral load tests on piles of circular, square, and H shape as well as circular piles with HDPE sheeting and a CMS. The test piles had similar material properties with comparable dimensions and moments of inertia to allow direct comparison of lateral resistance. The H pile was oriented about its weak axis which is common to current construction practices. To provide a full view of the pile response, the experiment was documented with instruments that measure lateral deflection, lateral load, heave, pile rotation, and pile moment. As a method

of analysis, the measured load tests where compared to current lateral design methods to gauge accuracy in predicting lateral resistance. The use of p-multipliers in an LPile analysis provided a reasonable method of predicting the lateral resistance of square and H piles.

1.3 Thesis Organization

This thesis is organized in seven chapters, this introduction being the first. The second chapter will provide a brief review of the technical literature related to laterally loaded pile theory, p-y curves, and methods of estimating the effect of pile shape and pile sleeves. Chapter three explains the layout of the test site, the piles used, soil compaction and the loading system. Chapter four describes how the test was instrumented. Chapter five reports the load test results with a brief discussion on observations. Chapter six provides the analysis of the test results in comparison with current methods to explain the lateral resistance of shaped piles. Conclusions of the findings of this research can be found in the final chapter, chapter seven.

2 LITERATURE REVIEW

In preparation for a study of the influence of pile shape and piles sleeves on lateral resistance it is necessary to become familiar with current literature on the subject. In this section, a brief summary of basic theory and contributing articles on the subject matter have been provided regarding the influence of pile shape, wrapped piles, and corrugated metal sleeves (CMS). A discussion of laterally loaded piles will introduce methods for computing the expected lateral resistance through p-y curves. The API method for calculating p-y curves in cohesionless sand will be explained along with the computer program LPile. A basic explanation of the iterative method of computing pile response will be provided including additional characteristic equations to be used to further describe soil properties. The practice of using pile sleeves will be introduced along with implications that the literature provides on such uses to lateral response. It will be apparent that full-scale data on these topics will be a welcome contribution to the literature and can be the basis of future recommendations for design.

2.1 Laterally Loaded Piles

Pile foundations are often subjected to lateral loads such as:

- Earth pressures on the back of retaining walls
- Wind Loads
- Seismic Loads
- Berthing loads from ships as they contact piers or other harbor structures
- Downhill movements of earth slopes
- Vehicle acceleration and braking forces on bridges

- Eccentric vertical loads on columns
- Ocean wave forces on offshore structures
- River current forces on bridge piers
- Cable forces from electrical transmission towers or electric railway wire support towers
- Structural loads on abutments for arch or suspension bridges. (Coduto, 2001)

The transfer of these lateral loads between a deep foundation and the ground is an interactive process. As a deep foundation is loaded it deflects into the soil which provides resistance against the load. The amount of resistance the engaged soil provides is dependent on the degree to which the pile has deflected into the soil. This concurrent process can be modelled at the most basic level as a beam using dynamic beam theory. Figure 2-1 represents a free body diagram for a deep foundation, namely a long pile (L>10D), considering lateral deflection, slope, moment and shear found in a long foundation under a lateral load. This figure demonstrates how maximum magnitudes for deflection and pile slope occur at the ground surface, whereas maximum pile moment occurs at a depth below the ground surface. The soil-pile interaction, represented as the shape and magnitude of these plots, depends on many factors. Three of these factors include: the type of load that is applied (axial, shear and moment) as well as their magnitude; the relationship between resistance and deflection in the soil (known as the p-y curve); and properties of flexural rigidity such as the modulus of elasticity (E) and the moment of inertia (I) of the pile. These factors have been the subject of much research and theoretical analysis. However, the influence of pile shape and pile sleeve elements on lateral resistance has received relatively little attention.

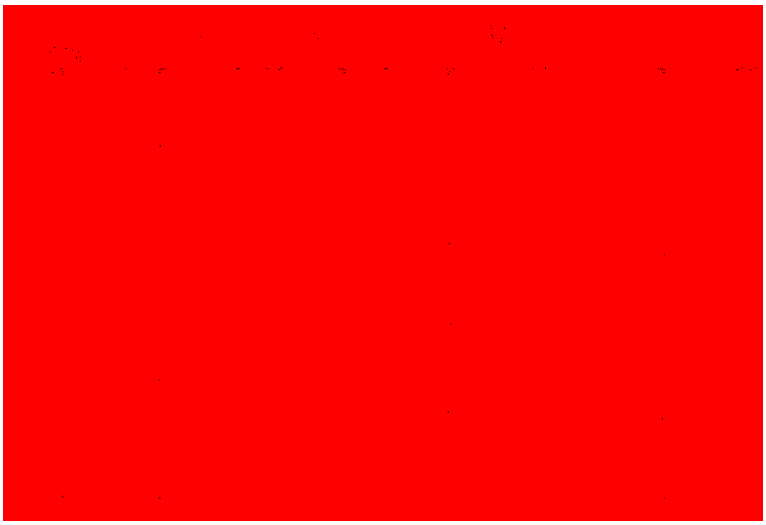

Figure 2-1: Deflection, Slope, Moment and Shear for a Pile Subject to Lateral Loading (After Isenhower and Wang, 2015)

The connection of the pile head to the rest of the structure can prescribe the type of loads that can be expected. Three basic types of connection restraints include; free-head condition, restrained-head condition, and pure moment condition. When designing a deep foundation it is important to identify the connection to determine the boundary conditions of the pile's movements. In practice, designs should incorporate all the expected loading of a pile. This study will isolate pile head shear forces and its effect on pile response.

Pile length is an important attribute in the design of deep foundations. With respect to lateral loading, pile length can be indicative of the failure mechanism that occurs when overloaded. Deep foundations are divided into two categories: short and long. Short or "stubby" foundations that are laterally loaded lack the depth required to anchor the toe against rotations. Often it is the soil that fails first when ultimate loads occur, that is to say the soil yields before the flexural capacity of the pile can be reached. Long foundations provide greater embedment establishing the pile toe as essentially fixed. Piles are classified as long or short according to

their stiffness and the lateral resistance provided by the soil. Generally, stiffer piles, such as one made of steel, is considered long if $D/B \leq 10$.

2.2 The P-y Curve

First proposed by McClelland and Focht in 1956, the p-y curve is an elementary soil model vital to the analysis of a laterally loaded pile (Isenhower & Wang, 2015). This curve demonstrates, at any depth z, the correlation of soil resistance per unit length of pile, p, and the lateral displacement of the pile, y. At a basic level, the p-y curve actually comes from two components: the Q-y curve, defining the development of the passive resistance on the face of the pile, and the F-y curve, defining the development of shear resistance along the side of the pile as illustrated in Figure 2-2 (Briaud et al., 1983). This relationship is also described in Equation (2-1).

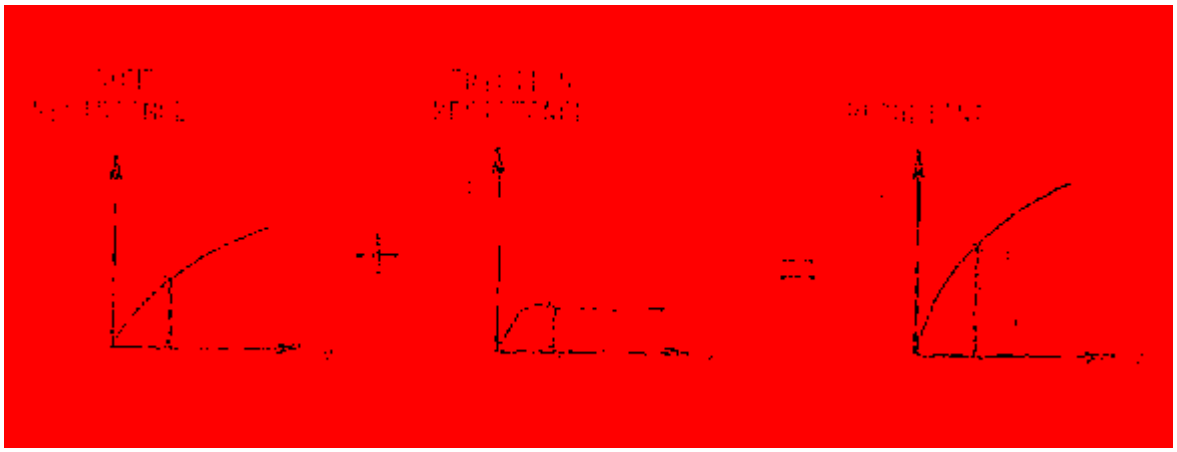

Figure 2-2: Lateral Load Mechanism (after Briaud et al., 1983)

$$P = Q + F \quad \textbf{(2-1)}$$

Where:

P = the total lateral resistance of a pile

Q = the passive force contribution to lateral pile resistance on the pile face

F = the shear resistance contribution to lateral pile resistance on the side of the pile

The significance of both components of lateral resistance have been displayed by pile tests. Briaud et al. (1983) performed a test analyzing the predicted soil interaction of 4 design methods versus the actual soil behavior. The test pile was a three foot diameter drilled shaft embedded 20 ft in a stiff clay. At the rate of approximately five tons per day the load was applied at 2.5 ft above the ground surface. The soil resistance due to the face of the pile was calculated from pressure cell readings. Horizontal and moment equilibrium could not be obtained considering only the front or passive resistance of the pile and the side shear effects had to be included to describe the reaction of the pile to the loading. This example confirmed two points:

1. The shear resistance is an important part of the total resistance.
2. The shear resistance is fully mobilized before the passive resistance.

Trends in full-scale tests show that little movement (0.1 to 0.25 inches) is typically required to engage full shear resistance while passive forces require large amounts of movement to achieve maximum resistance (Smith, 1987). Load tests have proven the existence of separate passive pressure and side shear forces in lateral loading yet some design procedures lump the two sources into a more generic overall lateral resistance. Such as by the use of magnification factors based on pile shape and plasticity (Robertson et al., 1986). Nevertheless, some methods

are available that attempt to formulate passive pressure, Q-y curves, and side shear contributions, F-y curves, independently. (Smith, 1987).

The pressuremeter method is a common procedure used to distinguish the Q-y and F-y contributions. The expansion of a pressuremeter probe in soil is analogous to the lateral movement of a loaded pile. Correlations to expected lateral stiffness and strength can be made according to the pressure readings. Direct techniques for producing the Q-y curve and the F-y curve can also be derived from the pressuremeter curve (Briaud et al., 1983; Smith, 1987; Cosentino et al., 2006). Thus the pressuremeter method can be used to provide more accurate p-y data. From test data the components of side shear and passive pressure can be combined to describe the soil-pile interaction as the pile is laterally loaded. The pressuremeter can be used to produce p-y curves for a specific soil and it has also increased the accuracy of theoretical methods that use soil and pile parameters to produce p-y curves.

2.2.1 API Method for Calculating P-y Curves for Piles in Sand above the Water Table

The American Petroleum Institute (API) has published a method to calculate load-deflection curves for round piles in sand. Printed in RP 2A-WSD (2010) it is included in the recommended practice for planning, designing and constructing fixed offshore platforms using a working stress design. This method accounts for soil properties; such as, effective unit weight, friction angle, and modulus of subgrade reaction, as well as pile diameter, depth, and loading condition. Initially, the lateral bearing capacity of the sand material can be calculated with Equation (2-2) and Equation (2-3) for shallow and deep depths respectively.

$$P_{us} = (C_1\, x + C_1\, d)\, \gamma\, d \qquad \textbf{(2-2)}$$

$$P_{ud} = C_3\, d\, \gamma\, x \qquad \textbf{(2-3)}$$

Where:

p_u = ultimate resistance (force/unit length), lbs/in.

s = shallow

d = deep

γ = effective soil weight, lbs/in^3

x = depth, in.

φ = angle of internal friction of sand, deg.

C_1, C_2, C_3 = Coefficients determined from Figure 2-3 as a function of φ

d = average pile diameter from surface to depth, in.

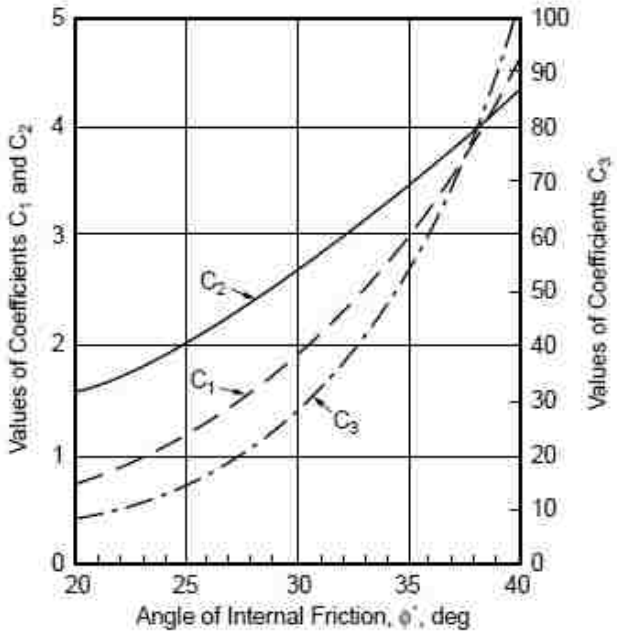

Figure 2-3: Soil Coefficients; C_1, C_2, and C_3 (After *RP 2A-WSD*, 2010)

The ultimate lateral bearing capacity for sand can vary at a certain depth therefore the smaller of the two lateral bearing capacities should be used as the ultimate bearing capacity, p_u. With the ultimate bearing capacity designated, the resultant soil resistance, P, can be calculated using Equation (2-4). This equation considers the loading condition, subgrade modulus, depth, and lateral deflection. The factor for loading condition can be found with Equation (2-5) whereas the subgrade modulus, *k*, can be determined with Figure 2-4 as a function of φ. The resultant soil resistance P, in lbs/in., explains the soil resistance at a depth given a certain lateral deflection of the soil.

$$\boldsymbol{P = A\,P_u\,tanh\left[\frac{k\,x}{A\,P_u}y\right]} \qquad \textbf{(2-4)}$$

$$\boldsymbol{A = \left(3.0 - 0.8\frac{x}{d}\right) \geq 0.9 \text{ for static loading}} \qquad \textbf{(2-5)}$$

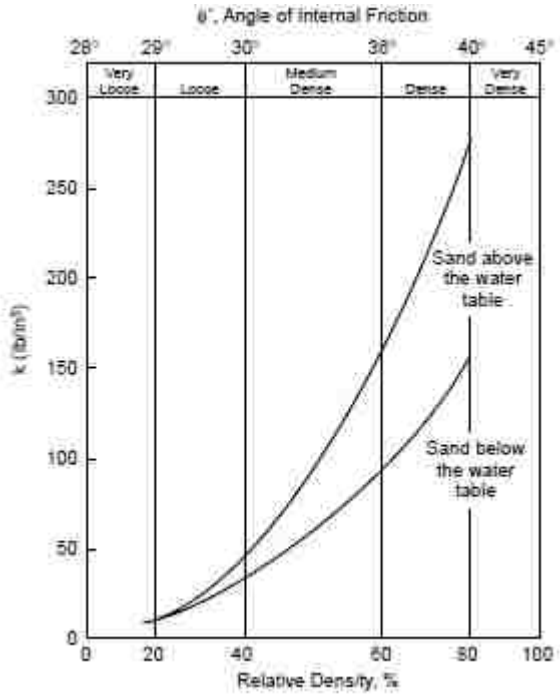

Figure 2-4: Subgrade Modulus as a Function of Friction Angle (After *RP 2A-WSD*, 2010)

The API method effectively correlates the soil properties with a lateral bearing capacity to produce p-y values. Given various deflection values, this method may be used to calculate enough soil resistance values at a certain depth to formulate a p-y curve. It should be noted that neither pile width nor shape effect was considered in the above equations. That is because this method was designed specifically for steel cylindrical (pipe) pile foundations. It is recommended that this method should be used in a general setting and in the absence of more definitive information (*RP 2A-WSD*, 2010). Despite this limitation, the basis of this method is similar to other procedures for calculating the resistance of laterally loaded piles such as the LPile procedure for calculating p-y curves.

2.2.2 LPile Analytical Method

LPile is a widely used computer program which specializes in the analysis of piles and drilled shafts under lateral load. The development for the commercial distribution of LPile by Dr. Lymon C. Reese began in 1985. However, it was preceded by general pile theory and methodology similarly used in the computer program COM624 developed for mainframe computers. The current version used in this work is LPile version 2015.8.03 which will be referred to as LPile throughout the remainder of this document. LPile computes deflection, shear, bending moment and soil response as a function of depth in nonlinear soils. The user interface allows for the consideration of various soil types as well as pile configurations. These features qualify its use in this study.

In an LPile model the soil around the pile is replaced with a series of nonlinear springs representing the soil resistance over a length, p, as a nonlinear function of pile deflection, y (Figure 2-5). The pile is typically divided up into 50 to 100 nodal points, and p-y curves

appropriate for the soil type and soil strength are computed at each node. In an iterative process, the lateral resistance at each node is adjusted until it is consistent with the deflection computed at that node based on the p-y curve defined for that node.

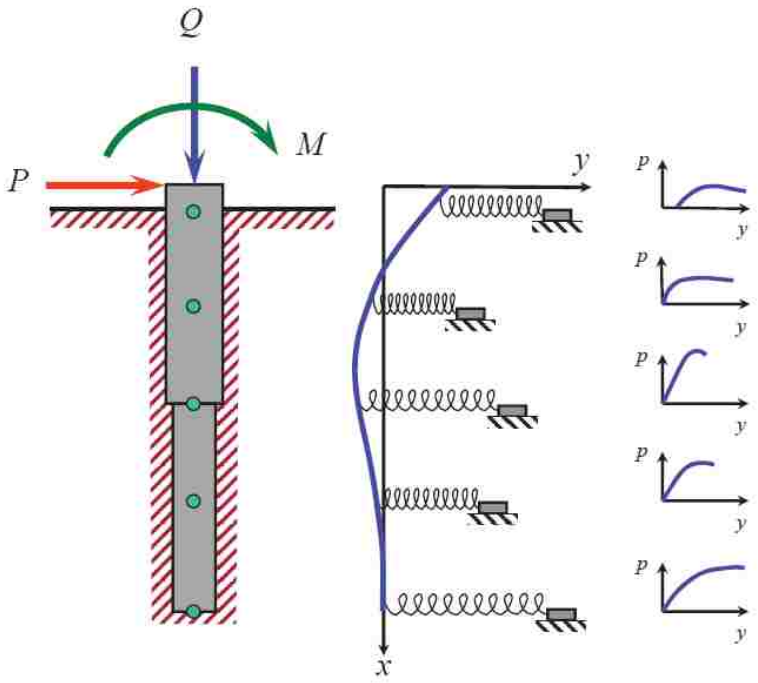

Figure 2-5: Theoretical Model of a Pile under Lateral Loading and p-y Curves (after Isenhower and Wang, 2015)

The basic differential equation governing the lateral load behavior of a pile in a soil profile is given by the equation

$$EI\frac{d^4y}{dx^4} + Q\frac{d^2y}{dx^2} - p + W = 0 \qquad \textbf{(2-4)}$$

Where:

Q = axial thrust load in the pile,

y = lateral deflection of the pile at a point x along the length of the pile,

p = soil reaction per unit length,

EI = flexural rigidity, and

W = distributed load along the length of the pile.

The first term governs the influence of pile flexural resistance, the second term deals with p-delta effects from the axial load on the pile as it deforms laterally, the third term accounts for the soil resistance along the length of the pile and the last term accounts for distributed load. The differential equation can only be solved by application of boundary conditions at the top of the pile which define applied load or moment, rotation or deflection.

There are 8 assumptions made in deriving the differential equation (2-6) for pile analysis:

1. The pile is initially straight and has a uniform cross section
2. The pile has a longitudinal plane of symmetry; loads and reactions lie in that plane
3. The pile material is homogeneous
4. The proportional limit of the pile material is not exceeded
5. The modulus of elasticity of the pile material is the same in tension and compression
6. Transverse deflections of the pile are small
7. The pile is not subjected to dynamic loading
8. Deflections due to shearing stresses are small (Isenhower and Wang, 2015)

With integration of equation (2-6), other useful formulas can be obtained such as Equations (2-7), (2-8) and (2-9).

$$V_v = EI\frac{d^3y}{dx^3} + Q\frac{dy}{dx} \quad \textbf{(2-5)}$$

$$M = EI\frac{d^2y}{dx^2} \quad \textbf{(2-6)}$$

$$S = \frac{dy}{dx} \quad \textbf{(2-7)}$$

Where:

V_v = horizontal shear in the pile,

M = bending moment in the pile,

S = slope of the elastic curve relative to the x-axis of the pile.

Some may recognize this process because it resembles conventions used in beam mechanics. A pile may be thought of as a beam with loads, reactions, moments, and even torsion. The process increases in complexity because the reaction of soil depends on the movement of the pile and vice versa. These equations are matched with the p-y curves that explain the soil resistance with depth according to the deflections calculated using the pile deflection equations.

The LPile procedure for developing p-y curves for cohesionless soils is similar to the procedure for cohesive soils but with the additional consideration of cohesive effects. Because abutment piles are typically located in cohesionless soils associated with approach fills, this review will focus on this material type.

The initial slope of the p-y curve is approximately linear with depth. Terzaghi (1955) suggested the following Equation (2-10) representing the p-y curve as straight lines as the slope increases with depth.

$$E_s = kx \quad \textbf{(2-8)}$$

In this equation k is a variation of the soil modulus while x represents the depth below the ground surface. Terzaghi's k values were merely results of a literature review taking place in the 1950s. Since then, values derived from full scale testing have given more accurate estimates of the subgrade modulus. Figure 2-6 shows the correlation between friction angle and k used in LPile for fine sands, this is a variation of Figure 2-4 used by API. If the user specifies a k value of zero then LPile will assign a default value using Figure 2-6. If an input value for the friction angle is higher than 45° a k value corresponding to 45° will be assigned. If the soil profile shows coarse or well-graded sand, a higher value of k may be considered. Although experimental data is sparse, it can be appropriate to use a k value 10 to 50 percent higher when dealing with dense and very dense well-graded sands that do not contain compressible material (Isenhower & Wang, 2015).

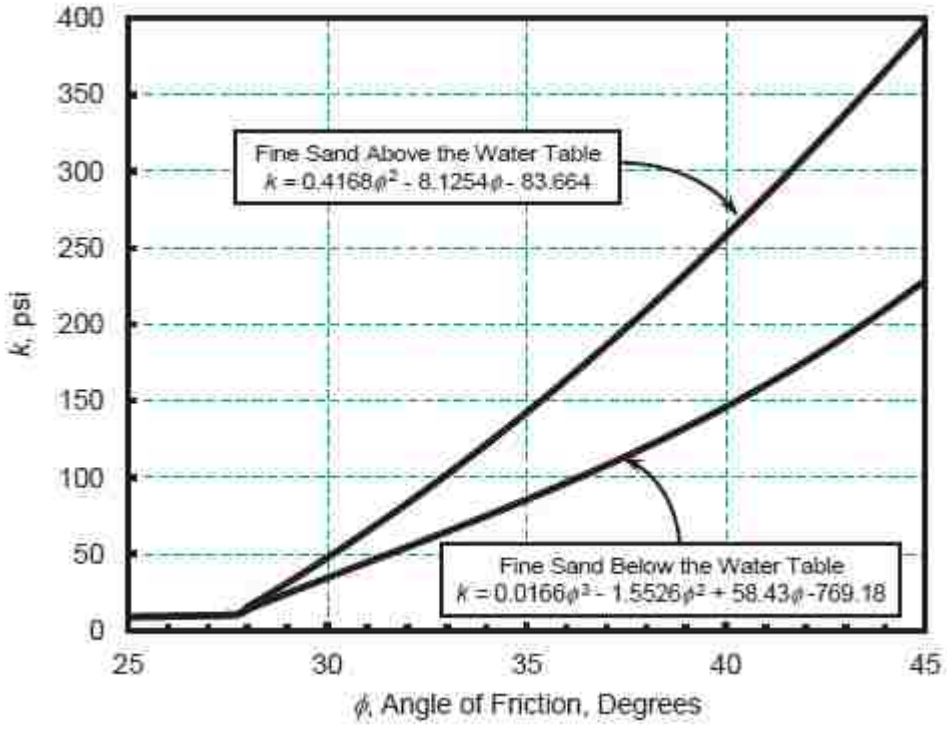

Figure 2-6: Value of *k* versus Friction Angle for Fine Sand Used in LPile

Other soil values have been suggested by Isenhower & Wang (2015) that can be used to further describe soil response, such as the passive, K_P, at rest, K_0, and active, K_a, earth pressure coefficients developed using equations (2-11) through (2-13);

$$K_P = tan^2\left(45° + \frac{\varphi}{2}\right) \quad \textbf{(2-9)}$$

$$K_0 = 0.4 \quad \textbf{(2-10)}$$

$$K_a = tan^2\left(45° - \frac{\varphi}{2}\right) \quad \textbf{(2-11)}$$

Equations (2-14) through (2-16) define the soil coefficients; C_1, C_2, and C_3, which can be found in the LPile technical manual (Isenhower & Wang, 2015),

$$C_1 = tan\,\beta\left\{K_P\,tan\,\alpha + K_0\left[tan\,\varphi\,sin\,\beta\left(\frac{1}{cos\,\alpha} + 1\right) - tan\,\alpha\right]\right\} \quad \textbf{(2-12)}$$

$$C_2 = K_P - K_A \quad \textbf{(2-13)}$$

$$C_3 = K_P{}^2(K_P + K_0 tan\varphi) - K_A \quad \textbf{(2-14)}$$

These equations can be used in conjunction with the API method to develop p-y curves in cohesionless sand above the water table.

There are two models used while solving for the ultimate resistance of piles in sand. These two models allow approximations for $(p_u)_{sa}$ and $(p_u)_{sb}$ to be developed as a general limit and magnitude of the ultimate soil resistance. The first model assumes a passive failure wedge develops at shallow depth while the second model assumes that the soil flows around the pile at depth. The lowest ultimate resistance is used. The passive wedge failure model is shown in Figure 2-7. The total lateral force F_{pt} (Figure 2-7) is a summation of the passive force, F_p subtracted by the active force F_a which is computed with the use of Rankine Theory. To quantify F_p it is assumed that the Mohr-Coulomb failure condition is satisfied on the vertical wedge side planes ADE and BCF as well as the wedge surface AEFB.

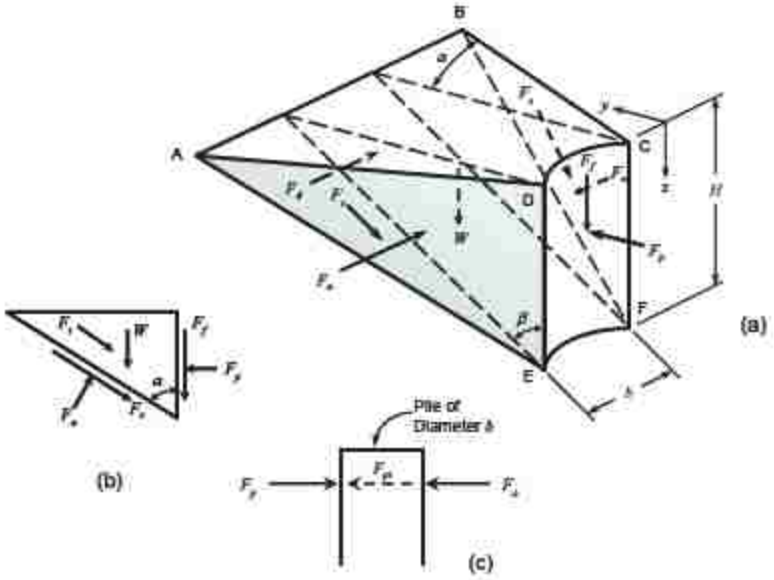

Figure 2-7: Geometry Assumed for Passive Wedge Failure for Pile in Sand (After Isenhower and Wang, 2015)

The resulting Equation (2-17) is to solve for F_{pt} based off of the passive wedge failure model.

$$F_{pt} = \gamma H^2 \left[\frac{K_0 H tan\phi tan\beta}{3\tan(\beta-\phi)cos\alpha} + \frac{tan\beta}{\tan(\beta-\phi)}\left(\frac{\beta}{2} + \frac{H}{3}tan\beta tan\alpha\right)\right] \quad \textbf{(2-15)}$$
$$+\gamma H^2 \left[\frac{K_0 H tan\beta}{3}(tan\phi sin\beta - tan\alpha) - \frac{K_A b}{2}\right]$$

Where:

α = the angle of the wedge in the horizontal direction

β = the angle of the wedge with the ground surface.

b = pile diameter

H = height of the wedge itself

K_0 = at rest earth pressure coefficient

K_A = active earth pressure coefficient

The ultimate soil resistance per unit length of pile near the ground surface can be obtained by differentiating Equation (2-18) with respect to depth.

$$(P_u)_{sa} = \gamma H\left[\frac{K_0 H tan\phi sin\beta}{\tan(\beta-\phi)cos\alpha_s} + \frac{tan\beta}{\tan(\beta-\phi)}(b + Htan\beta tan\alpha)\right] + \gamma H[K_0 H tan\beta(tan\phi sin\beta - tan\alpha) - K_A b] \quad \textbf{(2-16)}$$

Values of α can range from φ/3 to φ/2 for loose sand to nearly φ for dense sand according to Bowman (1958). The value of β can be approximated using equation (2-19).

$$\boldsymbol{\beta = 45° + \frac{\phi}{2}} \quad \textbf{(2-17)}$$

Another soil model considering flow around failure for ultimate resistance at any depth below the ground is shown in Figure 2-8. This model incorporates stresses before the pile and behind the pile which are assumed equal or at least σ_1 greater than σ_2 else active soil failure could ensue. Due to the two dimensional nature of the model it is subject to uncertainty. With these assumptions the ultimate soil resistance for horizontal movement can be expressed as Equation (2-20).

$$\boldsymbol{(p_u)_{sb} = K_A b\,|\,H(tan^8\beta - 1) + K_0 b\,|\,H\,tan\phi\,tan^4\beta} \quad \textbf{(2-18)}$$

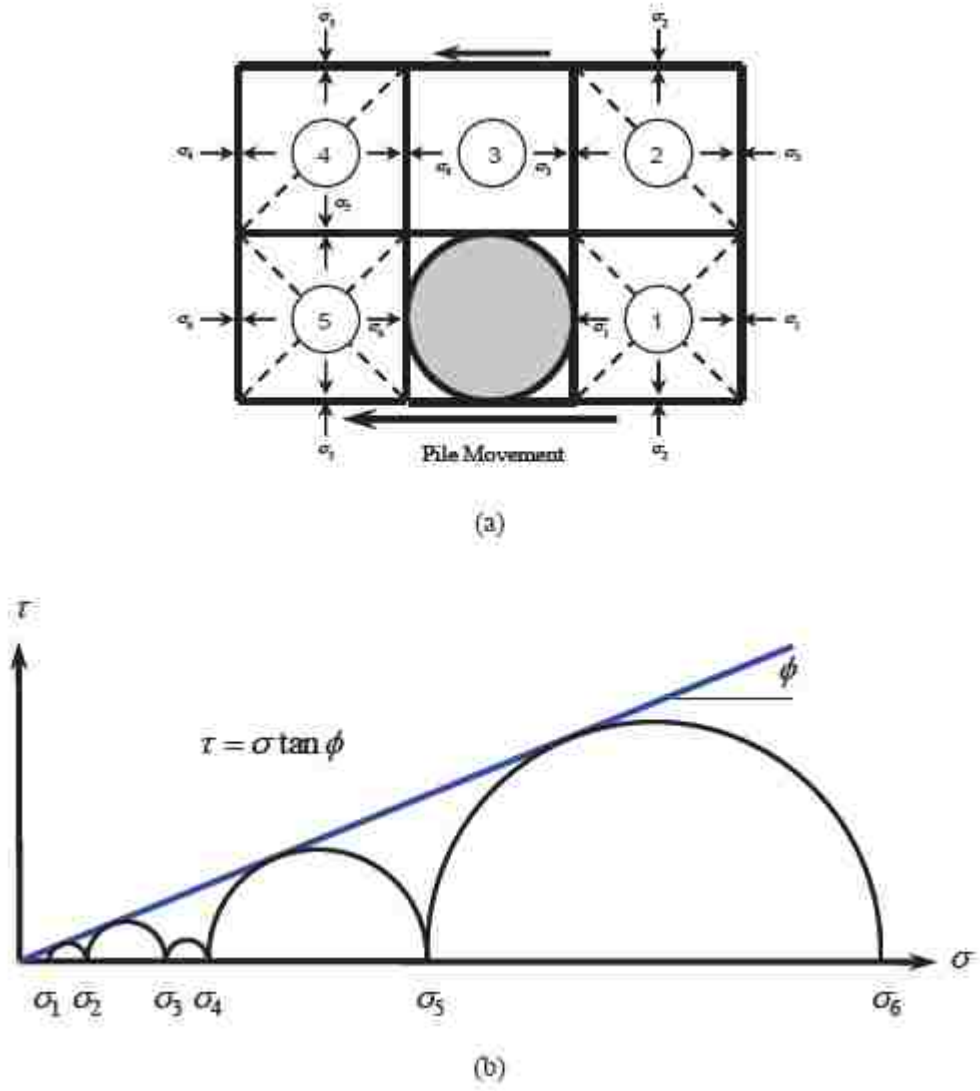

Figure 2-8: Assumed Mode of Soil Failure by Lateral Flow around Pile in Sand, (a) Section through Pile, (b) Mohr-Coulomb Diagram (After Isenhower and Wang, 2015)

After an analysis in LPile is completed results with depth are immediately displayed for deflection, bending moment, mobilized soil reaction, and shear force. The presentation charting utility can generate a total of 28 different types of graphs as a way of displaying results of the analysis (Isenhower and Wang, 2015). Along with those mentioned previously, p-y curves can

also be produced at user specified depths, which is a function that will be used in proceeding sections. Results can be compared in the program itself or exported for further analysis.

Influence of Pile Properties

2.3 Influence of Pile Shape

Pile shape is an attribute that effects the p-y curve as well as the structural stiffness of the pile. Although the pile shape is routinely considered in computing the moment of inertia, I, for a pile, potential effects of pile shape are commonly neglected. Theory on the lateral resistance of piles such as the passive wedge failure method are based on the assumptions of a round pile and most field tests reported in the literature have involved circular piles. As a result, the lateral soil resistance for piles of all shapes are typically based on that developed for round piles and is likely conservative for square shaped piles. Despite the uncertainty in the pile shapes effect on lateral resistance, non-circular piles are commonly used in practice.

A survey conducted by Filtz et al. (2013) presented questions about the use of steel H piles in bridge abutments to different Departments of Transportation (DOTs) across the United States and Canada. A total of 45 DOTs were invited to participate and 27 responses were received. More than half of the responding agencies reported using H piles more than other shapes in the construction of bridge abutments. In response to a question regarding the orientation of the H pile 21 agencies responded as follows: 15 of the responding agencies reported orienting the H pile with the weak axis perpendicular to the bridge centerline; 3 agencies orient steel H piles with the strong axis perpendicular to the bridge centerline; while 3 agencies orient the H pile in either direction. Out of all the responses, none of the agencies provided a design methodology that supports the use of a particular pile orientation. More information regarding the influence of pile

shape could be useful to pile design which otherwise must rely on current shape theory as a basis of design.

Figure 2-9 shows from a conceptual standpoint how each pile shape resists stresses induced by lateral loads. In this figure, the loading force is coming from the left and arrows directed to the left represent the normal stress and shearing stresses on the piles.

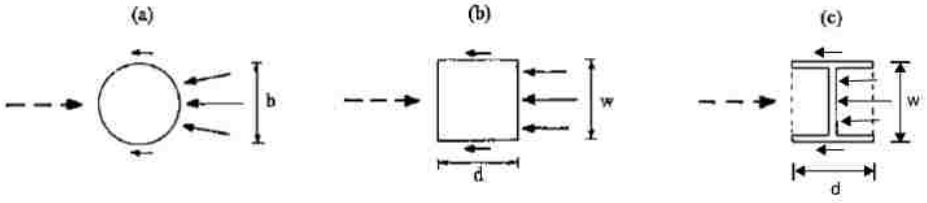

Figure 2-9: Sketch demonstrating shape influence on perceived stresses (After Reese and Van Impe, 2001)

As a first approximation, one could assume that a square pile and a circular pile having the same width would have the same lateral soil resistance. Although the projected areas of the piles are similar, the shear resistance developed along the side of the piles will be different. As a round pile is loaded laterally, the back half of the pile loses contact with the soil and therefore no shear resistance is developed on this surface. In contrast, the side of a square pile remains in contact with the soil during lateral loading and therefore has a longer side length to develop shear resistance. As a result, a square pile will have greater lateral soil resistance than a round pile of the same width. The H pile loaded about its weak axis may have about the same width and depth as the square pile therefore, it should develop similar side shear resistance. However, it should be noted that the moments of inertia of the two shapes are understandably different. In addition, to the differences in side shear, differences in passive resistance might be anticipated based on

pile shape. For example, the normal force arrows for a square pile are all parallel to the direction of load while for a round pile the normal force arrows would have a component parallel and a component perpendicular to loading which might be expected to reduce lateral soil resistance. Like the bow on a ship through water, the shape of the round pile face can penetrate the earth easier therefore the effectiveness of the round pile in resistance lateral force must be less than that of a flat surface (Czerniak, 1957). Although an H pile loaded about its weak axis would also have a normal force arrow parallel to the applied load, there could be some differences in passive resistance owing to compression of the soil between the flanges.

As a method to quantify these differences in geometry and soil-pile interaction, Reese and Van Impe (2001) suggest a method for calculating an equivalent diameter, b_{eq} for square cross sections using Equation (2-21).

$$\boldsymbol{b_{eq} = w\left[\frac{P_{uc}+2\left(d-\frac{w}{2}\right)f_z}{P_{uc}}\right]} \quad \textbf{(2-19)}$$

Where:

w = width of section

d = depth of section

P_{uc} = ultimate resistance of a circular section with a diameter b equal to w

f_z = Shearing resistance along the sides of the rectangular shape at depth z below the ground surface

For cohesionless soils, the unit side resistance, f_z, may be computed using equation (2-22).

$$\boldsymbol{f_z = K_z|_z \tan(\phi_z)} \quad \textbf{(2-20)}$$

Where:

K_z = lateral earth pressure coefficient

γ_z = effective vertical soil stress at depth z

ϕ_z = interface friction angle (between the soil and the wall of the pile)

The value of K_z will also be related to the manner in which the pile is installed and ϕ_z will turn out to be lower than the soil friction angle. The values of equivalent diameter will vary according to the shear strength, soil characteristics, and depth. It may be practical to calculate the equivalent diameter at various depths and average the values to obtain an inclusive equivalent diameter for the length of the pile. The resultant b_{eq} may then be introduced into p-y calculations, such as those previously mentioned, as a modified pile width, b.

Other methods have also been devised to consider shape factors in lateral pile design. Czerniak (1957), explaining the overturning resistance of piles, detailed a reduction to allowable lateral earth pressure of 0.636 for circular piles. Another method by Smith (1987), based on applying vertical shear pressuremeter methods to lateral effects, proposed a tentative procedure that separated the shapes effect on side shear and passive resistance. His method for calculating the ultimate shear reaction used shape factors of 0.79 and 1.76, for circlular and square shapes respectively. Shape factors for the passive resistance was suggested as 1.0 for square piles and 0.75 for circular piles. These factors were an adjustment from a previous study performed by Briaud et al. (1983) which suggested a passive resistance factor of 0.8 for circular piles instead of 0.75 as well as a shape factor of 2.0 for square piles and 1.0 for circle piles in regard to the side shear contribution. Currently, there are no suggested shape factors for the design of H piles.

Although these concepts on the influence of pile shape seem correct conceptually, there is a lack of full scale testing data that could verify the theorized methods. It is possible that this

uncertainty is the reason why current pile analysis programs, such as LPile, do not apply a shape factor in calculations and only consider the shape's effect on the moment of inertia. Full scale testing of round, square and H piles in close proximity could increase the accuracy of non-circular pile models and confidence in their results.

A study preliminary to this one performed by Bustamante (2014) was completed in response to this lack of data. Bustamante tested the influence of pile shape by laterally loading square, circle, and H piles. His test consisted of piles driven 18 ft into native soil with 15 ft of soil backfill added around the piles. These different shaped piles had similar dimension and comparable moment of inertia so the shape effect could be compared. The results of the tests, shown in (Figure 2-10), demonstrated that the square piles provide more lateral resistance than the round pile. The H pile was observed to have less lateral resistance than the round pile but it should be noted that it was loaded about its weak axis having a moment of inertia of 59% of that of the round pile. It is suggested that an H pile with a moment of inertia equal to the round would provide more resistance than the round pile. Further analysis suggested that this increase was a result of higher resistance from side friction and normal stress components of the H and square piles.

As part of the analysis, Bustamante also created a model of the square and H pile in LPile to better match the load test data. His findings showed that the current procedure for analyzing square and H piles under lateral loads insufficiently predicted the resistance of each shape. Better agreement could be acquired with the use of p-multipliers along the entire depth of the pile. P-multipliers of 1.2 for the square pile and 1.35 for the H pile provided the best agreement with the load test data as shown in Figure 2-11. These modification factors can be used in the lateral design of square and H piles to better predict the lateral capacity of such piles.

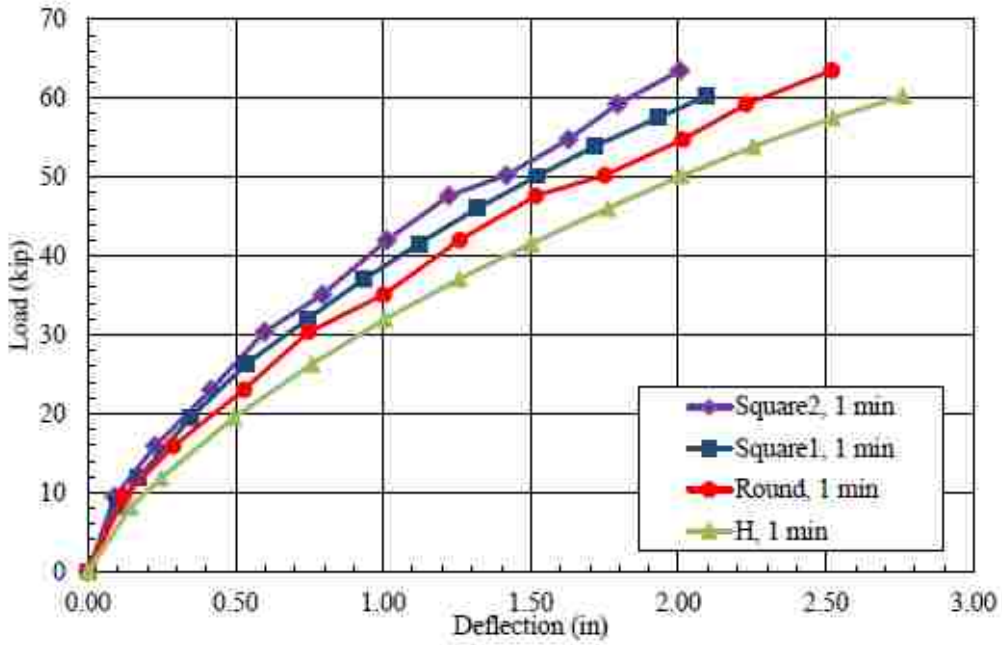

Figure 2-10: Load Tests on Square, Round, and H Piles (After Bustamante, 2014)

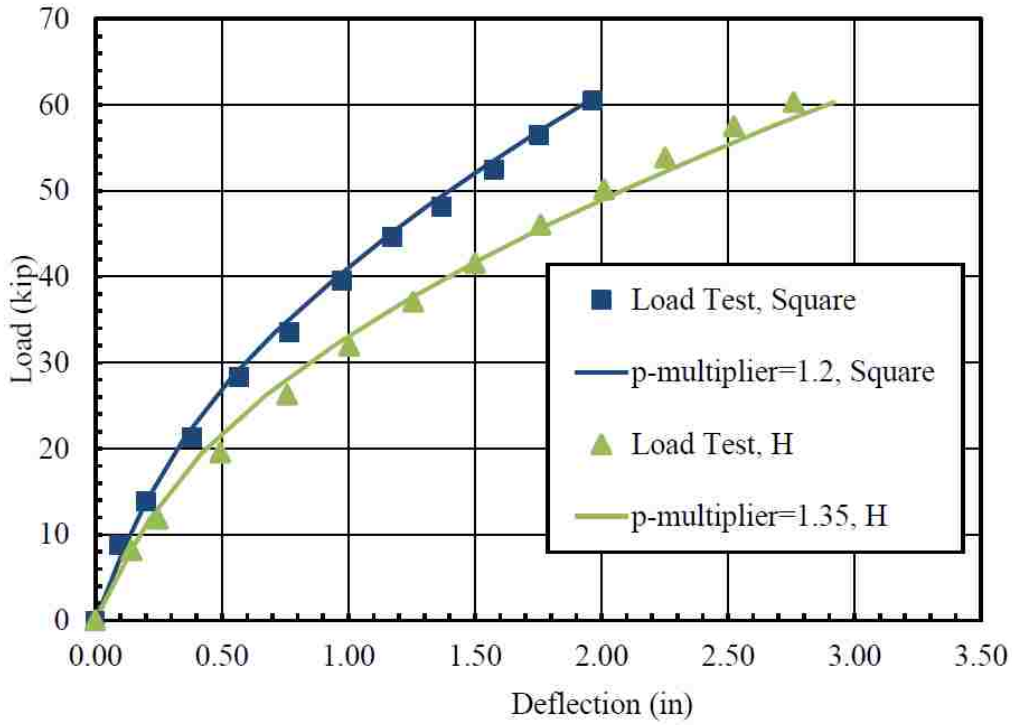

Figure 2-11: Model for Square and H Piles with P-multipliers (After Bustamante, 2014)

The study by Bustamante appears to be the first of its kind in the lateral pile resistance literature. Further tests like this can provide more insight on the shape effect of these non-circular piles. The study presented in this document will build on the research done by Bustamante, literally and academically. In an effort to provide more data to compare with Bustamante's results, the round and H piles were retested after sufficient compaction of the disturbed material and an additional 5 ft of backfill has been added. A different square pile was also tested to compare with the square pile previously tested. Similar analysis to that of Bustamante was performed to verify the p-multipliers suggested for the square and H piles.

2.4 Wrapped Piles

One concern with the use of piles in deep foundations is called downdrag. Piles that are situated in compressible soil can experience negative skin friction due to the downward shear forces that accumulate along the length of the pile. The same vertical side friction which prevents the pile from settling in the soil is capable of pulling the pile downward as the soil compresses around it. There are several methods to reduce this negative skin friction. (1) Preloading to reduce soil settlement following pile installation; (2) pile casing to prevent direct contact between the pile and the surrounding soil; and (3) coating the pile with bitumen or wrapping the pile with plastic sheeting to ease the effect of relative settlement. The 3rd method is often the most cost effective.

Polyethylene wrapping, applied similarly to Figure 2-12, can also be used for certain pile configurations that require the advantage of the vertical capacity of a pile but not the lateral resistance of a pile. Piles such as those in bridge abutments demand the vertical capacity of a deep foundation but need the flexibility to allow certain amounts of deflection.

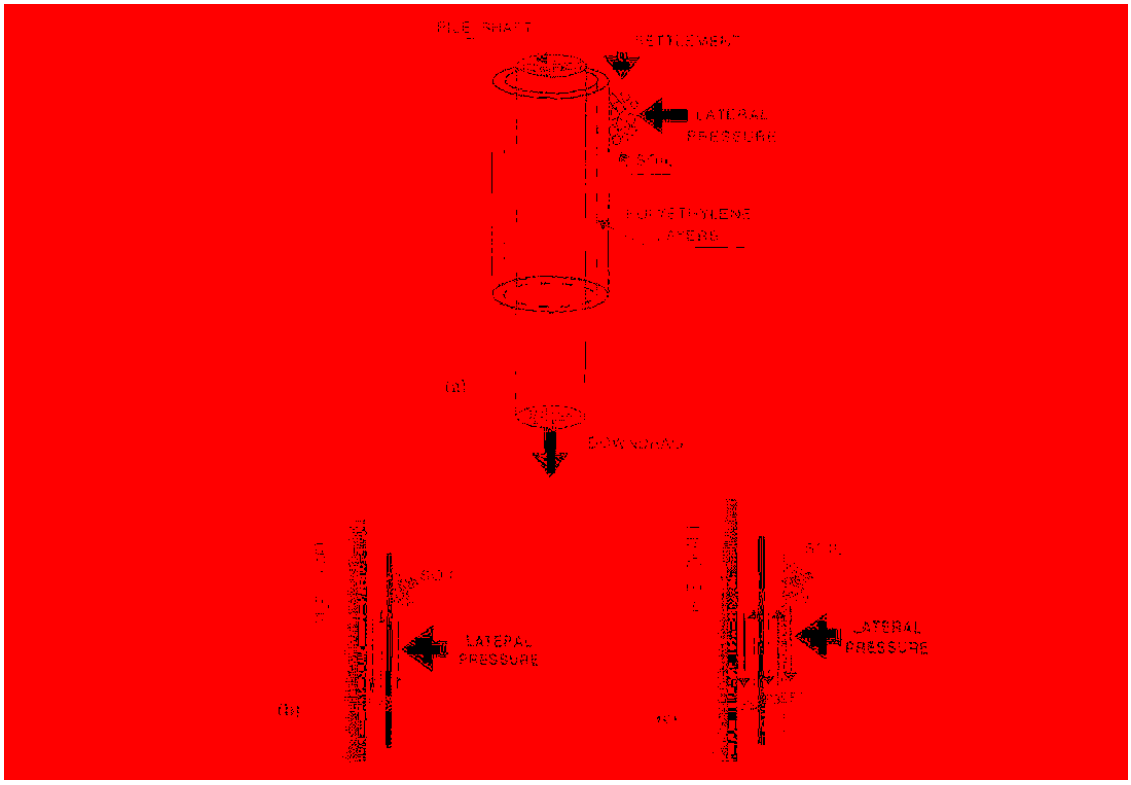

Figure 2-12: Plastic Sheeting for Downdrag Reduction: (a) Schematic; (b) One plastic Layer; and (c) Two Plastic Layers (After Caliendo and Tawfiq, 1995)

Caliendo and Tawfiq (1995) demonstrated the reduction in negative skin forces through tests performed using a direct shear apparatus as shown in Figure 2-13. Concrete blocks reinforced with wire mesh were fashioned to represent the pile face as well as provide the bottom half of the direct shear apparatus. The soil in the apparatus was then sheared to model the friction mechanism between the concrete surface and the soil. A set of blocks where tested with the soil to obtain baseline shear values then another set of blocks were tested with various applications of plastic sheeting.

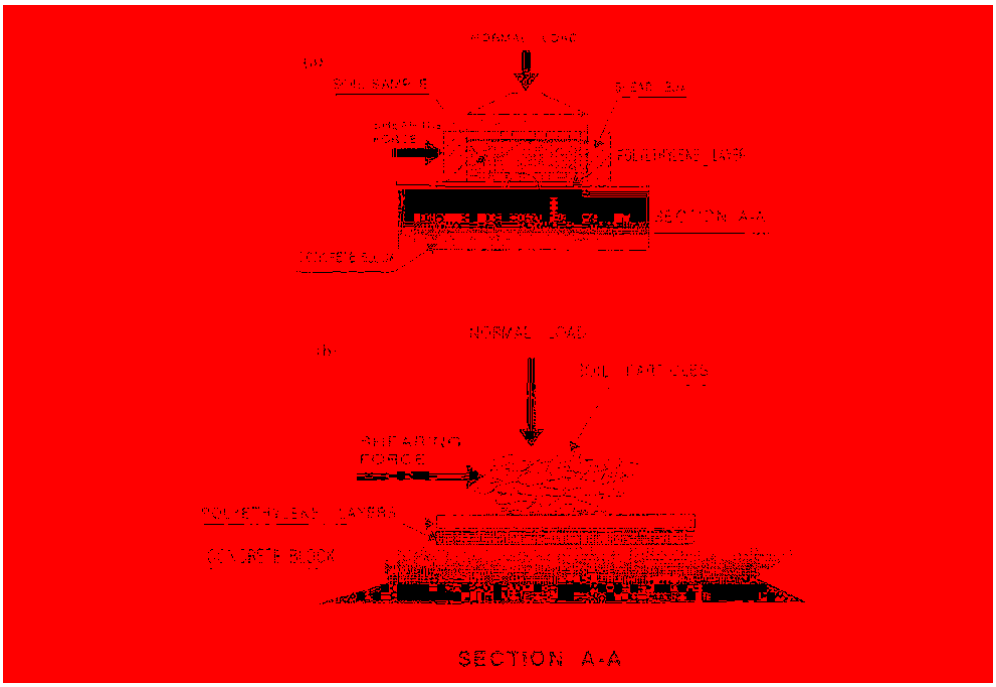

Figure 2-13: Direct-Shear Test on Concrete-Polyethylene-Soil Samples: (a) Full View; and (b) Section A-A (After Caliendo and Tawfiq 1995 page 7)

Two different types of soil samples were provided during the testing. The first being a reddish-brown sand with some fines and a natural water content, w_c, of 2%. The second soil type was a crushed Florida limestone with crushed fines, irregular surfaces and hard particles angular in shape. Two types of plastic sheets were used for the testing. The first type was a Textrud clear 0.15 (6 mil) polyethylene sheet and the second was Gundline high-density polyethelene (HDPE) with 1 mm (40 mil) thickness. To examine the effect of the boundary conditions on the friction characteristics of the polyethylene coating various layering arrangements were applied to the concrete testing blocks. These arrangements included: (1) one fixed layer; (2) one loose layer; (3) two fixed layers; (4) two loose layers; and (5) two loose oil-lubricated layers. The fixed layers were fastened to the concrete block while the loose layers were free to slide on the concrete surface during loading of the shear force. These various applications of the plastic

sheeting were chosen to evaluate the most effective negative skin friction reduction system. The tests were repeated with shear strain rates ranging from 1.3 x 10-6 s^{-1} to 5.25 x 10-3 s^{-1} as well as at temperatures of 5°C, 25°C and 56°C to examine the effects that these variables might have on negative skin friction reduction.

The results of the testing showed that temperature, deformation rate, and soil particle size had no effect during the various arrangements of plastic sheeting to reduce the negative skin friction forces. The effectiveness of a 40-mil polyethylene sheet in reducing friction resistance was around 60%. The single 6-mil, which was the smoother of the two sheets, had an effectiveness around 67%. When two free layers of polyethylene were tested the effectiveness rose to 77%. When mineral oil was applied between two free layers of polyethylene sheets the skin friction was reduced by 80-98%. A further set of experiments was conducted with smooth steel plates. A single 6 mil loose polyethylene sheet was effect in reducing skin friction by 80%. This demonstration gives evidence that the material surface of the pile influences the effectiveness of the plastic sheeting in reducing the negative skin friction of the pile.

A full scale test was performed by Price (2012) using 16" piles double wrapped with 10 mil (0.25mm) thick sheet of low-density polyethylene (LDPE). Down drag was expected to be significant around the piles as the fill around the pile was compacted. The test pile TP4 was placed at a distance of 6.9ft (5.2D) from the Mechanically Stabilized Earth wall which is considered far enough to be unaffected by the wall. Their models showed that the computed lateral resistance was 60 to 80% higher than what was measured. This overestimation in the model and lower measured resistance appears to have been a consequence of double wrapping the pile.

It can be assumed that because side friction is a component of lateral resistance then reducing vertical side friction would also reduce the lateral side friction of a pile. Full scale comparable testing between wrapped piles and non-wrapped piles under the same conditions would provide further proof that a reduction should be included when analyzing lateral load resistance of a pile prepared with negative skin friction reducers such as polyethylene sheeting.

2.5 Corrugated Metal Sleeves

A practice becoming more common with the construction of bridge abutments is the use of corrugated metal pipes placed around the upper portion of a pile as a sleeve. These CMSs can potentially reduce the dragload or downdrag forces that piles near bridge abutments experience during soil compaction. CMS piles also allow greater flexibility in the support which is needed in the construction of jointless bridges as shown in Figure 2-14.

Figure 2-14: Piles in Corrugated Metal Sleeves near a Bridge Abutment

A nation-wide survey of state Departments of Transportation (DOTs) and construction companies using piles in integral abutment bridges indicated that 11 of the 20 responding agencies reported the practice of placing a corrugated metal pipe or a corrugated metal sleeve (CMS) around piles in the design of integral abutment bridges. In this practice the void space between the CMS and the pile is typically filled with loose sand to provide an increased ability for lateral movement of the pile while preventing buckling under axial load. For integral abutments, where expansion and contraction of the bridge is accommodated at the abutment, it is desirable to provide a more flexible foundation. In particular many reported using CMS piles for abutment piles offset from an adjacent MSE wall. Of the surveyed agencies using the CMS filled with sand the offset distance ranged from 3 to 5 feet while those not using CMSs range from 3 to 5.6 feet. The average distance for both is approximately 4.5 feet suggesting that the use of a CMS does not influence the offset distance used in practice (Filtz et al., 2013).

Although the survey indicates that CMS piles are being used throughout the country, a review of the published technical literature does not provide any full-scale test data to provide any information on the lateral pile resistance provided by these systems. Many engineers apparently assume that there is little or no lateral resistance in the CMS piles.

To provide some guidance related to the performance of CMS piles, Filtz et al. (2013) conducted a finite element analysis using FLAC3D. The numerical model represented a steel pipe pile surrounded by sand encased by a steel membrane within a soil mass shown in Figure 2-15. Three sand infill mediums were introduced into the model designated as loose, medium, and dense. Specifications for the infill material as well as the steel and backfill material can be found in Table 2-1.

Table 2-1: Material Properties of Numerical Model (After Filtz et al, 2013)

Material	Elastic Modulus E, psf	γ pcf	ϕ deg	Constitutive Model	Poisson Ratio ν
Steel	4,177,000,000	485	-	Elastic	0.3
Loose Sand	280,000	115	30	Elastic-plastic, Mohr-Coulomb	0.3
Medium Sand	540,000	120	34	Elastic-plastic, Mohr-Coulomb	0.3
Dense Sand	800,000	130	38	Elastic-plastic, Mohr-Coulomb	0.3
Backfill	800,000 to 1,300,000	120	38	Elastic-plastic, Mohr-Coulomb	0.2

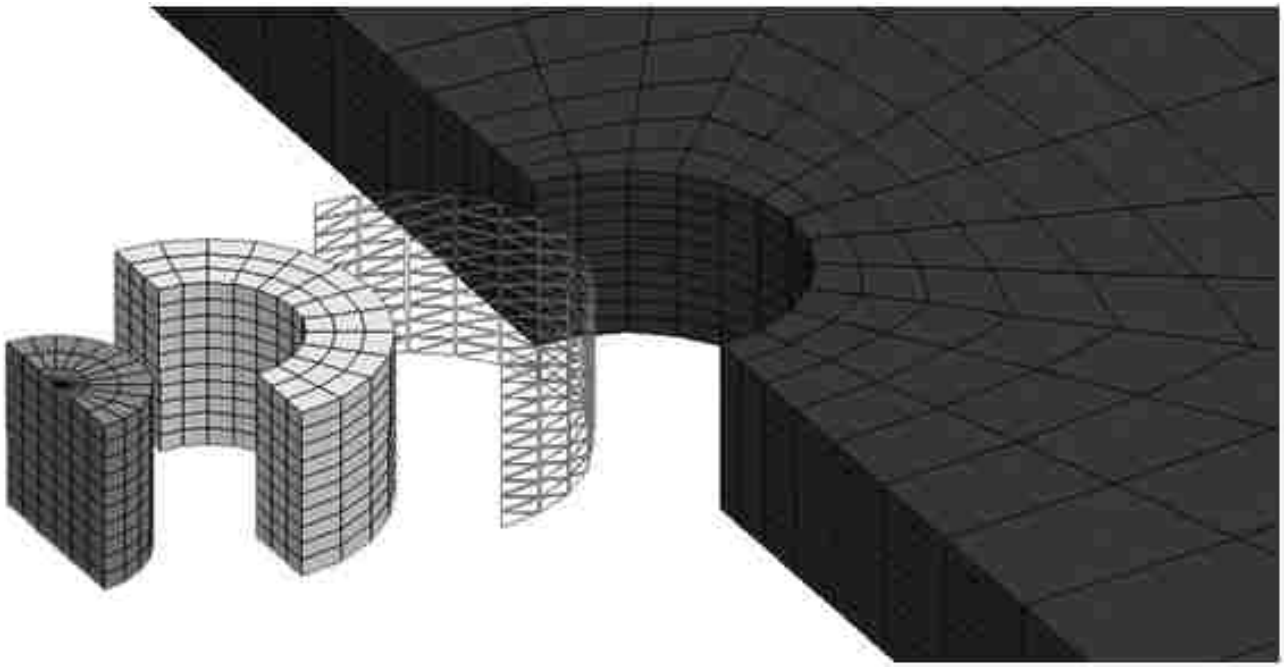

Figure 2-15: View of 3D Numerical Model, from Left to Right: Pile, In-fill Sand, Steel Sleeve and Surrounding Backfill Soil (After Filtz et al., 2013)

A first case analysis subjected the model to self-weight forces followed by a vertical pressure of 1300 psf with lateral displacement constraints. After the model reached equilibrium the lateral loading sequences were applied. The second case analysis consisted of "monotonic" or progressively increasing loading to a deflection of 0.6 feet as shown in Figure 2-16. The second loading sequence represented cyclic lateral loading resembling 365 daily thermal cycles of displacement superimposed on one annual thermal cycle of displacement followed by monotonic loading to 0.6 feet of displacement as shown in Figure 2-17. This sequence was meant to represent thermal expansion cycles resembling a jointless bridge about 320 ft long and subject to a temperature variation of 80 °F.

Figure 2-16: Second Case Analysis with Monotonic Loading (After Filtz et al., 2013)

Although decreasing the density of the infill decreased the computed lateral pile resistance, the use of the loose backfill did not reduce the lateral resistance to some very small value as is

often assumed in design. It is shown in Figure 2-16 and Figure 2-17 that the one year cyclic thermal displacement loading has actually caused the pile resistance to stiffen. The loose soil under the cyclic loading in Figure 2-17 shows greater resistance than the loose soil in Figure 2-16. These results indicate that infilling the CMS surrounding the pipe pile with sand will not eliminate the loads on the pile partly because of the stiffening that occurs due to cyclic loading. This is a topic of further investigation considering the lack of data to support the practice.

Figure 2-17: Second Case Analysis with Cyclic then Monotonic Loading (After Filtz et al., 2013)

3 TEST LAYOUT

This section will describe in detail the components of the test and how they contribute to the results found hereafter. The location of the test site will be described followed by an introduction to the pile sizes, shapes, and properties that were used in this test. The use of plastic sheeting and corrugated steel pipes along with their properties will also be detailed. The soil properties, such as gradation information, unit weight and compaction efforts, is an essential component to the resistance of piles, a description of such can be found in this section. The sequence of the piles that were tested as well as the procedure of loading will then be explained in detail. This section will provide context that should be understood before progressing through following sections.

3.1 Location of Test site

An undeveloped area of land located between Bluffdale and Lehi, Utah was chosen for the test site (see Figure 3-1). The location can be found using coordinates 40°27'10.95" N 111°53'54.63" W. Access to the plot of land was provided by Geneva Rock who formerly used it as a gravel pit. This rather isolated location with granular native soil was a desirable site for testing.

Figure 3-1: Test Site Location (Google Earth 2013)

3.2 Piles Tested

With the intent of collecting data on the soil-pile interaction, nine piles of various shapes were selected for testing. Table 3-1 provides a summary of the properties of the piles chosen for testing. There were four round 12.75X3/8" piles, four square HSS 12X1/4" piles, and one H shaped HP 12X74 pile used in testing. The pipe piles and square tube piles were donated by Atlas Steel while the H pile was donated by Spartan Steel. The tubular round piles conform to the American Society for Testing and Materials (ASTM) A252-10 GR 3 specification and have a yield strength of approximately 57 ksi. The non-compact H pile conforms to ASTM A572-50 specifications with a minimum yield strength of 50 ksi while the steel of the square pile conforms to ASTM A500-10A Grade B&C specifications having a minimum yield strength of

46 ksi. Figure 3-2 illustrates the layout of the piles and test sequence which will be explained further in this section. Piles of similar dimension were selected so that they could be relatively comparable in width despite differences in geometric shape. Although square steel tube piles are not common, steel was selected for this pile shape so that differences in pile-soil interface friction could be avoided. An H pile shape with a smaller cross sectional area, such as an HP 12x53, could have been used however inelastic global buckling in the flanges would reduce the moment capacity by about 20%. The HP 12x74 shape was chosen for a theoretical capacity of 90% of the yield moment capacity so that failure in the soil could be observed before buckling in the pile became a concern. The piles were intended to act as a long pile therefore the pile length of 40 ft was deemed an appropriate pile length with a length to width/diameter ratio (D/B) of nearly 40.

Table 3-1: Pile Properties

Type	Diameter/ Depth (in)		Wall Thickness (in)		Cross Sectional (in^2)	Moment of Inertia (with angle iron) (in^4)	E (ksi)	F_y (ksi)
Round 12.75X3/8	12.75		0.349		14.57	279 (314)	29,000	57
CMP	24		0.064		4.8	0.454	29,000	57
HSS 12x12X1/4	12		0.233		14.8	248 (335)	29,000	46
HP 12X74	12.1	12.2	0.605	0.61	22.6	186 (186)	29,000	50
	Flange Depth	Flange Width	Web Thickness	Flange Thickness				

Deseret Deep Foundations, Inc used an ICE I-30V2 diesel hammer to drive the test piles 18 ft into native soil. The tubular piles were driven open ended which resulted in a soil plug with a length of 10.4 ft to 12.1 ft above the toe of the pile. The piles were left hollow so that the non-

linear behavior of cracked concrete did not have to be considered which better facilitates back analysis using the program LPile. After the piles were driven compacted granular backfill was compacted around the test piles to an elevation 20 ft above the native soil surface. This left about 2 feet of pile above the ground surface.

Along with pile shape, two other pile geometries common to pile design were tested; namely, round piles with a corrugated metal sleeve (CMS), as well as a round pile wrapped with high density polyethylene sheeting (HDPE). Figure 3-2 shows two round piles on the right end of the test site with a circle around them, these two piles where surrounded by a CMS. Following a practice common for bridge abutments, a galvanized corrugated metal pipe 2 ft in diameter was placed around the top 20 feet of a round pile, as a CMS. This CMS was placed after the round piles were driven and prior to soil compaction around the top 20 ft of the pile. A picture of the round pile with a CMS during compaction is provided in Figure 3-3 (Right). It is common practice to fill the annular void with a loose uncompacted backfill material. The annular void of the CMS encased pile on the far right was filled with loose gravel while the annular void of the other CMS pile was filled with loose sand.

The third pile from the left in Figure 3-2, shown with a black upper half, is a round pile that was wrapped with 8 layers of 6 mil high density polyethylene sheeting. A photo has been provided of the round pile with HDPE prior to recompaction in Figure 3-3 (Left). Although these practices are meant to reduce downdrag during soil compaction around the piles, the effect on lateral resistance has not yet been evaluated with full-scale tests. After the piles were driven along with the CMS and HDPE sheeting applied to their respective piles, the backfill was placed in 4 phases of compaction.

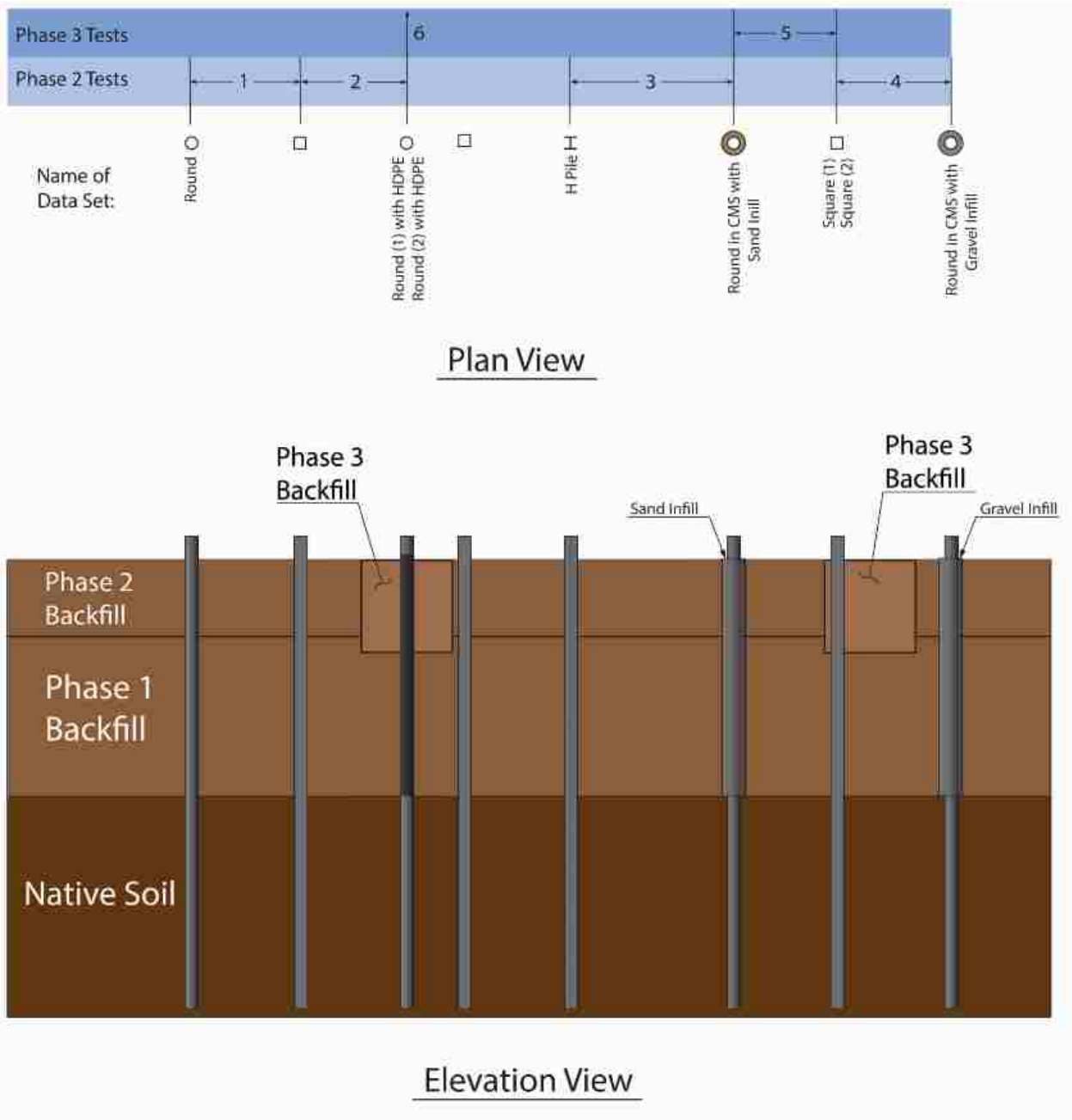

Figure 3-2: Pile Layout

Figure 3-3: (Left) Round Pile with HDPE, (Right) Round Pile with CMS

3.3 Soil Compaction

Compacting the soil around the piles was a meticulous endeavor constituting a total of 20 ft of backfill. The last lift of compaction reached a grade line about 2 ft below the top of the piles. The backfill material was selected as a silty sand with gravel while two separate materials were selected for the annular infill material between the round piles and the CMS. Particle size distribution curves for each material type were developed based on mechanical analysis to better define the soil used and its constituents.

3.3.1 Backfill Material

The silty sand with gravel backfill material was provided by Geneva Rock. The backfill classified as an A-1-a material according to the AASHTO classification system or an SM material according to the Unified Soil Classification System. A sieve test showed a mean grain size (D_{50}) of 2.3 mm, a coefficient of gradation (C_c) of 1.6, a coefficient of uniformity (C_u) of 40 and a fines content of 14% (Table 3-2). The results of a gradation test is plotted in Figure 3-4. A standard Proctor test produced a maximum density of 126.7 pcf and an optimum moisture content of 7.8%. Further information on this backfill material can be found in subsequent sections explaining the compaction of the backfill.

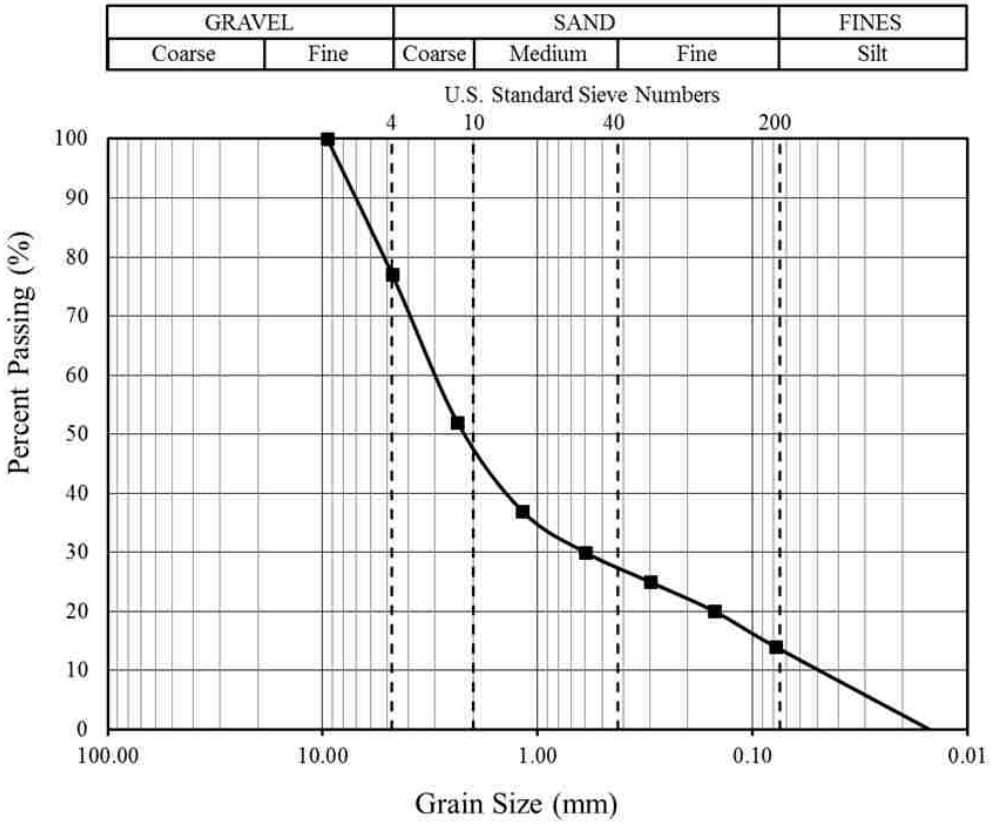

Figure 3-4: Particle Size Distribution Curve for Selected Backfill

3.3.2 Infill Material

A variety of materials could be used in practice for the annular infill material between the round piles and the CMS. In this study a poorly graded sand and a sand with gravel have been chosen to represent two possible options for infill. Gradations have been performed on the two materials to produce the following information. The sand infill consists of 97.7% sand fraction and falls under the AASHTO classification of A-1-b or SP according to the Unified Soil Classification System. A sieve test showed a mean grain size (D_{50}) of 0.81 mm, a coefficient of gradation (C_c) of 0.93, a coefficient of uniformity (C_u) of 5.31 and a fines content of 1.4% (Table 3-2). The gradation curve from the sieve analysis is presented in Figure 3-5. The other material can be classified as an A-1-a according to AASHTO and it qualifies as an SP, a poorly graded sand with gravel, by the Unified Soil Classification System. The material has a mean grain size (D_{50}) of 3.7 mm, a coefficient of gradation (C_c) of 1.29, a coefficient of uniformity (C_u) of 2.9 and a fines content of 1.4% (Table 3-2). Hereafter, for simplicity, it will be referred to as a gravel material to distinguish it from the poorly graded sand. The gradation curve of the gravel material is shown in Figure 3-5. How these two different materials affect the lateral pile resistance will be a topic of further investigation.

Table 3-2: Gradation Information

Material	AASHTO Classification	USCS Classification	D_{50} (mm)	C_c	C_u	Percent Fines
Sand Backfill	A-1-a	SM	2.3	1.6	40	14%
Gravel Infill	A-1-a	SP	3.7	1.29	2.9	1.4%
Sand Infill	A-1-b	SP	0.81	0.93	5.31	1.4%

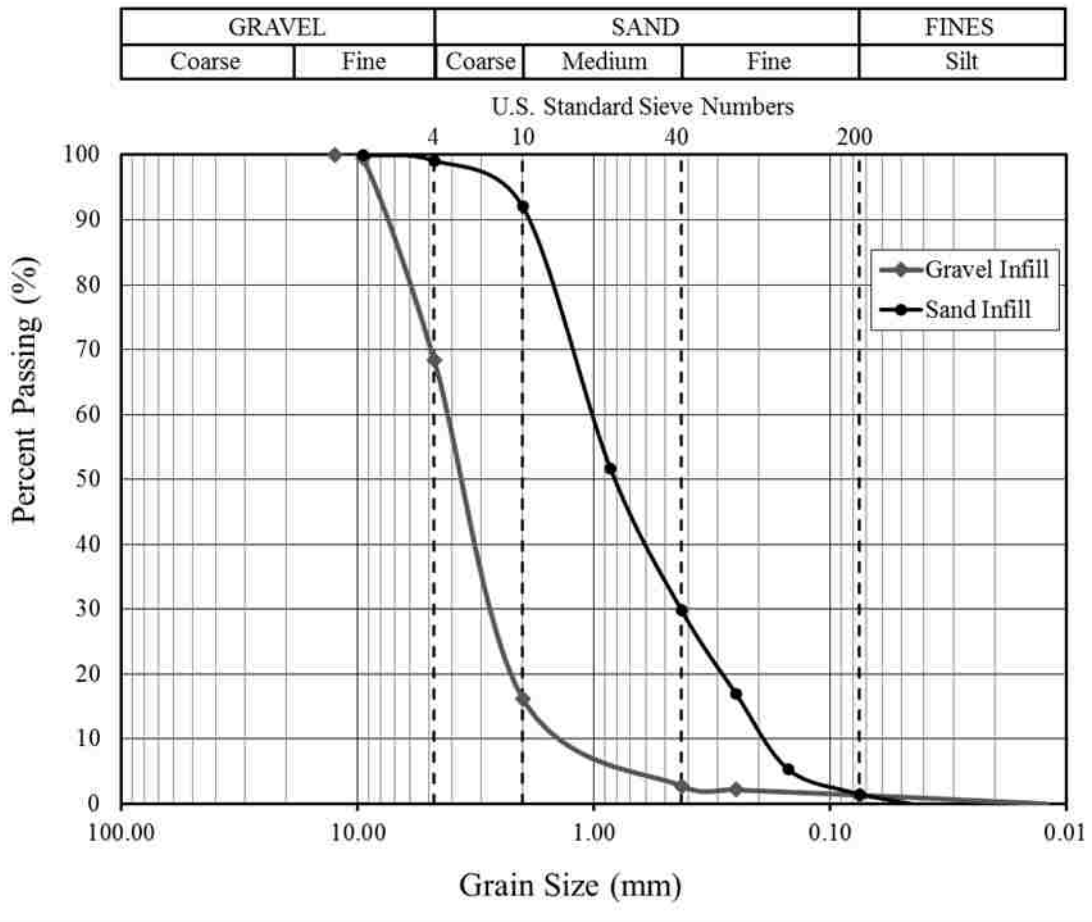

Figure 3-5: Particle Size Distribution Curve for Gravel and Sand Infill Material

3.3.3 Compaction

There were three phases of soil compaction at this test site. An explanation of each of these phases is provided in this section. Figure 3-2 has been provided as a visual aid to show the layout of the test piles and the compaction phases as an elevation and plan view. The initial phase of soil compaction consisted of 15 ft of backfill material to be compacted on top of the native soil. This material was placed in twelve inch lifts and compacted by a vibratory roller compactor. The material was moisture conditioned to sustain optimum levels throughout compaction. Lateral load tests on four piles were performed at this level including two square, one round, and one H pile. The first test was performed by reacting a round pile against a square pile while the second

test reacted another square pile against an H pile. A more detailed discussion of these test results and a detailed analysis was performed by Bustamante (2014). These tests will be mentioned in subsequent chapters for comparison.

The second phase of soil compaction added five more feet of backfill on top of phase 1 reaching 20 ft of backfill over the native soil. Four load tests were performed in phase 2 compaction. Similar to the compaction in phase 1, phase 2 used a vibratory roller compactor with 12 inch lifts as shown in Figure 3-6 and Figure 3-7. In phase 1 and 2, a jumping jack type compactor, as shown in Figure 3-8, was used to compact immediately around the test piles where the roller could not fit, such as between the two piles within close proximity to each other as shown in Figure 3-7. There was a larger section between the two piles in The material in phase 2 was moisture conditioned, as shown in Figure 3-7, to achieve optimum moisture conditions.

Figure 3-6: Phase 1 compaction

Figure 3-7: Phase 2 Compaction

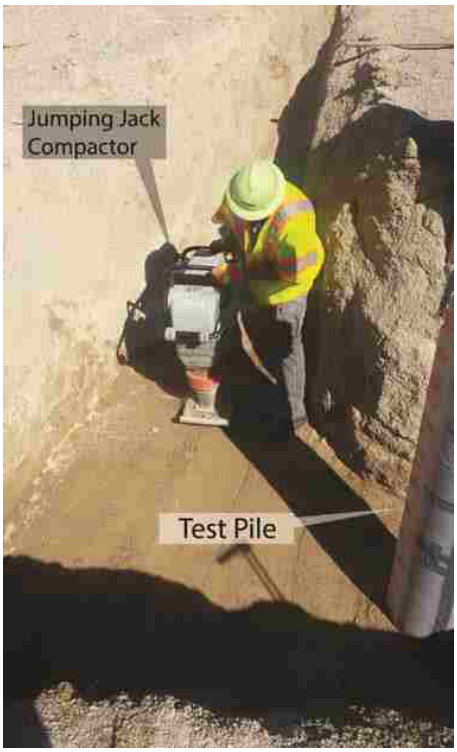

Figure 3-8: Jumping Jack Compactor in Phase 3 of Compaction.

Phase 3 was a recompaction phase which allowed the re-testing of two piles; the round pile with HDPE sheeting and the square pile at the right end of the test site. A procedure was designed to effectively remove any disturbed soil from previous tests and place re-compacted soil in the direct zone of influence around the piles to be re-tested. According to supportive literature (Duncan et al., 1994) and results from the tests done in phase 2 it was decided that the majority of lateral resistance is developed within the top 5-10 ft of soil. A pit measuring 6 ft wide, 6 ft long and 6 ft deep was excavated around the two piles on the side that the piles were to be pushed toward. Because of the size of the pit, a jumping jack compactor had to be used for compaction although the effectiveness in compaction of the jumping jack compactor compared to a vibrating roller was in question. To promote uniformity between phases of compaction, phase 3 re-compaction was performed with six inch lifts rather than twelve inch lifts because of the limited zone of influence of a jumping jack compactor. Special effort was made to provide compactive energy in the immediate vicinity around the piles where compaction is likely to have significant effects on lateral resistance at small deflection levels. This method was used for the last two tests, the (2) square and (2) round – HDPE load tests. Effort was directed to ensure uniformity between all lifts of compaction.

According to common practice, the CMS infill material was poured into the annular void from the top of the pipe after final grade had been reached. Compaction was impossible in such a confined space and the pipe was not vibrated to increase infill density. Therefore, the infill material can be considered loose.

Nuclear density tests were performed to check conformity to at least 95% of the standard proctor dry density and near optimum moisture content. Based on these measurements, the

moisture content, dry unit weight, calculated moist unit weight and relative compaction of the measured soil properties for phase 2 and phase 3 are shown in Table 3-3. The overall average, standard deviation, and coefficient of variation have been calculated and are also reported in this table. Although these measurements indicate that the soil densities are relatively uniform throughout the test site, the extent of this data should be explained. The nuclear density gauge was set to depths of six to eight inches during density testing. While this ensures that the phase 3 data, which was laid in six inch lifts, is uniform, it can introduce a level of uncertainty for the phase 2 data, which was laid in 12 inch lifts. The compaction data for the phase 2 tests reports satisfactory compaction results although this data is only representative of the depth to which the soil was tested. It is possible that at depths below that which was tested, from eight to twelve inches, lower amounts of compaction were reached. It is common practice to use a roller compactor for twelve inch lifts although in smaller areas where a jumping jack compactor was used for a twelve inch lift, there is a higher probability that proper compaction was not reached at greater depths. The moisture conditioning was applied in a uniform manner throughout all the layers and the moisture content of the material was kept within an acceptable range to provide sufficient compaction in the regions that were tested. In retrospect, this is shown with the results of the round (1) pile with HDPE sheeting. The close proximity of this pile to an adjacent square pile required a jumping jack compactor to be used on twelve inch lifts. Load test results in future sections will reveal the inconsistency in compaction around this pile while all other load tests show trends that conform to the expected level of resistance.

Table 3-3: Soil Properties

Phase of Soil Compaction			Moisture Content (%)	Dry Unit Weight (pcf)	Moist Unit Weight (pcf)	Relative Compaction (%)
	2	Round	5.9	122.7	129.9	96.9
		1 Round - HDPE	6.5	123	131.0	97.05
		H	6.1	123.0	130.4	97.05
		1 Round - CMS	8.5	121.6	131.9	96.0
		2 Round - CMS	8.0	123.1	132.9	97.2
		1 Square	7.1	123.9	132.6	97.8
	3	2 Round - HDPE	5.6	121.9	128.8	96.3
		2 Square	6.5	121.9	129.8	96.2
		Average	7	123	131	97
		Standard Deviation	1.02	0.77	1.45	0.59
		Coefficient of Variation	0.15	0.006	0.01	0.006
		Optimum	9.7	126.7	139	95

3.4 Loading System

The load source for the tests was a 300 kip hydraulic jack with a maximum stroke length of 13 inches. To provide redundancy in load measurements, a load cell was placed between the hydraulic jack and the pile and load was read from a calibration with the pressure transducer on the pump. This generally provided two measurements for load readings. A steel C - channel or steel plate was welded to each test pile to provide a flat surface to attach clevis pin and protect the strain gauges. This setup allowed for fixed connections at every joint except where the tie-rod load cell met the clevis pin. This pinned connection was intended for safety purposes. The load apparatus was applied to each pile one foot above the ground surface. The piles were tested in sets of two, each pile acting as a reaction for the load applied to the other pile. The loading sequence can is shown in Figure 3-2. The order is numerical starting at test 1 and test 6 being the

last. Each load test followed a specific loading procedure to ensure consistent and comparable results.

The procedure for loading in these tests followed similar procedures as those employed in lateral load tests conducted previously by Bustamante (2014). The loading was controlled by the lateral deflection of the pile. Deflection increments of 0.25 inches were chosen with an initial increment at 0.125 inches to better describe initial loading conditions. After the specified deflection increment had been reached, the fluid flow into the jack was locked off while load and deflection came into equilibrium over a 5 minute period. The initial deflection state of 0.125 inches was held for only half the 5 minute period. Figure 3-9 shows a typical loading procedure as recorded by the data acquisition system during the loading program.

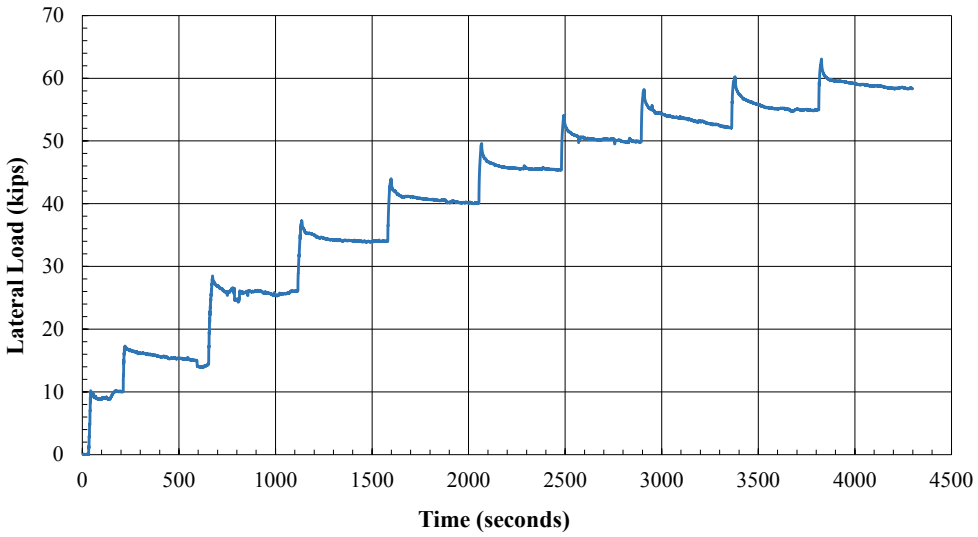

Figure 3-9: Typical Loading Procedure

This plot represents how the load was applied with time. The load increases to the next deflection state and reaches a peak. When the fluid flow is locked off during the five minute

hold, the load initially decreases quite rapidly for about one minute and then reaches an equilibrium in which load is relatively stable or decreases very slowly. Pile deflection typically remain constant or increases slightly during this period. After the five minute hold, the load is increased to the next deflection increment. This specific pile was pushed to 2.25 inches of deflection at around 60 kips of load. All tests were performed in this consistent manner with similar methods of instrumentation.

4 INSTRUMENTATION

Various data collection methods were used during the load tests to record the magnitude of the load applied, deflection of pile, pile rotation at head, ground heave, deflection at the ground surface and strain along the length of the pile. These observations were critical toward explaining pile performance and for making comparisons between the individual piles. This section explains the instrumentation used during each test.

4.1 Load Cell and Pressure Transducers

The load applied during each test was recorded by a strain gauge cell as well as an electronic pressure transducer in line with the hydraulic pump. The cell was located immediately in front of the hydraulic jack as it transferred the load from the hydraulic pump to the piles. A variety of steel struts were used to span the distance between test piles. During testing the load was verified with the pressure transducer which measured the hydraulic pressure from the hydraulic jack. Figure 4-1 provides a photo showing the load cell, jack and strut set-up between two test piles. To eliminate the buildup of a moment at the load point, the loading strut was pinned to a clevis on one pile while two spherical end platens were located on the opposite pile for the same purpose. These pin connections, shown in Figure 4-2, were also added to ensure safety in testing. Measurements were recorded by a Megadac computer data acquisition system at a rate of two readings per second. The same instrumentation procedure was used in all of the tests.

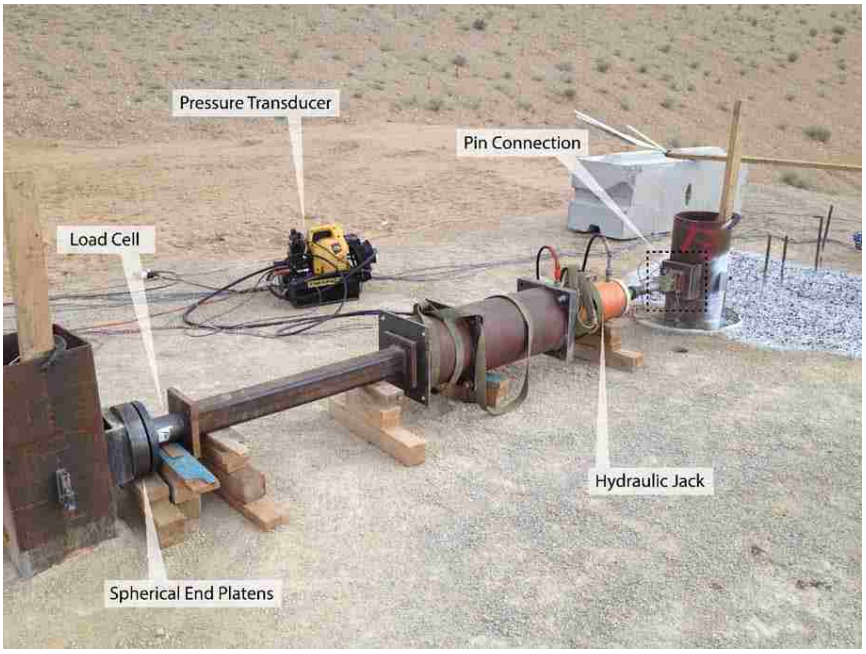

Figure 4-1: Load Test Arrangement

Figure 4-2: Pin Connection

4.2 String Potentiometers

The displacement and rotation of the pile as well as the displacement of the ground surface immediately around the pile were measured using string potentiometers or string pots, as shown in Figure 4-3. Independent reference frames were constructed out of two pre-cast concrete blocks weighing around 3600 lbs spaced at about 8 ft on either side of the test pile. The string potentiometers were attached to this reference frame as well as their different points of observation. The pile head displacement was recorded by attaching a string potentiometer to a location on the pile one ft above grade using a magnetic clip. This was also the elevation at which load was applied. Another string pot was fixed to the pile at a location three feet above the load point to measure pile deflection. Pile rotation could then be computed by taking the difference in lateral deflection between the two points and dividing by the vertical distance between them.

Stakes were placed in the ground at measured increments from the pile with string potentiometers attached in order to measure ground surface displacement. Figure 4-3 (left) shows how the string potentiometers were set up for the first test. During a few of the first tests the lateral deflection reading at the first stake, closest to the pile, showed inconsistent results. As failure planes propagated through the soil, this stake had a tendency to rotate toward the pile, giving false deflection readings. A new system using a metal plate with three stakes at the bottom to be driven in the ground and one upright stake to hold the string line proved a more efficient way to measure lateral ground deflection.

Figure 4-3: String Potentiometers in Place during Testing

4.3 Strain Gauges

To calculate pile moment with depth, waterproof electrical resistance type strain gauges were installed along the length of each pile prior to driving. In order to protect the gauges during driving, the line of strain gauges was covered with a steel angle which was tack welded to each pile between strain gauge locations as shown in Figure 4-4. The strain gauges were placed on the pile at depths of 2, 4, 6, 9, 12, 15 and 18 ft below the ground surface. Two strain gauges were placed at each depth on opposite exterior sides of the pile and in line with the direction of loading. This allowed the collection of strain measurements on the pile as the pile face was subjected to tension or compression during loading. Strain gauges were placed on the web of the H pile whereas the square round pile had strain gauges on the face of the pile in line with loading. Trial readings were taken before hand to calibrate the data collection system to the strain gauge readings.

Figure 4-4: Strain Gauges Encased in a Steel Angle

4.4 Digital Image Correlation Camera System

Relatively little information is available in the literature regarding ground heave and displacement patterns in soil adjacent to a laterally loaded pile. To better capture the heave around the piles two data collection methods were used in this experiment. Digital Image Correlation equipment and conventional surveying equipment were both used to record heave of the soil immediately around the pile. The survey station was set up prior to each test at a distance unaffected by the load test. Elevation measurements were taken with a leveling rod before and after the loading was applied. The elevation measurements were correlated to a backsight reading of a known benchmark that was independent of the testing. This method recorded elevation differences at one foot distances from the pile face to a distance of five feet from the pile, where space permitted. Elevation readings were also taken at the edge of the CMS which was six inches

from the face of the round central pile. This traditional method will later be compared to newer technology to ensure consistency with the new method.

The method of Digital Image Correlation (DIC) was used in this study to provide detailed measurements of ground heave around the piles during loading. This appears to be the first application of this technology for this purpose. The DIC system, manufactured by Dante Dynamics, collects data by using two digital cameras placed at a known height from the ground and spaced at a fixed distance apart from each other. The cameras were oriented so that their line of sight overlapped with the companion camera creating a field of vision approximately 8 ft x 6 ft. Corresponding shots were taken by each camera of the same object at the same time. The analysis software then uses a correlation algorithm to recognize displacements of thousands of points in the x, y and z direction. With this information, color contour plots can be generated of displacement, deformation, and strain. The setup of the data collection system in this test is shown in Figure 4-5. Ground heave was expected on the side of the piles opposite to the loading and the DIC cameras were installed to measure the deformation of the ground in that area. Objects with a high contrast pattern provide the most accurate data so the ground was painted white to contrast against the black painted gravel that was arranged in the camera view as shown in Figure 4-6. The system is sensitive to measurements down to 1/100,000 of the field of view (Measurement Principles of DIC). This setup resulted in a calculated measurement uncertainty of three thousandth of an inch (0.003 in). Digital images were taken immediately after each load increment during the test and again after the five minute hold period.

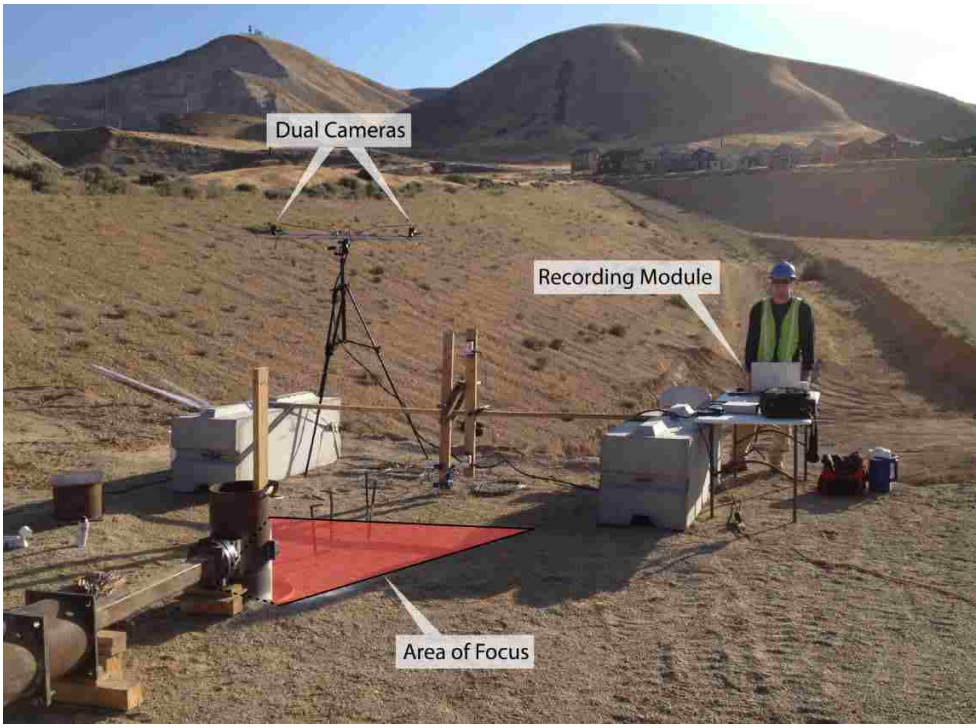

Figure 4-5: Test Apparatus with Independent Reference Frame and DIC Cameras

Figure 4-6: Contrast Grid for DIC Cameras

5 LATERAL LOAD TESTING

This section reports the result of each individual lateral load test while providing explanations on these results. This section was organized to best compare how each pile type behaved in relation to similar pile types. The following sub sections will show the aspects of comparison for the lateral load tests: failure planes, load-displacement curves, pile rotation, bending moment vs. depth diagrams, ground displacement and ground heave. Further analysis and the implications of the test results can be found in Section 6.

5.1 Failure Planes

As each of the piles were loaded failure planes started to propagate in the soil originating from the pile face. Failure planes that reached the surface were directly observable as surface cracks running through the soil. These cracks are a result of the soil failing in tension as the failure wedge mobilizes. These failure planes are another indicator of the influence of the laterally loaded pile on the surrounding soil. Figure 5-1 shows the surface cracks around each pile with the cracks highlighted with red paint for better visibility. The fan angle (α) of the most prominent failure plane has been measured for the square and the H piles. The H pile failure wedge spanned out to an α of 43° in each direction whereas the square pile showed an α of 45° on one side and 37° degrees on the other. These α measurements are close to those recorded by Rollins and Bustamante, (2015) as 38-45° for the H pile and 34-36° for the square pile. Passive wedge failure theory suggests an α ranging from the friction angle to half the friction angle

Bowman (1958). In this case, expected friction angles for the soil could range from 43° degrees and higher.

Figure 5-1: Failure Plane around the Piles: Round (top left), H (top right), Square (bottom left), Round in CMS (bottom left)

The failure planes shown around the round pile with a CMS gives insight into the soil pile interaction of this pile combination. As the applied load increases, the influence of the round pile on the loose infill increases, eventually engaging and mobilizing the CMS. The CMS then transmits this pressure onto a larger area of soil which is visible in Figure 5-2. This is a clear representation of how the use of a CMS increases the effective width of the pile. These failure planes will be further investigated in subsequent sections through measurements of vertical and

horizontal soil movement at distances from the pile. These methods will create a better description of the failure "wedge" or "bulb" for each pile shape.

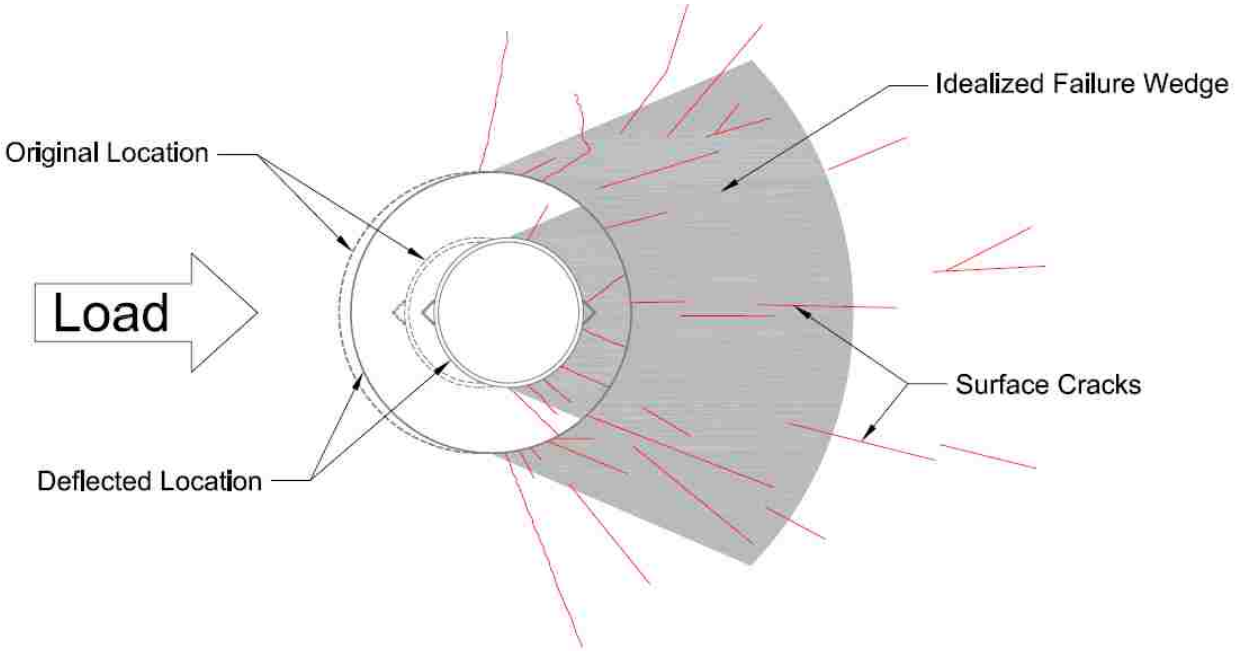

Figure 5-2: Idealized Failure Plane around Round Pile in a CMS

5.2 Pile Deflection

Lateral deflection measurements were taken at 1 foot above the ground. This was also the point where the load was applied and can be referred to as the pile head. These deflection measurements at the pile head have been used to create load versus displacement curves for the various load tests. Each curve is based on the average load and displacement readings over a 30 second interval one minute after the peak load. These curves will provide a basis in which to compare the lateral resistance of each pile type. This section will present the differences and

discuss the implications of the displacements of each pile type with load. Further insight based on observations made during the testing and pile properties will be provided.

Deflection measurements were also taken at 3 ft above the load point or 4 ft above the ground. The two measurements of pile deflection were used to calculate pile rotation at the pile head. This metric allows an interpolation of lateral deflection down to the ground level which can be used to normalize the ground displacement versus distance plots. Pile rotation also provides a glance at the slope of the pile face above the ground surface as it deflected under lateral loading. Along with the load-deflection curves, pile rotation will also be provided in the following shape sections.

5.2.1 Round Pile Performance

Many pile analysis methods are formulated considering round pile behavior. This section shows the results of the round pile tests which can later be used as a control in which to compare other pile results. Figure 5-3 shows the load versus displacement curves for two separate tests. One curve is for a round pile that was tested in phase 2. The other load deflection curve is from a lateral load test performed in phase 1 by Bustamante (2014) with similar soil conditions and pile properties. The results for that test as well as a calculated average of the two tests are shown as a comparison.

It is shown in Figure 5-3 that the load-deflection curve for the round pile test in phase 2 is very similar to that for the round pile reported by Bustamante (2014). Similar resistance trends are found up to 0.25 inches of deflection and at ultimate loads near 60 kips. At one inch of deflection the round Bustamante (2014) pile shows less resistance with varying slope, but the differences are less than 15%. It is possible that this small difference is due to slightly differing

states of soil compaction which would cause lower resistance compared to the round test in phase 2. Considering the initial response, matching ultimate loads, and general pile shape it can be said that these two load-deflection curves are comparable and display the same trend in soil-pile interaction. The calculated average of the two load tests will be used in comparisons with an H pile in similar soil conditions.

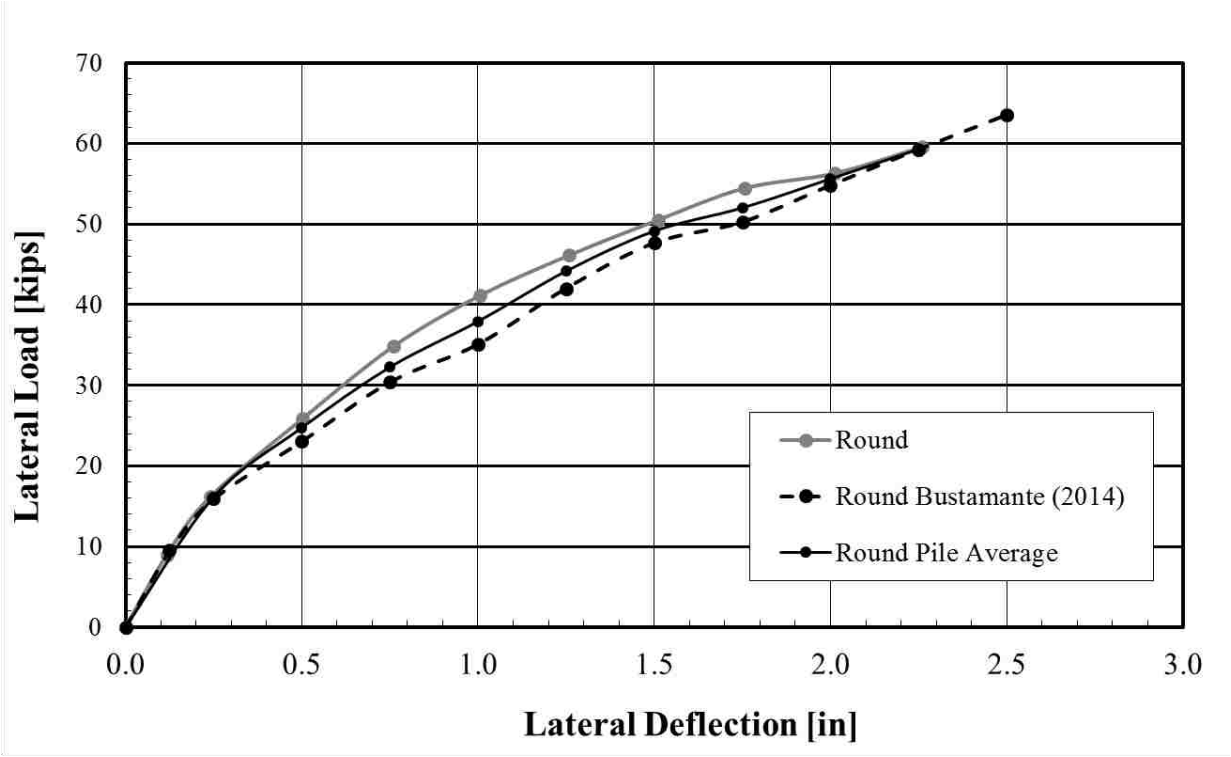

Figure 5-3: Lateral Load versus Deflection Curves for Round Piles

The round pile from Bustamante's load tests in phase 1 had an embedment length of 33 ft considering the 15 ft of compacted backfill on top of 18 ft native soil. This is less than the round pile tested in phase 2 with 20 ft of compacted backfill atop of the native soil amounting to 38 ft of total embedment. The agreement between these two load tests supports the hypothesis that this

difference in embedment length did not affect the lateral response of these piles. It is known that piles of shorter embedment react differently under lateral loads than piles considered to be long. These results indicate that embedment length doesn't have as much effect on lateral resistance after a certain embedment length has been reached.

Two separate tests were performed with a round pile wrapped with high density polyethylene (HDPE) wrapping, round (1) with HDPE and round (2) with HDPE. Plots of load-deflection curves for the two piles are shown in Figure 5-4. It was expected that the wrapped pile would show a decrease in lateral resistance when compared with the average round pile results owing to a decrease in interface friction. The lateral load versus deflection plot shows the round (1) with HDPE curve to have lower resistance than the average round curve. On the contrary, the round (2) with HDPE pile shows more resistance than the average round curve. It was expected that these two piles would both show resistance values lower than the regular round pile due to the effect of the HDPE sheeting. With the higher resistance values of the round (2) with HDPE pile it is apparent that there is another variable which is affecting the results.

These load tests come from piles of the same shape, loaded in the same manner and under similar conditions. The only factor that is seemingly a variable is the compaction of the soil around the pile. The soil around the round (2) with HDPE was sufficiently compacted with 6" inch lifts by a jumping jack compactor. This is different than the phase 2 compaction around the round (1) pile with HDPE which was placed in lifts of one foot. There is also reason to believe that less compactive effort was exerted on the side of the round pile (1) with HDPE in the direction that it was pushed due to close proximity to a surrounding pile. A jumping jack compactor was used on 12 inch lifts in this small area where the roller compactor could not fit. Although soil density tests in Table 3-3 show relatively uniform results for this pile, it has been

explained that this data may not fully explain the compaction at the bottom end of the 12 inch lifts. This difference in compaction has resulted in lower resistance values. The load tests are inconclusive in determining the effect of the HDPE sheeting on the lateral resistance of a round pile. Later analysis in Section 6.5.2 will suggest that the frictional contribution is a small portion of the overall lateral resistance. If the HDPE sheeting only affects the frictional contribution then it can be assumed that HDPE sheeting has little to no effect on the lateral resistance of a pile. This would suggest that soil compaction is the biggest variable in these load tests. Although the round pile (2) with HDPE sheeting differs in compactive effort from the other round pile load tests, the same compactive effort was implemented on the two companion square piles. Therefore the round pile (2) with HDPE will be used for comparison with the square load tests.

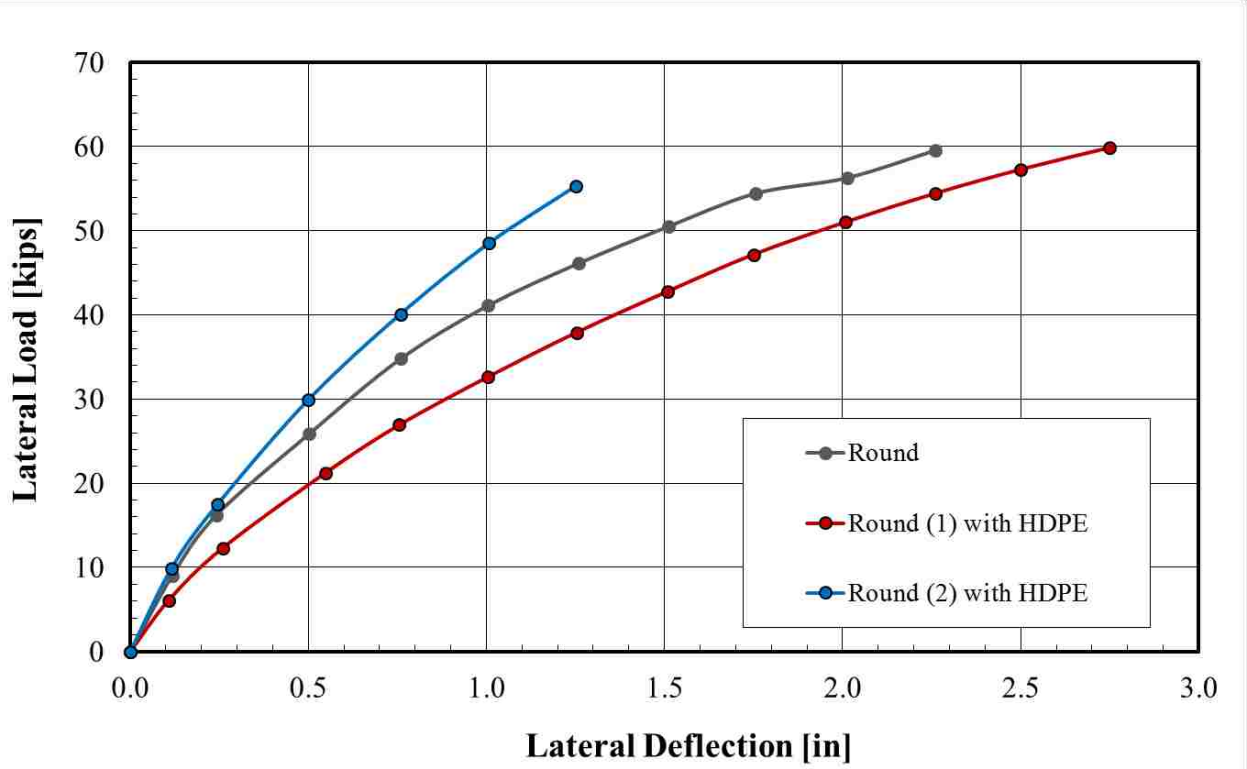

Figure 5-4: Load Test Results for Round Piles with HDPE Sheeting

The rotation of the round piles is shown in Figure 5-5. The round pile and the round (2) with HDPE sheeting display a similar pile rotation through all stages of loading. Meanwhile the round (1) with HDPE sheeting shows more rotation than the other two piles. Understandably if the round (1) pile with HDPE sheeting deflects more under load, shown in Figure 5-4, the pile will also have greater rotation. Unfortunately, the same cannot be said about the round pile and the round (2) with HDPE. Although the round pile showed less lateral resistance than the round (2) with HDPE, shown in Figure 5-4, both piles appear to have rotated similarly. The measurements from the string potentiometers, used to measure deflection which provided means to calculate rotation, have been checked for errors but none were found. An LPile analysis modelling these piles indicate that the round pile is showing less rotation than expected and should lie between the two piles with HDPE sheeting. The reason of this anomaly is inexplicable.

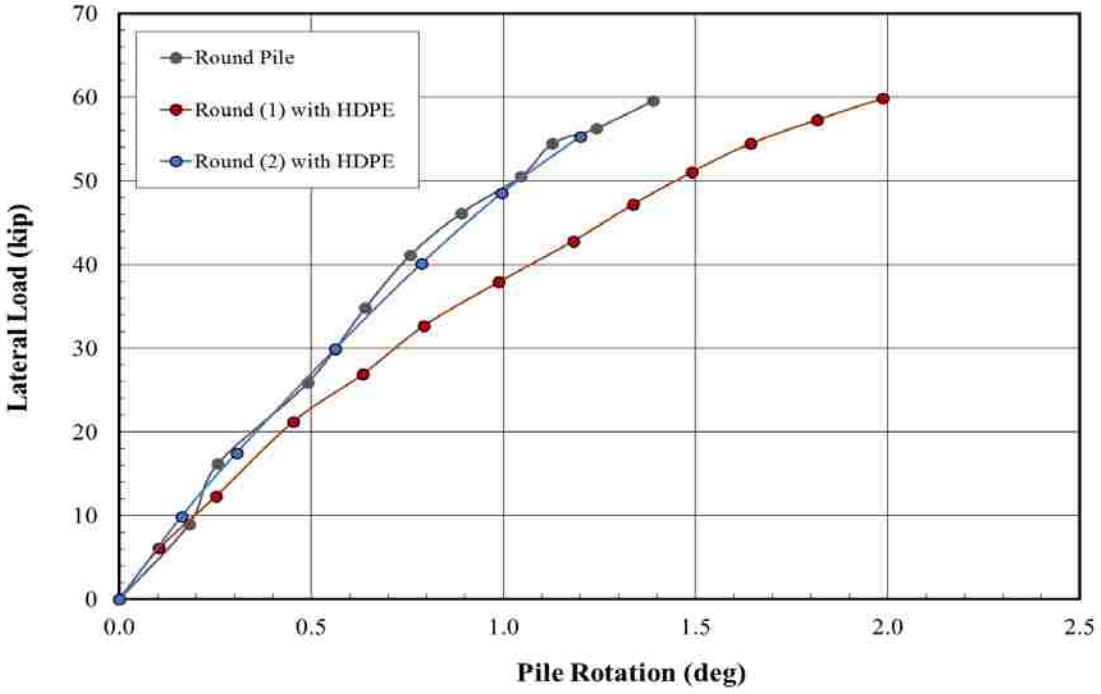

Figure 5-5: Rotation of Round Piles

5.2.2 Square Pile Performance

Two square piles were tested at this site. These piles were tested in compaction phases 2 and 3 with similar compactive effort provided by a jumping jack compactor. Every effort has been utilized to ensure similar quality in compaction around these square pile tests. The load-deflection curves for these two tests along with that for a companion round pile in a similar phase of compaction are presented in Figure 5-6. As listed in Table 3-1 the moments of inertia for the round and square piles are 314 in^4 and 335 in^4 respectively after considering the angle iron attached to cover the strain gauges. The closeness of these quantities rules out pile stiffness as a contributing factor to differing resistance values.

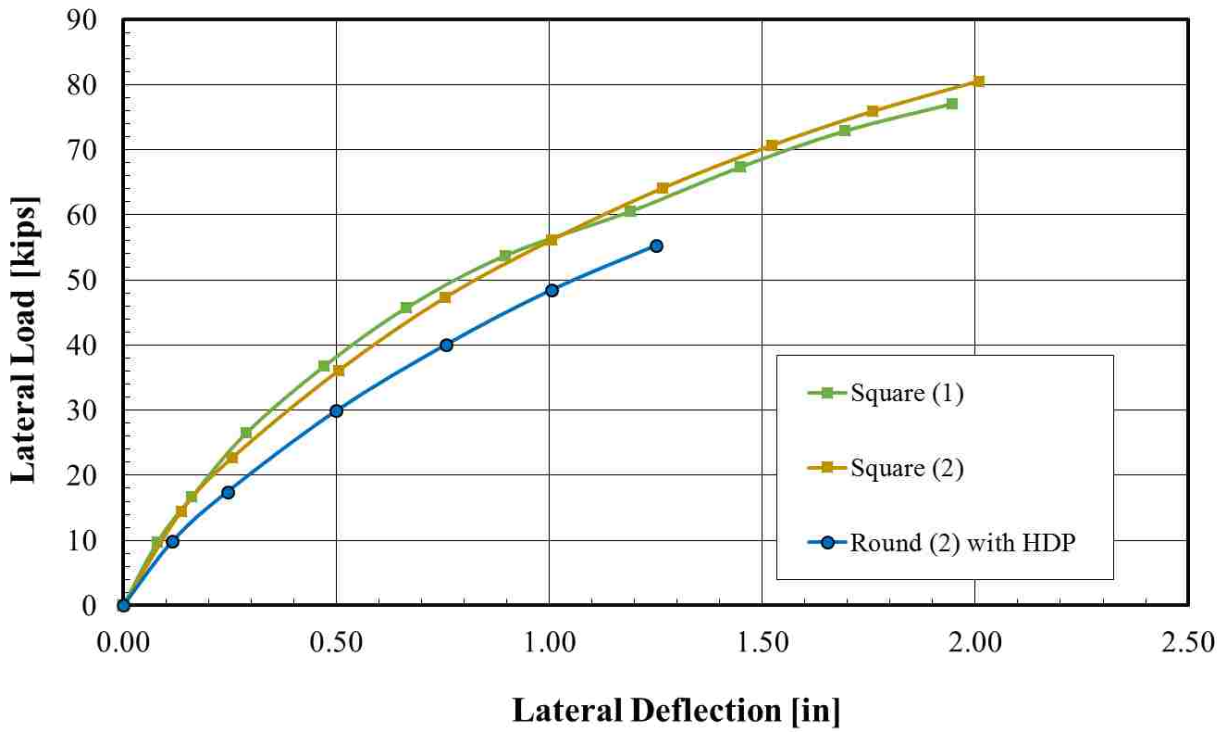

Figure 5-6: Square Pile Lateral Load versus Deflection Curves in Comparison with Round Pile Curve

The two square piles shown in Figure 5-6 have very similar load-deflection curves. This consistency indicates that these two piles reacted to the loading in the same manner and provide some confidence that the density state was similar in both cases as was indicated by the nuclear density tests. The initial slope of the two curves show similar stiffness and the progression of the curves overlap until an ultimate load of about 80 kips at 2 inches of deflection. These load tests on square piles show an increase in pile resistance when compared to the round pile which is significant. At ultimate loads, the square piles exhibited 16% more resistance than the round pile. These results are consistent with previous tests reported by Bustamante (2015), in which soil-structure interaction on the square piles provided somewhat greater resistance than that of the round pile. These load tests will provide a starting point toward quantifying the difference in the soil-structure interaction between these two pile shapes.

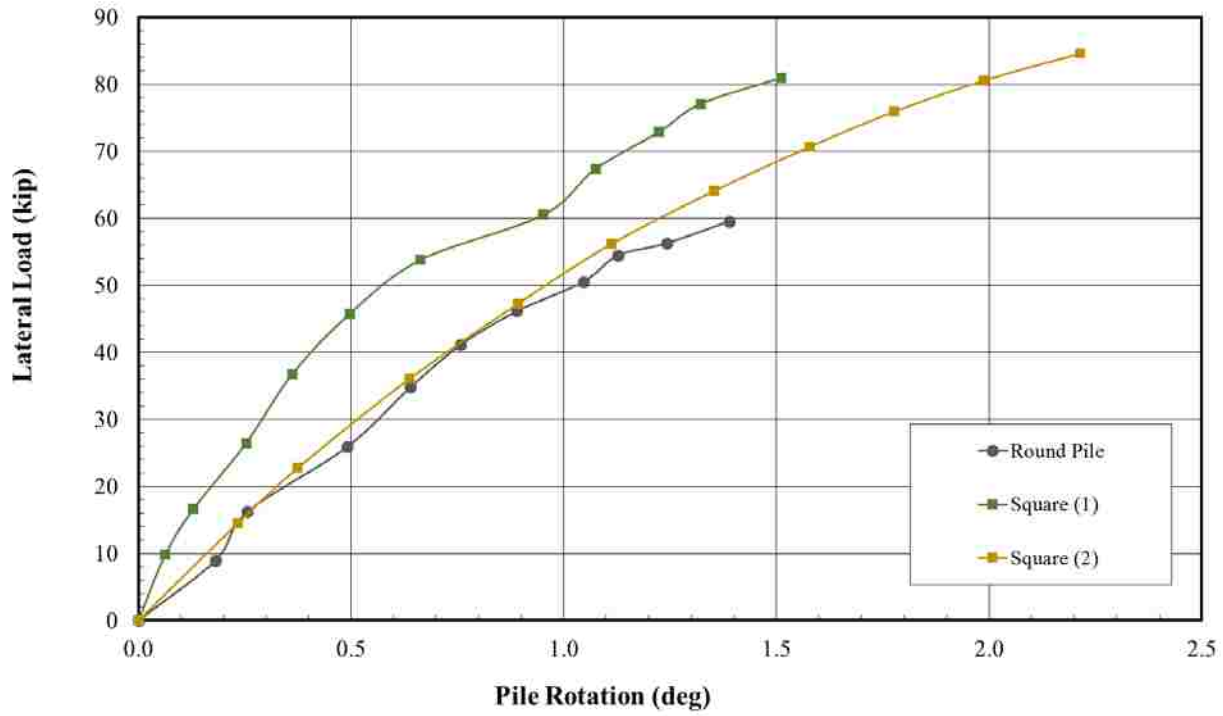

Figure 5-7: Rotation of Square Piles Compared to Round Pile

The rotation of the square piles is shown in Figure 5-7. The round pile and the square (2) pile display a similar rotation through all stages of loading. Meanwhile the square (1) shows less rotation than the other square pile, even though the square piles had similar values for load and deflection, as shownin Figure 5-6. It is difficult to say how the same pile shape in similar conditions reached the same deflection yet one of them rotated more than the other. The measurements from the string potentiometers, used to measure deflection which provided means to calculate rotation, have been checked for errors but none were found. An LPile analysis modelling these piles indicate that the square (1) pile is showing less rotation than expected and should have values closer to that of the square (2) pile. The reason of this anomaly is inexplicable.

5.2.3 H – Pile Performance

One H pile, tested in phase 2 of compaction, was laterally loaded for this study. Figure 5-8 shows the lateral load versus deflection curve for the load test as well as that that for a similar study which also tested an H-pile under lateral loading. The data from Bustamante (2014) comes from a lateral test using the same H pile. The previous H pile test was performed using a similar test procedure as the one described in Section 3 and was tested after soil compaction phase 1 with only 15 ft of backfill above native soil. The test on the H pile in this study was performed after the Bustamante (2014) test and with the addition of 5 ft of backfill. Considerable soil placement and recompaction had taken place to ensure that the Bustamante load test would not affect the results of further tests on that pile.

The two H pile tests show comparable resistance for the first inch of deflection. For deflections above one inch, the H pile from Bustamante (2014) develops 10 to 20% higher lateral

resistance for a given deflection and peaks at a load nearly 10 kips higher than the H pile. These two curves are reasonably comparable for lower deflections which are generally used in pile design. For analysis over a greater range of deflections an average load-deflection curve was computed as shown in Figure 5-8. This average, which peaks at 55 kips at 2.75 inches of deflection, will be used for further comparisons of the soil-pile interaction of an H pile such as in Figure 5-9.

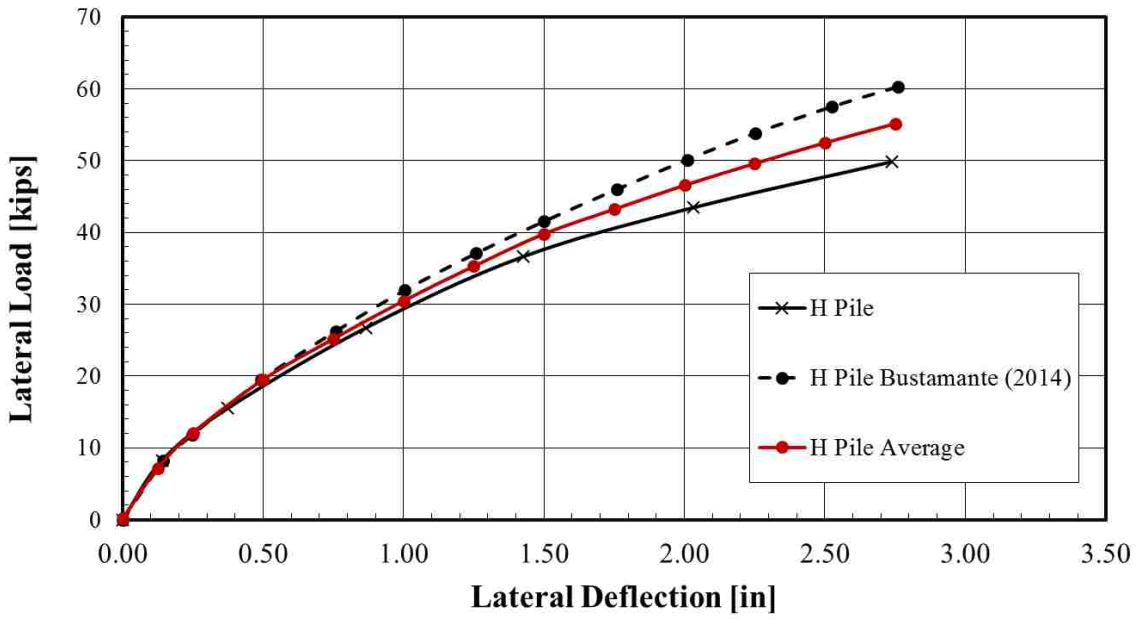

Figure 5-8: H Pile Lateral Load versus Deflection Curves

The round pile average in similar soil conditions demonstrates greater resistance then the H pile curve. It should be noted that the H piles in these tests were oriented about the weak axis to investigate a common construction practice. A survey of the use of H piles in integral abutment bridges reported that many agencies use H piles oriented about the weak axis as support for the

abutment foundations (Filtz et al., 2013). In these load tests, the moment of inertia (I) for the round pile is 314 in^4 whereas the H pile had an I of 186 in^4. The H pile has a smaller I by 41%. With this in mind it can be expected that the H pile will provide less resistance. From these load test results it appears that despite the orientation of the H pile, it still performs well in comparison to the round pile. Given equivalent values for I it appears that the H pile would provide more resistance than the round pile.

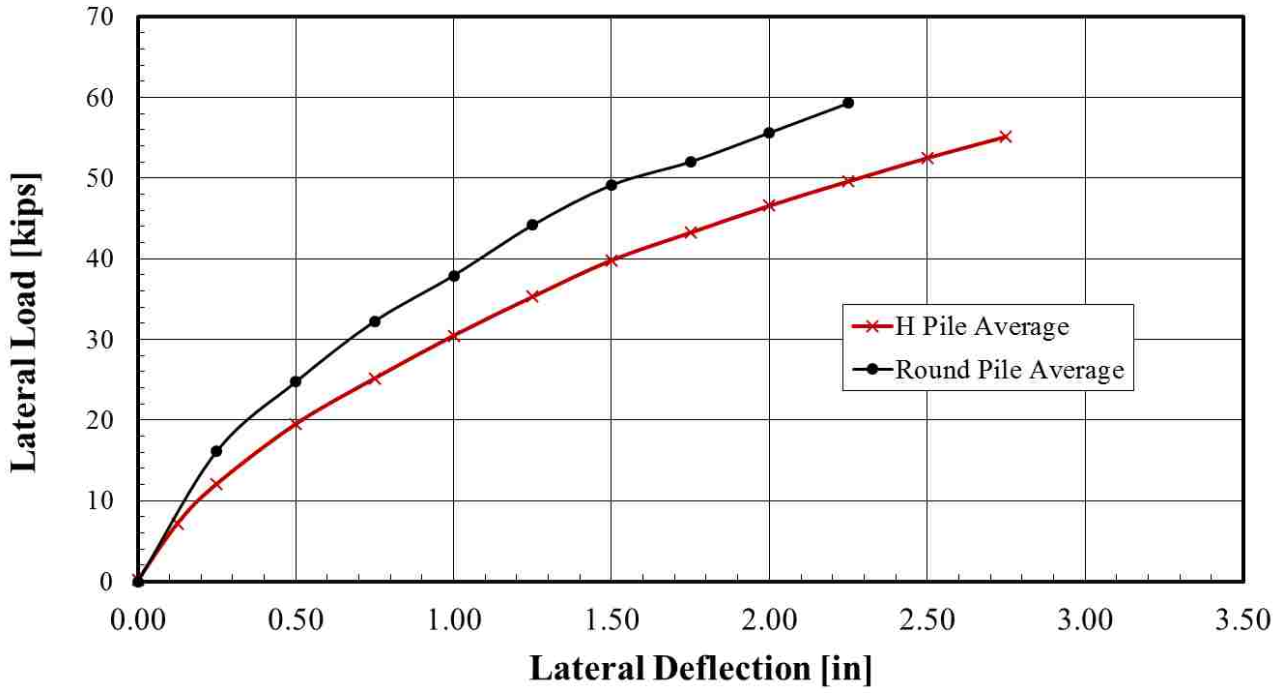

Figure 5-9: Load vs Deflection Curves for Round and H Load Test Averages

The load versus deflection curves (Figure 5-8) showed larger deflection for the H pile from these tests when compared to the round pile. A similar difference is apparent in the comparison of pile rotation for the H and round pile (Figure 5-10). The H pile rotation curve shows an initial

linear slop but gradually decreases as the pile is loaded through the yielding soil. The lower moment of inertia for the H pile must also affect the degree of rotation for the pile.

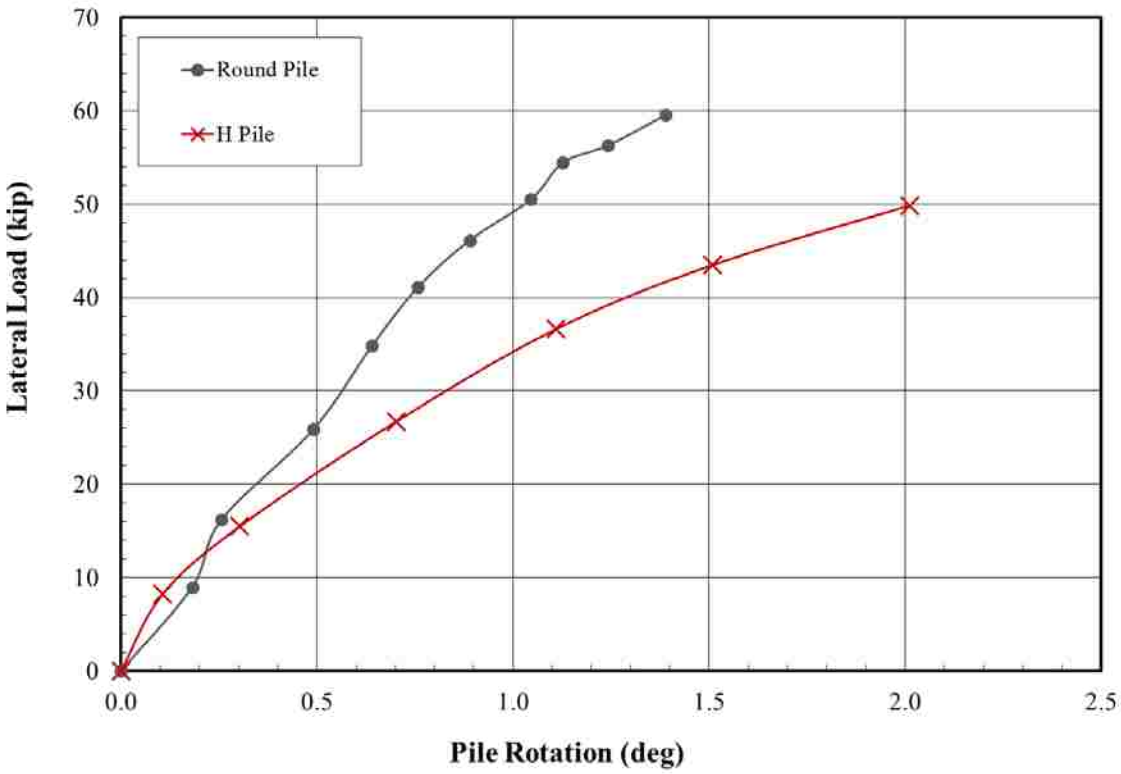

Figure 5-10: Rotation of an H pile Compared to a Round Pile

5.2.4 Performance of Round Piles with a CMS

This section describes the results of lateral load tests on two round piles each with a corrugated metal pipe (CMP) placed as a sleeve (CMS) over the upper 20 feet of the pile. The annular void space in one of the CMSs was filled with loose sand while the other was filled with loose gravelly sand. The load in both cases was applied to the round pile inside the CMS at a height of 12 inches. Plotted in Figure 5-11 are the load-deflection curves for the load tests performed on the round pile in CMS with sand infill and the round pile in CMS with gravel

infill. The load-deflection curve for the round pile surrounded by compacted backfill is also shown in Figure 5-11 purposes.

There is very little information dictating how these round – CMS combination piles should perform under lateral loading, only assumptions could be made up to this point. Generally, it is assumed that a round pile within a CMS filled with loose soil will provide relatively little lateral resistance. However, the results from these tests have been contrary to that expectation. These tests show that a round pile with a CMS will ultimately develop more resistance than a round pile in compacted granular backfill. For the first half inch of deflection the round – CMS piles show similar resistance to that for a round pile in compacted backfill. Moreover, after the first half inch of deflection, the round – CMS pile combinations develop higher lateral resistance than the round pile.

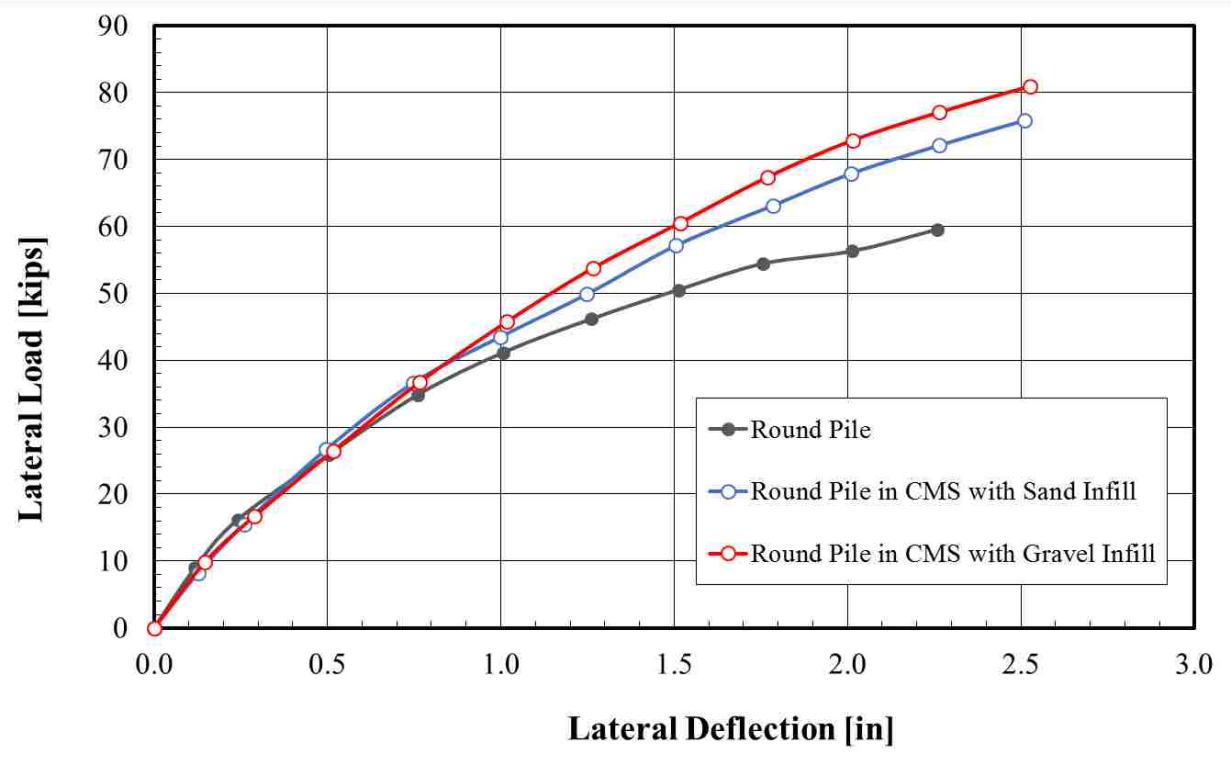

Figure 5-11: Round with CMS Lateral Load versus Deflection

The initial slope of the load-deflection curves indicates similar stiffness between all three curves at the beginning of loading. As the load increases, the soil around the round pile begins to yield and the slope flattens in all cases. However, the load-deflection curves have higher slopes than that for the regular round pile. There is also a difference in the load-deflection curves between the round – CMS pile combination with sand and the round – CMS pile combination with gravel infill. The gravel infill deflected less at higher loads than that of the loose sand infill. This might be expected because a gravelly sand often has a higher friction angle than a uniform sand. The increased resistance could also be due to greater compaction of the loose sand at higher loads as it was pressed against the CMS. The final resistance of the round – CMS pile combination with gravel infill reached 77 kips at 2.25 inches of deflection while the round – CMS pile combination with sand infill only provided 72 kips of resistance at the same deflection. These loads are 17 to 12 kips higher than that of the round pile in compacted backfill which is a large and unexpected difference. As these tests disproved the original thoughts on how these piles would perform, it is of importance to be able to explain this phenomenon and create a method of modelling these CMS piles.

The rotation of the round piles in the CMS give an interesting perspective when compared to the independent round pile. The pile rotation curve (Figure 5-12) show that the round piles in the CMS rotate more than the round pile until 50 kips of load. Both round piles in the CMS have a constant rate of rotation until 37 kips when the sand infill appears to give way allowing the pile to rotate more. It appears that using gravel infill in the annular void will cause less rotation to the central round pile in response to lateral load.

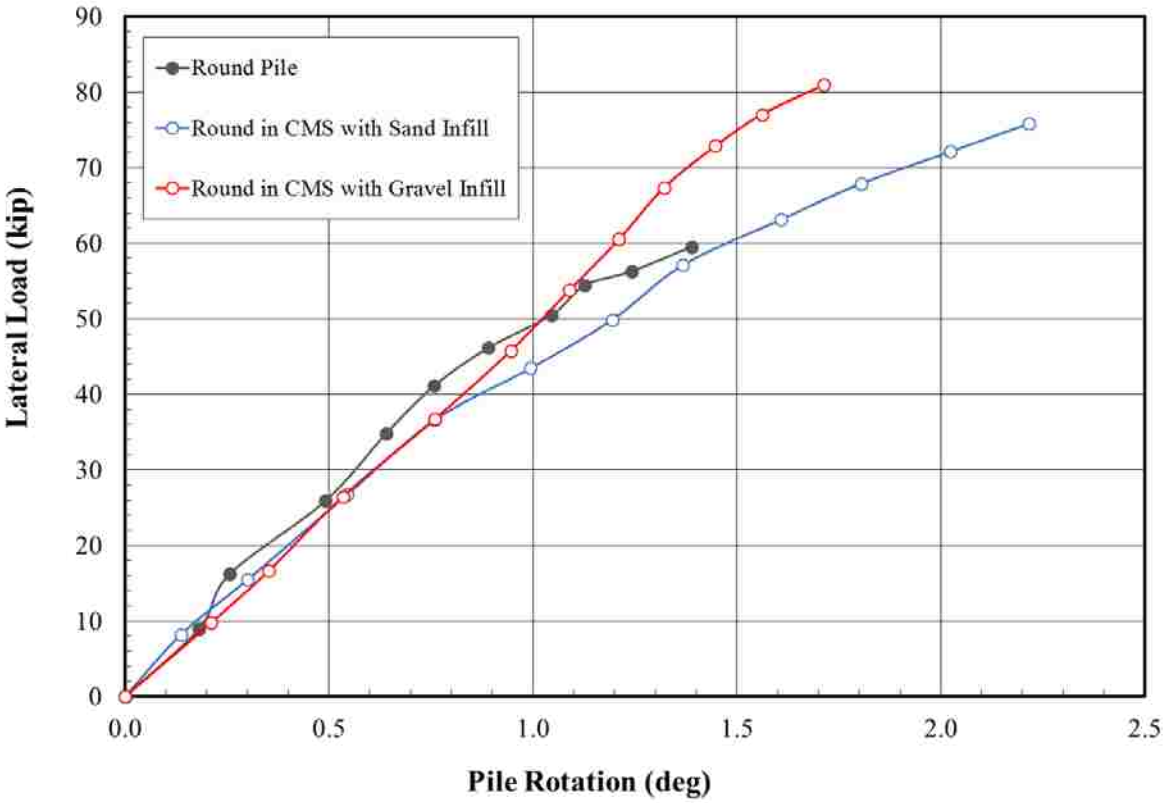

Figure 5-12: Rotation of Round Piles with and without a CMS

5.3 Pile Bending Moment vs. Depth Curves

The bending moment is directly tied with the deflection and soil resistance against the pile with depth. Obtaining information on the moment experienced in the pile will indicate the depth of influence for soil resistance. This section introduces the moment vs. depth plots obtained from lateral load testing. Section 6.6 will use the moment vs. depth curves to verify the accuracy of a model to explain the soil-pile interaction of the pile.

The bending moment, M, in inch-kips along each pile was computed using Equation (5-1).

$$M_i = \frac{EI}{2y}[(\mu\varepsilon_{it} - \mu\varepsilon_{ot}) - (\mu\varepsilon_{ic} - \mu\varepsilon_{oc})](10^{-6}) \quad \textbf{(5-1)}$$

Where:

E = modulus of elasticity of the pile (29,000 ksi),

I = moment of inertia of the pile (in^4),

$\mu\varepsilon_{it}$ = micro strain for the i^{th} data point on the tension (+) side of the pile,

$\mu\varepsilon_{to}$ = initial micro strain for the tension (+) side of the pile prior to loading,

$\mu\varepsilon_{ci}$ = micro strain for the i^{th} data point on the compression (-) side of the pile,

$\mu\varepsilon_{co}$ = initial micro strain on the compression side of the pile prior to loading, and

y = the distance separating the two strain gauges measured along the line of loading.

Micro strain values were collected from strain gauges on both sides of the pile, the tension and the compression side. Strain gauges were placed on the pile at depths of 2, 4, 6, 9, 12, 15, and 18 ft. These depths give an approximate depiction of the soil-pile interaction in the top half of the pile. The maximum moment of the pile will also occur within this depth range. Figure 5-13 shows an idealized bending moment diagram for a laterally loaded pile. The moment will also cross from positive to negative in this range. Figure 5-14, Figure 5-15, Figure 5-16 and Figure 5-17 respectively show the moment versus depth plots for round piles, a square pile, H pile and round piles in a CMS.

The moment vs. depth curves were plotted with a load of near 50 kips applied to the piles. The maximum moment typically occurs near 4 ft below ground for the round and square piles while the H pile experience the maximum moment at a depth of 6 ft (Table 5-1). The round piles in a CMS show maximum moments occurring at depths of seven and eight feet which is much deeper than the round piles. Typically, larger diameter piles develop maximum moment at

greater depth. This suggests that the CMS pile is acting as a round pile of larger diameter. The moment versus depth plots indicate that a large part of the soil resistance of a single laterally loaded pile occurs in the top 4 to 6 ft of soil which is in agreement to a previous laterally loaded pile analysis (Duncan et al., 1994). It is also interesting to note that the maximum moment in these tests tended to occur at a depth of four times that of the diameter or width of the pile as shown in Table 5-1.

Table 5-1: Summary of Maximum Moment and Depth for Each Pile Shape at 50 Kips Lateral Load

	Depth (ft)	Diameter/ Width (ft)	Max. Moment (kip-in)
Round	4	1.06	4700
Round (1) with HDPE	4	1.06	2531
Square (1)	3	1.0	1700
H Pile	6	1.01	2000
Round in CMS with Sand Infill	8	2.0	1650
Round in CMS with Gravel Infill	7	2.0	1830

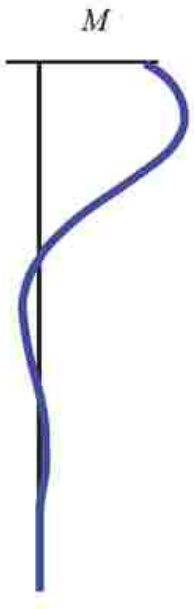

Figure 5-13 Idealized Bending Moment Diagram for a Laterally Loaded Pile

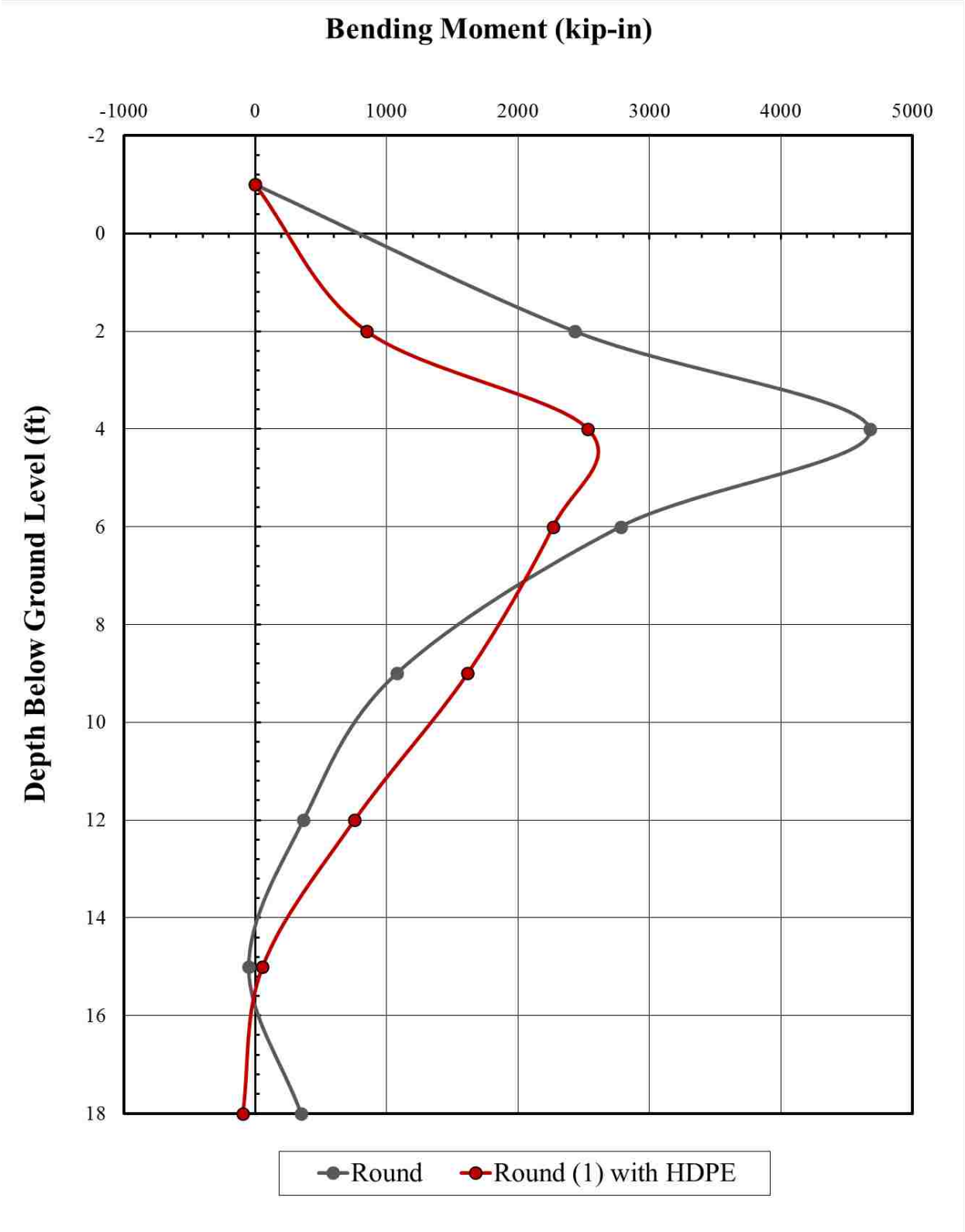

Figure 5-14: Bending Moment versus Depth for two Round Piles at 50 Kips Lateral Load

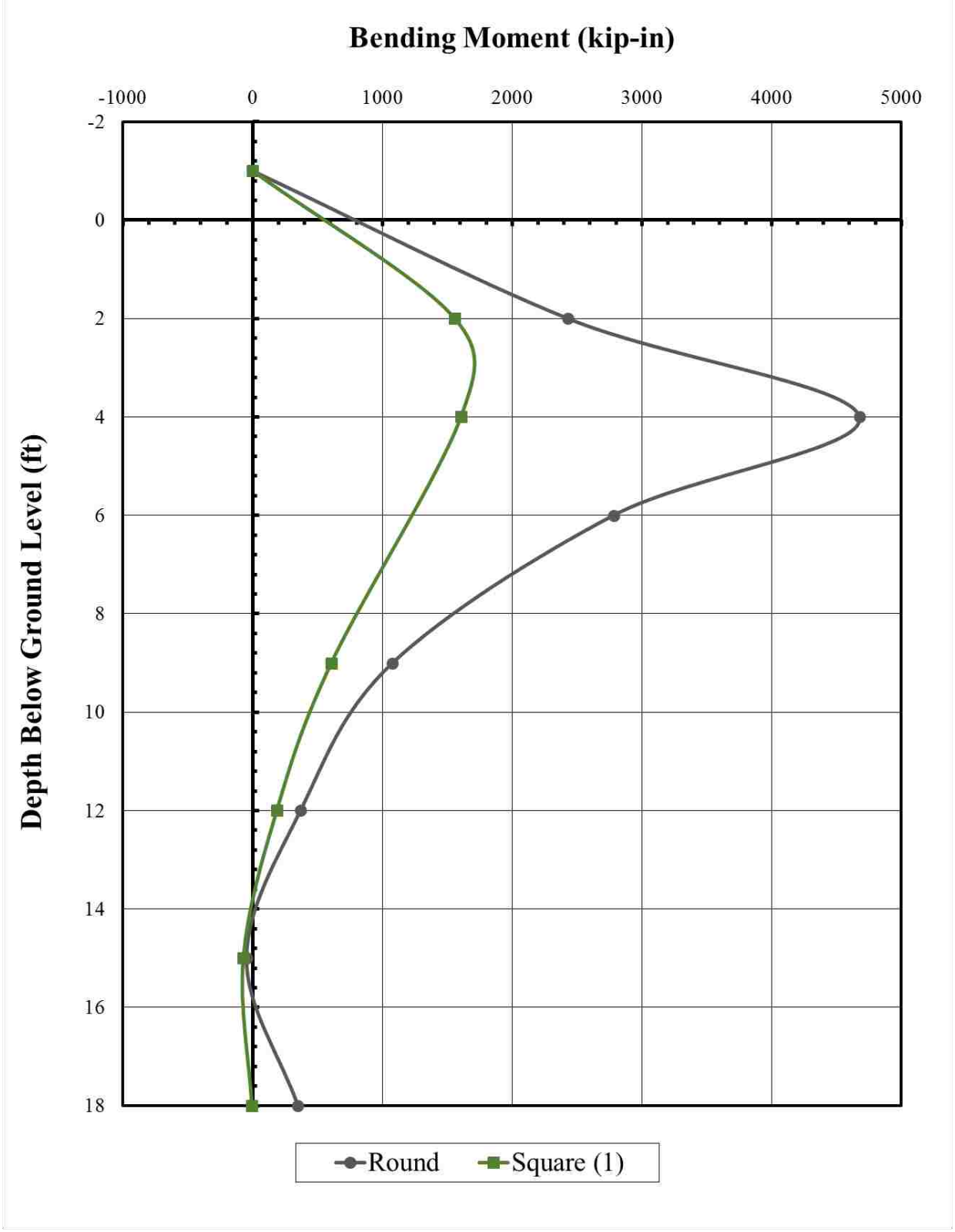

Figure 5-15: Bending Moment versus Depth for a Square and Round Pile at 50 Kips Lateral Load

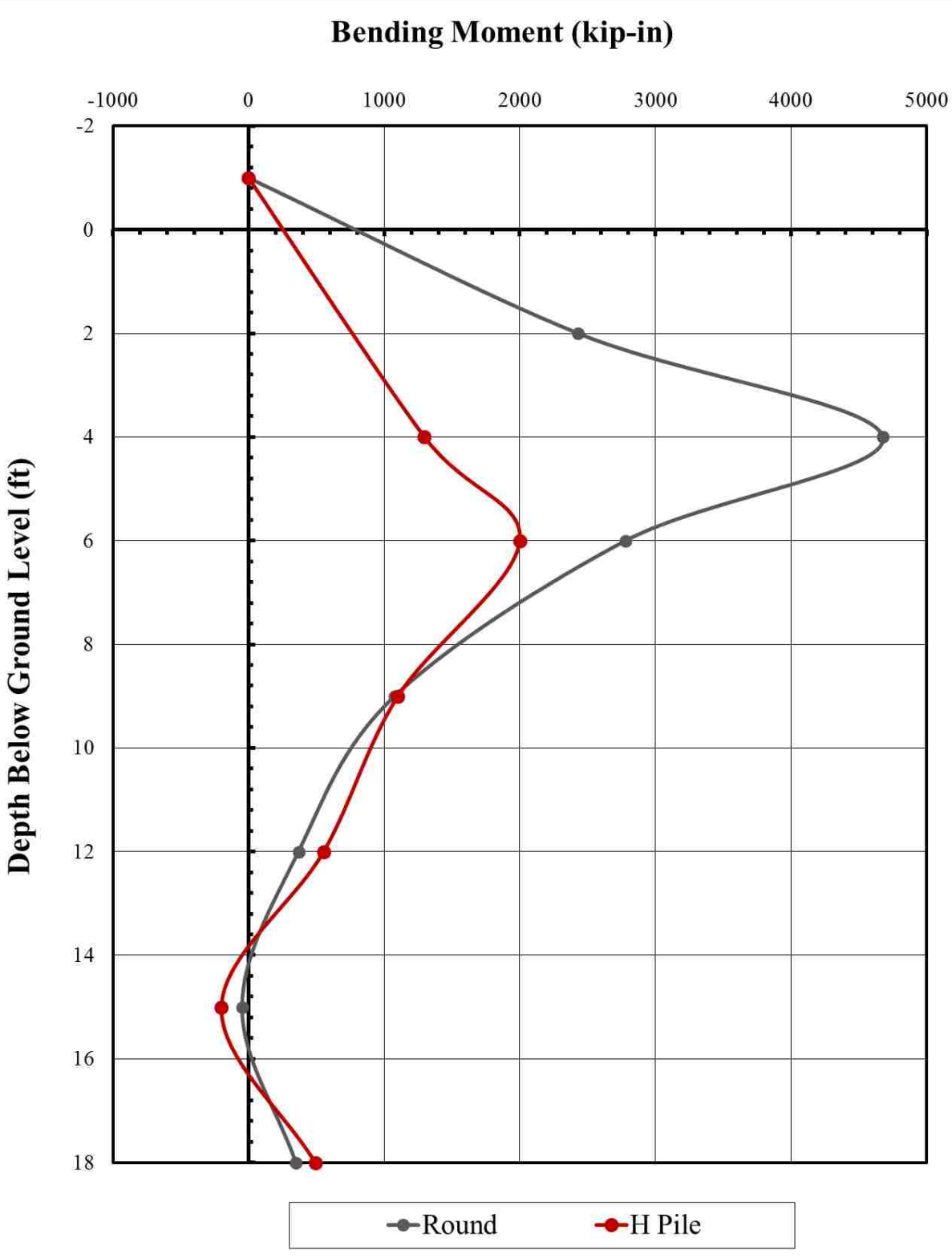

Figure 5-16: Bending Moment versus Depth for an H Pile at 50 Kips Lateral Load

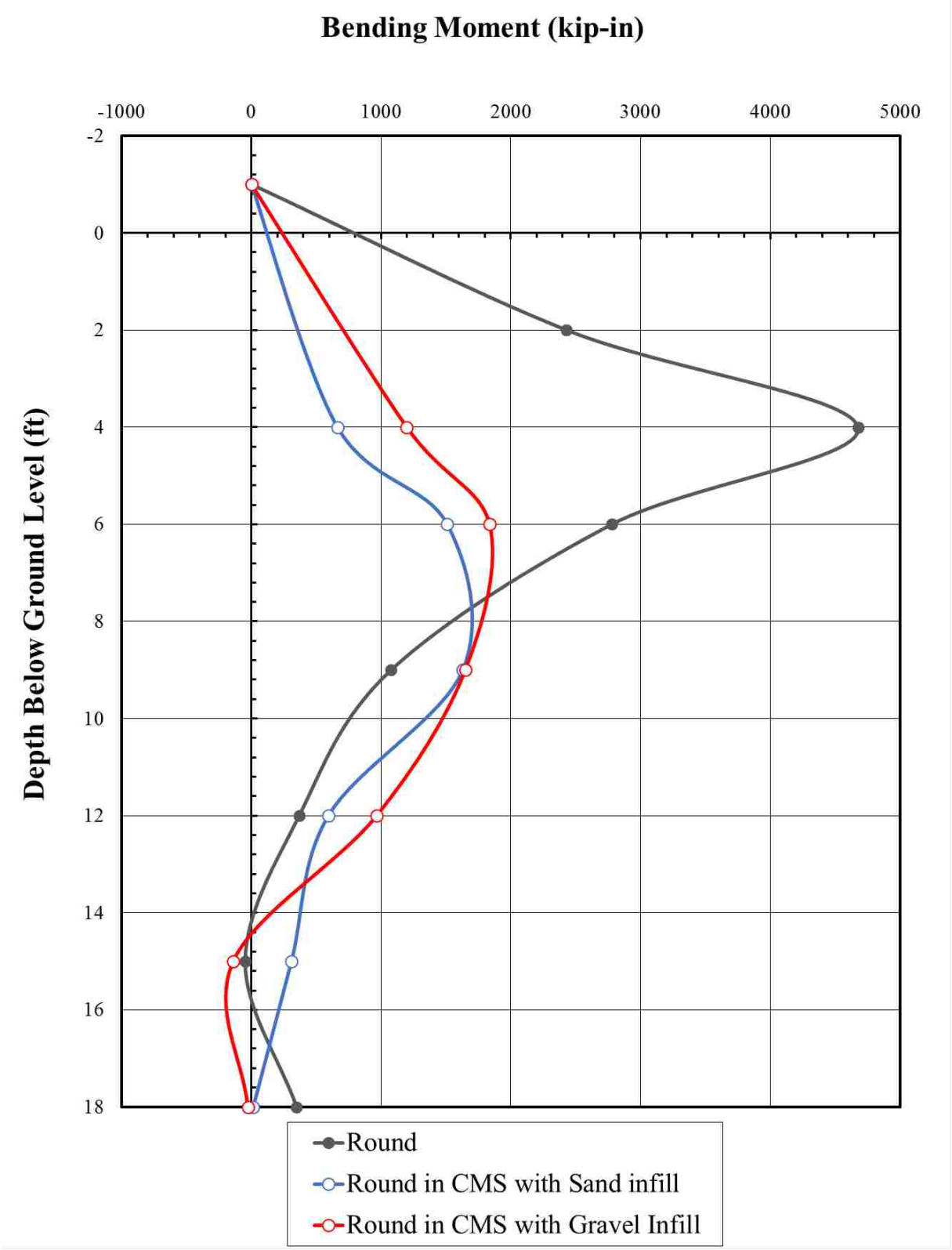

Figure 5-17: Bending Moment versus Depth for a Round Pile in a CMS at 50 Kips Lateral Load

5.4 Ground Displacement

As the pile was loaded during each test, pressure would be transferred to the surrounding soil causing the soil to displace. The lateral displacement of the ground at certain distances from the pile was measured using string potentiometers attached to stakes in the ground. These measurements help determine how lateral pile loading affects the ground around it and the extent of the failure wedge that is produced. The displacement around the piles at distances of up to 5.6 feet in front of the test piles shown in Figure 5-18 to Figure 5-21. In these figures the displacements at 0 feet from the pile, or the pile face, correlate to pile deflections near one inch after accounting for pile rotation.

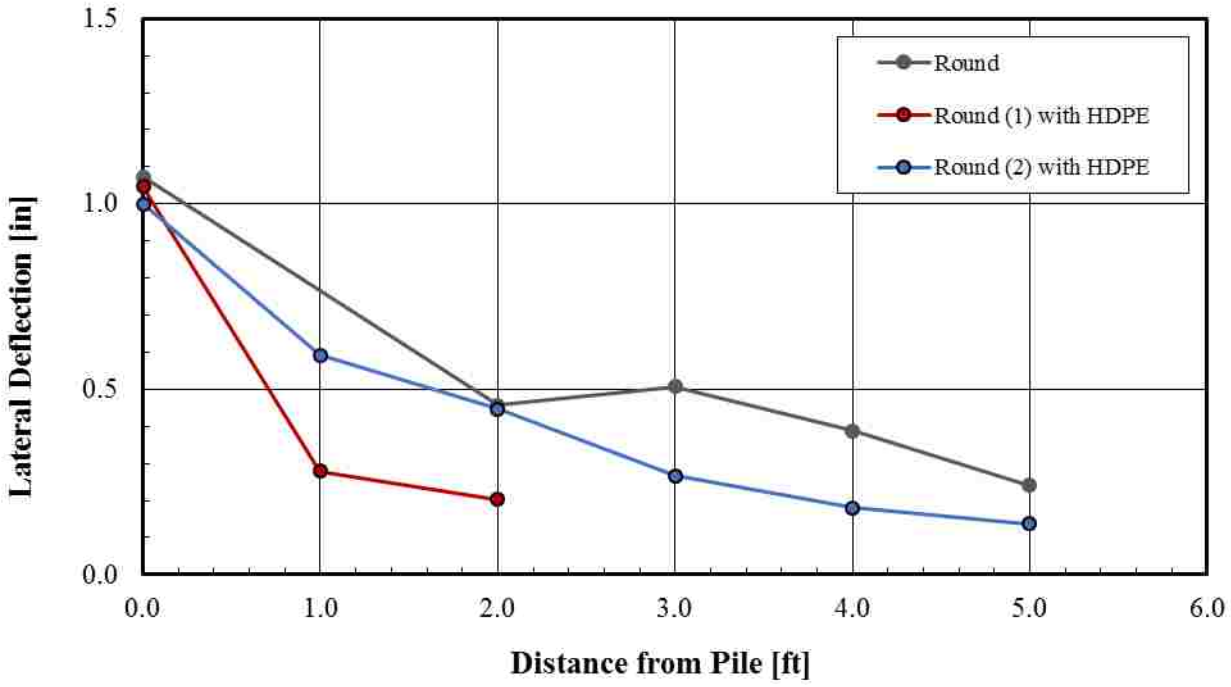

Figure 5-18: Displacement near Round Piles

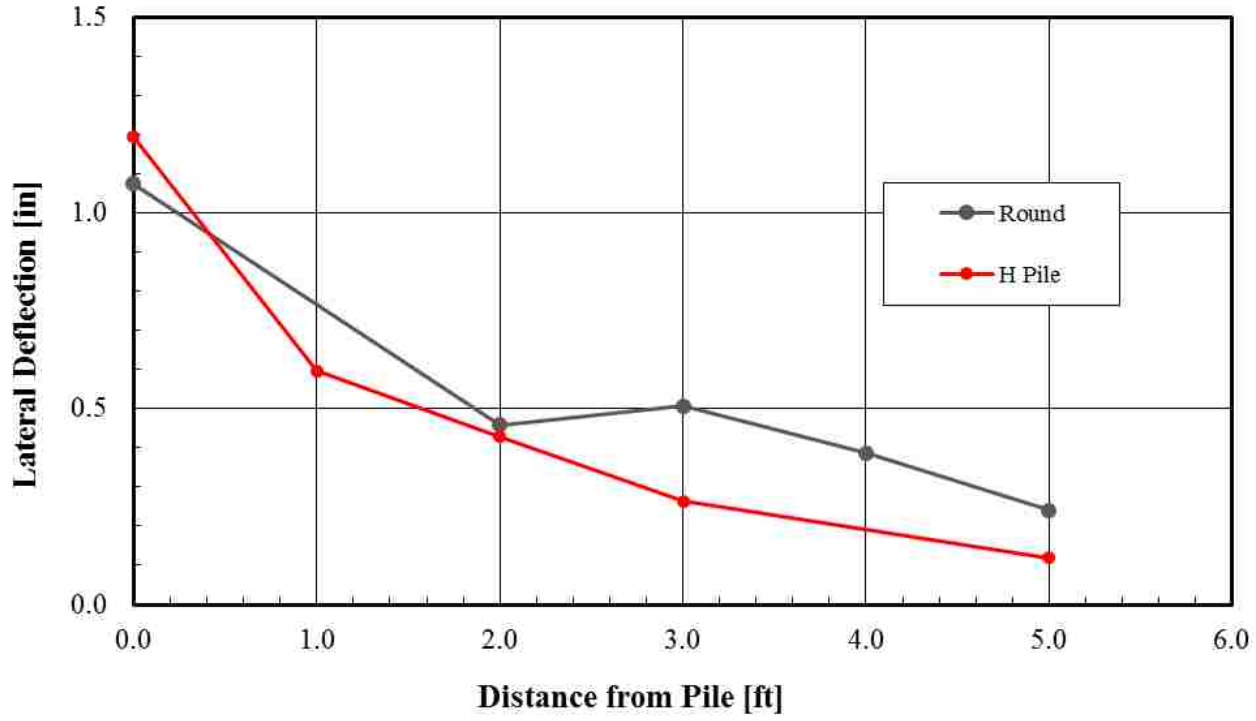

Figure 5-19: Displacement near H & Round Piles

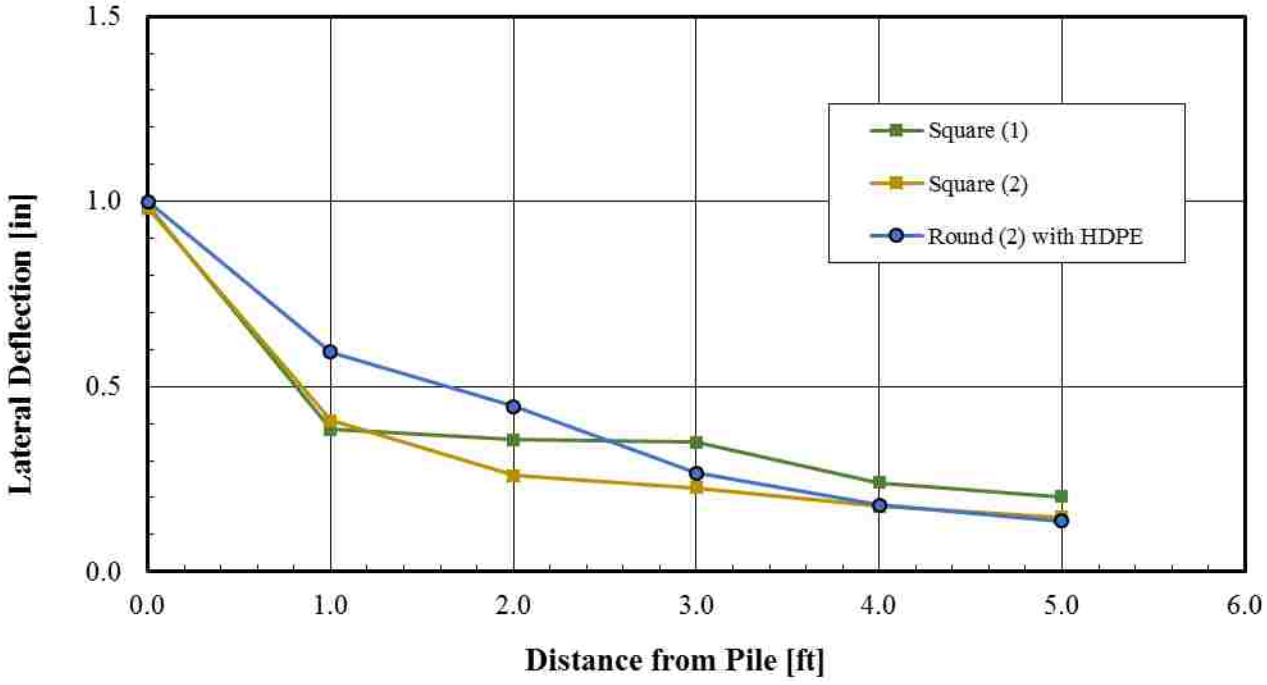

Figure 5-20: Displacement near Square Piles

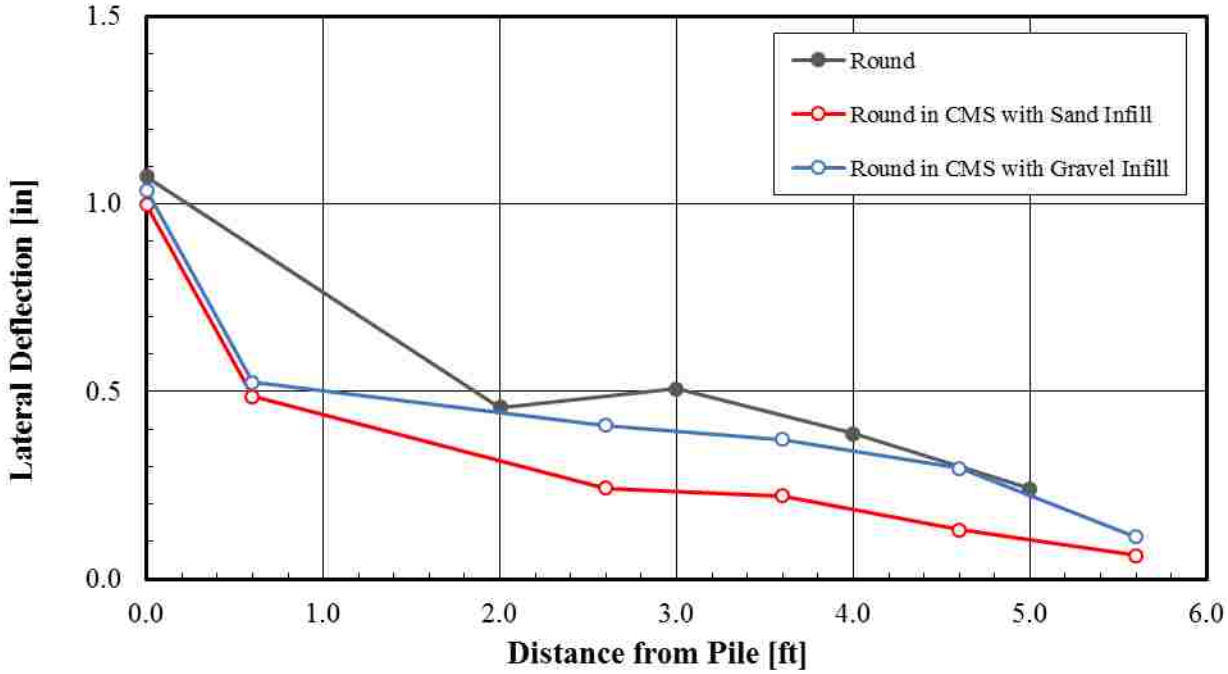

Figure 5-21: Displacement near Round Piles with CMS

The displacement figures show trends of decreasing displacement further from the pile. The round pile and round (1) wrapped pile show a drop in displacement at the one foot distance followed by a rise to the displacement at 2 foot. This is likely due to excess embedment of the reference stakes. The string potentiometers were attached to steel stakes used to mark the soil at that location. In these previously mentioned tests, lateral pile loading induced a failure plane in the soil that propagated to the stake causing rotation in the direction toward the pile. This would give artificially lower displacements than what actually occurred. This phenomena could also have occurred during the test for the H pile. The rest of the figures show that the effects of the lateral loading dissipate at distances further from the pile. The round piles with a CMS show displacement at a distance of 6 inches from the round pile which is where the outer diameter of

the CMS lies. In comparison to the results from the round pile it appears that the deflection of the CMS is similar to what the deflection of the ground would be without the CMS. Longitudinal ground displacements are close to zero at 5 feet from the pile. This indicates that at distances as low as 5 feet from the pile there is a small to negligible amount of influence from the loaded pile.

Knowing the amount of deflection at a given distance from the pile can be an indication of the pressure that the soil would exert on an object at that distance. In certain applications it is important to know how a laterally loaded pile will affect surrounding objects such as other piles in a pile group or spread footings. Normalized deflection versus normalized distance plots are presented in Figure 5-22, Figure 5-23, and Figure 5-24 with the equivalent loads that would cause 0.25, 0.5 and 1.0 inches of deflection at the pile face. These three curves have been combined into one plot with a best fit curve shown in Figure 5-25.This curve and Equation (5-2) can be used to estimate the deflection at certain distances from the pile face according to pile diameter and expected deflection at the pile face. Adversely, if the deflection limits are known this curve can be used to estimate the pile diameter needed to reduce horizontal displacement at a certain distance from the pile face. It should be noted that these curves are for sands at a 96% relative compaction so differences might occur for looser sands.

$$\boldsymbol{\delta = 0.0042d^4 - 0.0548d^3 + 0.276d^2 - 0.7125d + 1.0} \qquad \textbf{(5-2)}$$

Where:

$\boldsymbol{d}$ = distance from the pile face in diameters

δ = horizontal ground displacement as a percentage of displacement at the pile face

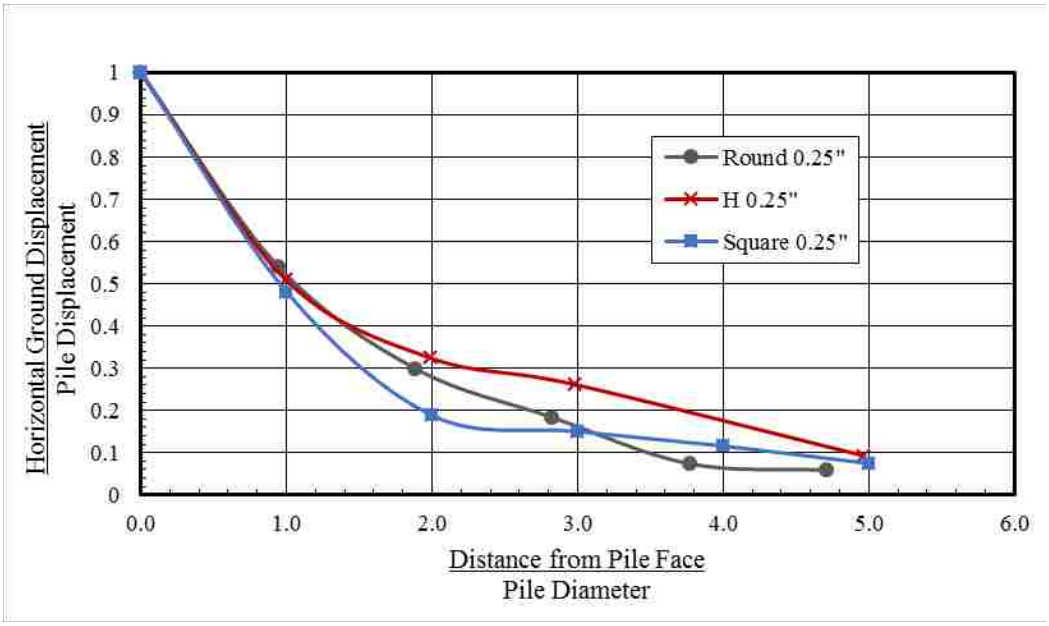

Figure 5-22: Normalized Deflection vs. Normalized Distance at 0.25" Equivalent Load

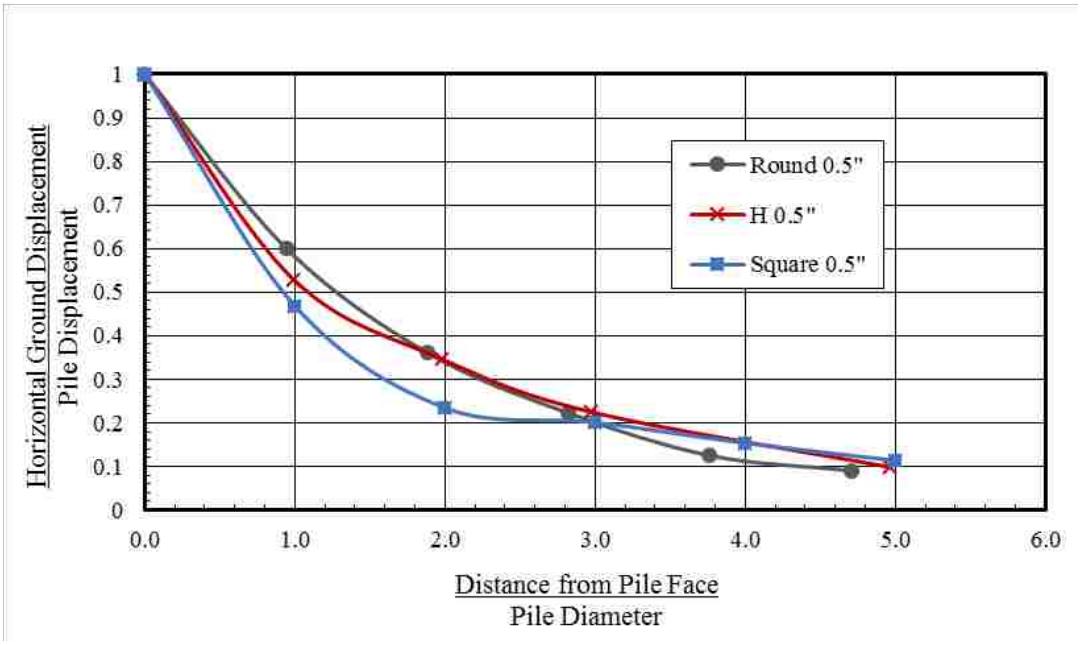

Figure 5-23: Normalized Deflection vs. Normalized Distance at 0.50" Equivalent Load

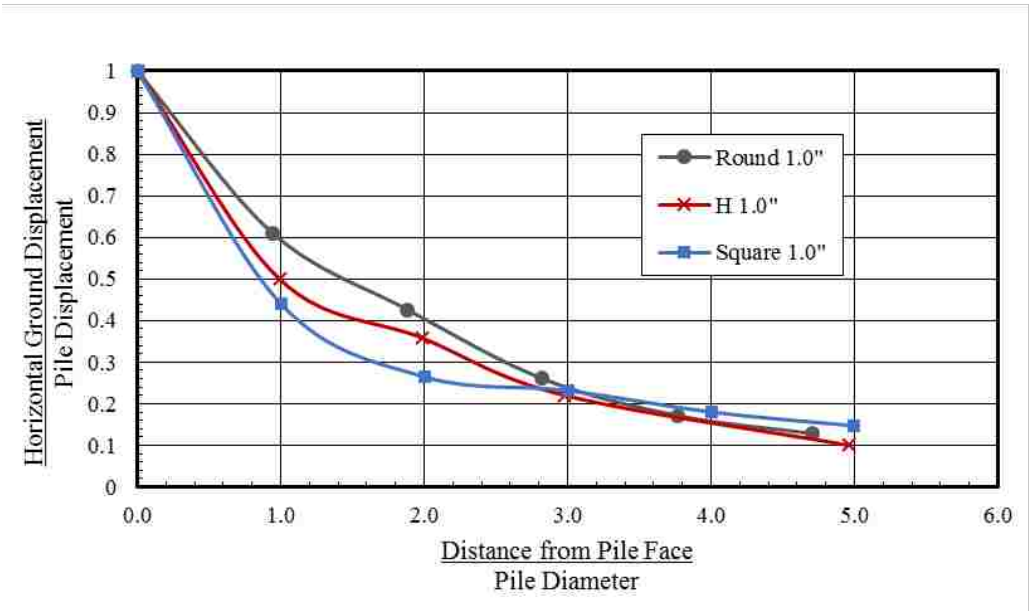

Figure 5-24: Normalized Deflection vs. Normalized Distance at 1.0" Equivalent Load

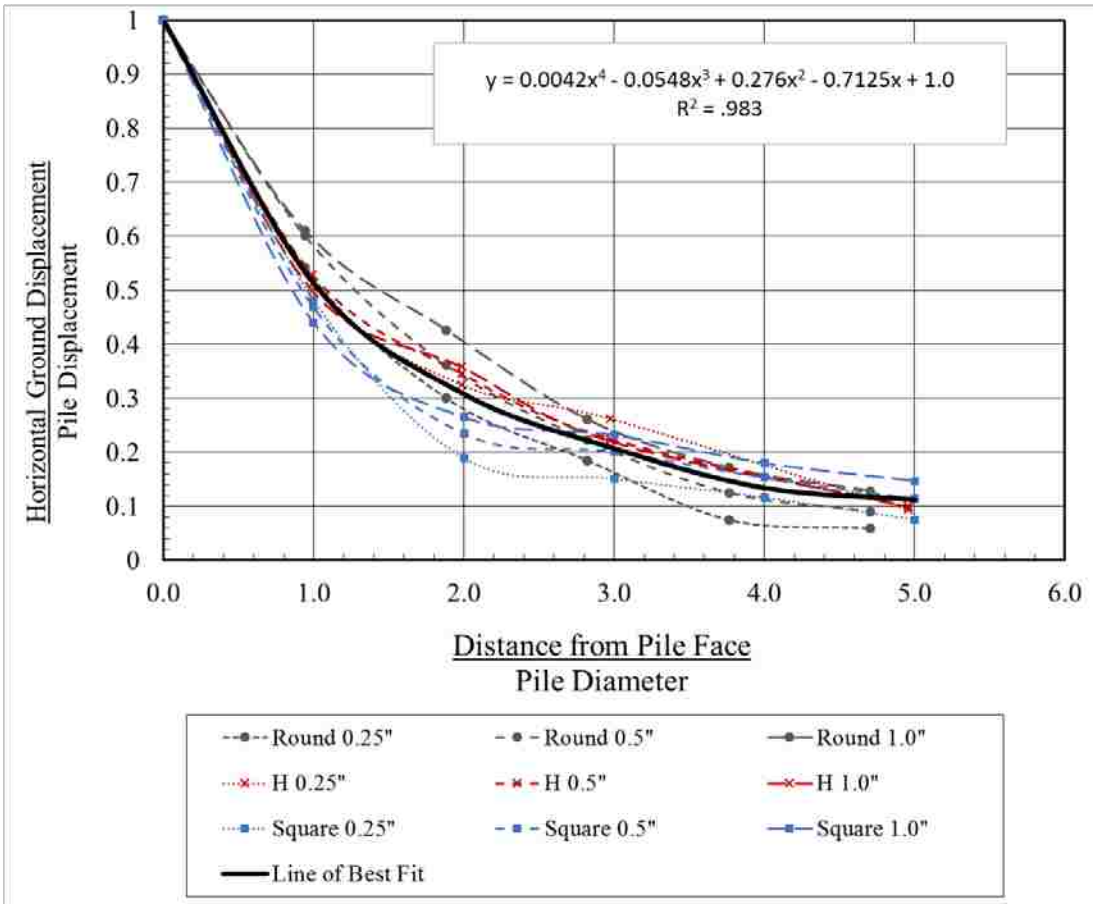

Figure 5-25: Normalized Displacement vs. Normalized Distance Line of Best Fit

5.5 Ground Heave

As each pile deflected laterally under the applied load the compacted soil around the pile would displace vertically. Measurements of this vertical displacement, or heave, at a distance from the pile can indicate the zone of influence in front of the pile itself. This information can influence the design of pile groups, bridge abutments, or structures near deep foundations. With the use of a level survey and DIC cameras, measurements were collected to observe this phenomena and determine how it might change for different pile shapes and the piles with a CMS.

Using a surveying level, ground elevation measurements were recorded before each lateral load test and after the final load was reached. The survey level was placed at a location independent of the load test with measurements in reference to a common datum. Measurements were taken at distances of 0, 1, 2, 3, 4 and 5 feet from the pile face, parallel to the line of loading. For the round piles with a CMS, the second measurement was taken at 6 inches from the pile face, which is where the CMS was located. Figure 5-26 to Figure 5-29 show the ground heave recorded using the survey level. A common trend among these plots is that ground heave is greatest at the pile face and comes back down to near zero at a distance of around 4 to 5 feet from the pile face. However, in the case of the CMS piles the ground heave increased from the pile face to the edge of the CMS, presumably as the loose fill in the annual space gradually compressed under load. Maximum heave occurred at the CMS face and then decreased with distance.

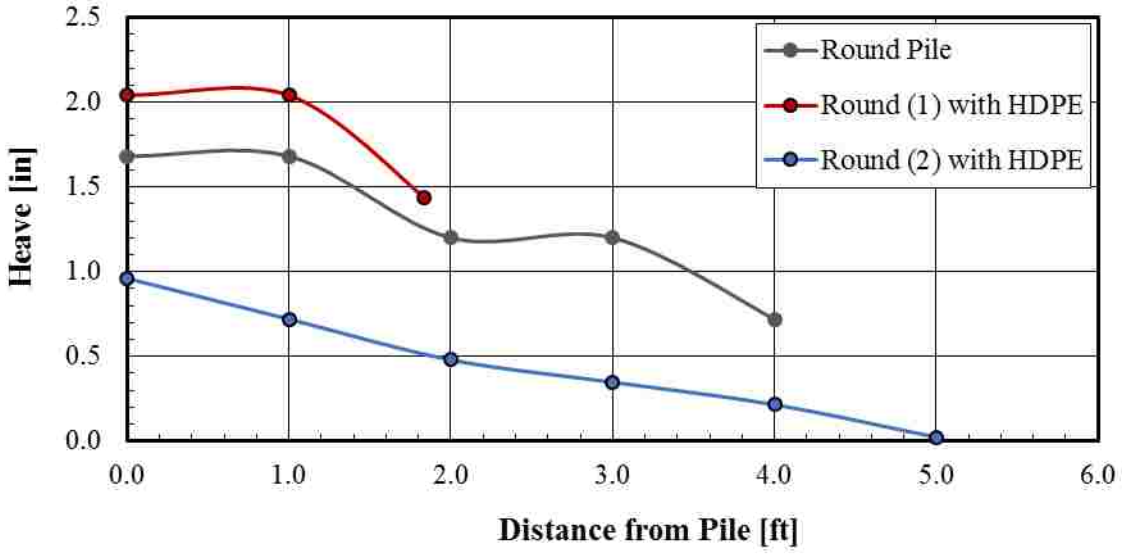

Figure 5-26: Ground Heave versus Distance in Front of Round Piles

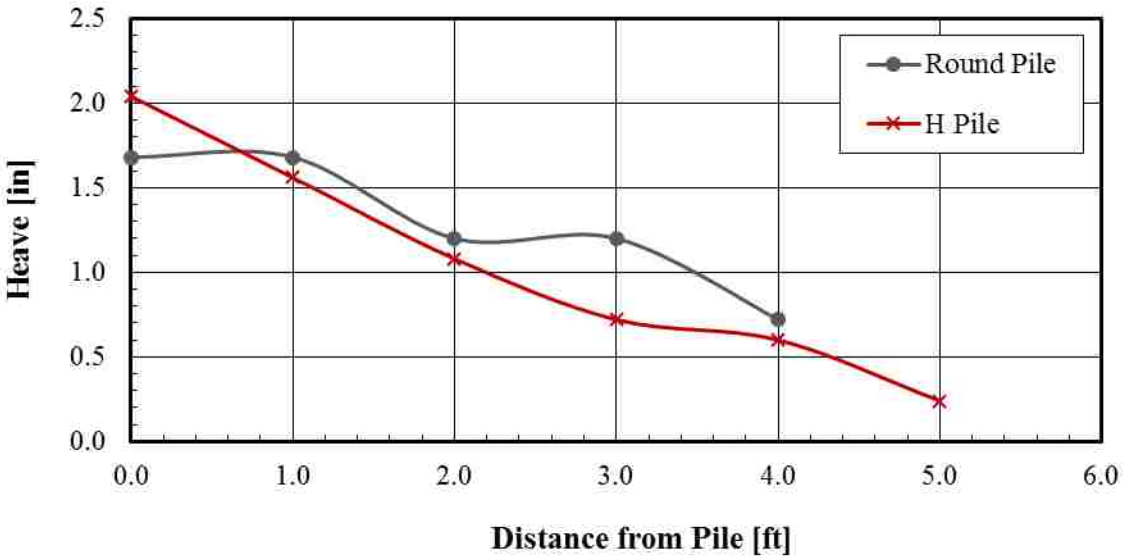

Figure 5-27: Ground Heave versus Distance in Front of an H Pile

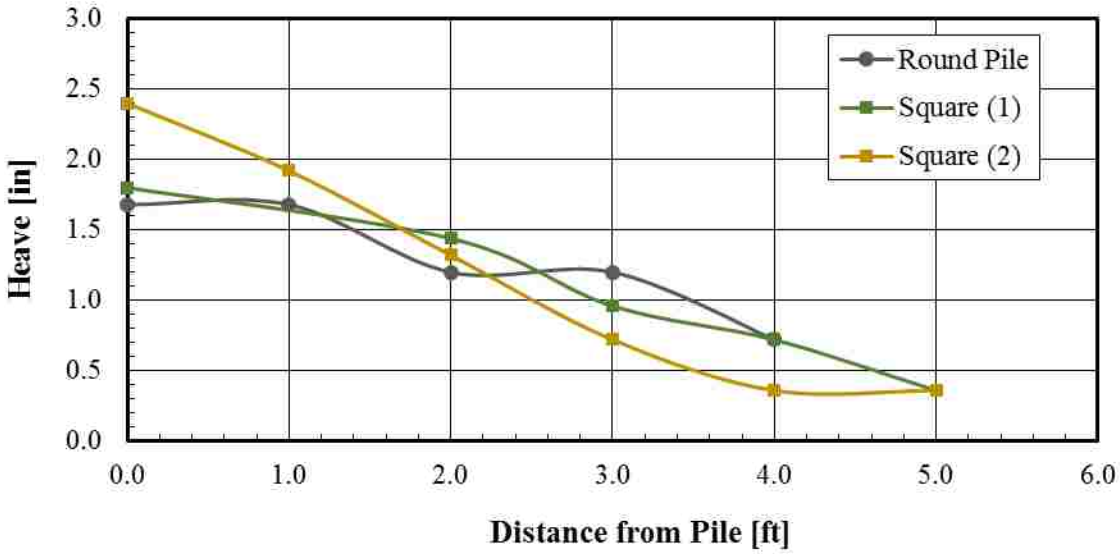

Figure 5-28: Ground Heave versus Distance in Front of Square Piles

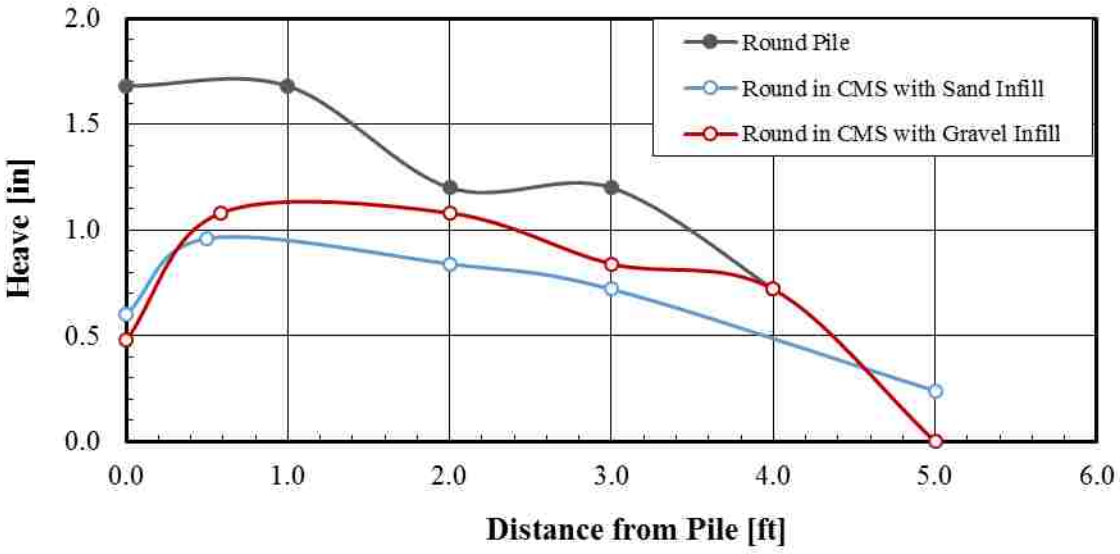

Figure 5-29: Ground Heave versus Distance in Front of Round Piles with CMS

Along with the survey measurements, a set of DIC cameras was placed around each test to record how the lateral pile loading displaced the soil around it. The DIC data provided a valuable perspective as it recorded thousands of data points at each step of loading. An initial comparison was made between the DIC data and the survey measurements to verify agreement in results. The heave versus distance plots from both methods is shown in Figure 5-30, Figure 5-31 and Figure 5-32 for the square pile, H pile and CMS pile, respectively. In these plots the heave in inches is recorded as a function of distance from the pile face in feet. The survey measurement curves, similar to those shown previously, represent the elevation difference before and after testing. The DIC reading curves represent the vertical displacement at the final load along the same line as the survey measurements. All three of the plots show reasonably comparable values for the two methods based on displacement at the pile face, displacement at the furthest distance and intermediate slope. The agreement between the two methods verifies the accuracy of the DIC analysis in estimating heave in front of the pile face.

For the square and H shaped piles, the heave versus distance plots show a nearly linear, decreasing slope to around four feet from the pile. Beyond a distance of four feet the slope appears to level off, indicating little or no effect from the loaded pile. Maximum heave occurs at the pile face for the square and H piles. In contrast, the CMS heave plot shows an increase in heave moving from the pile face to the CMS as discussed previously. Unfortunately, there was a shadow in the DIC data at the final load step where the camera could not pick up any readings for the first 8 inches from the pile face including 2 inches beyond the CMS so this behavior cannot be independently confirmed. However, DIC readings at smaller load levels indicate agreement with the survey measurement, in which the loose infill material does not heave as much as the compacted soil outside the CMS. After the first 8 inches, the two curves in Figure

5-32 fit nicely. From these results it appears likely that the loose material densifies during lateral loading before it shows signs of heave. Beyond the CMS it appears that the compacted backfill behaves similarly to that of the square and H piles with heave decreasing with distance.

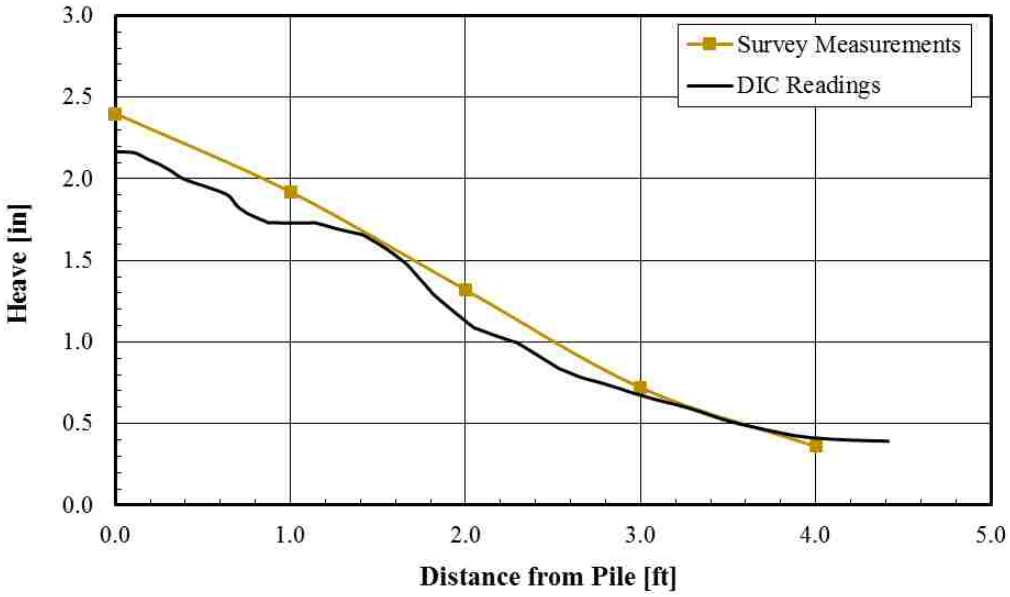

Figure 5-30: Heave Measurements for a Square Pile

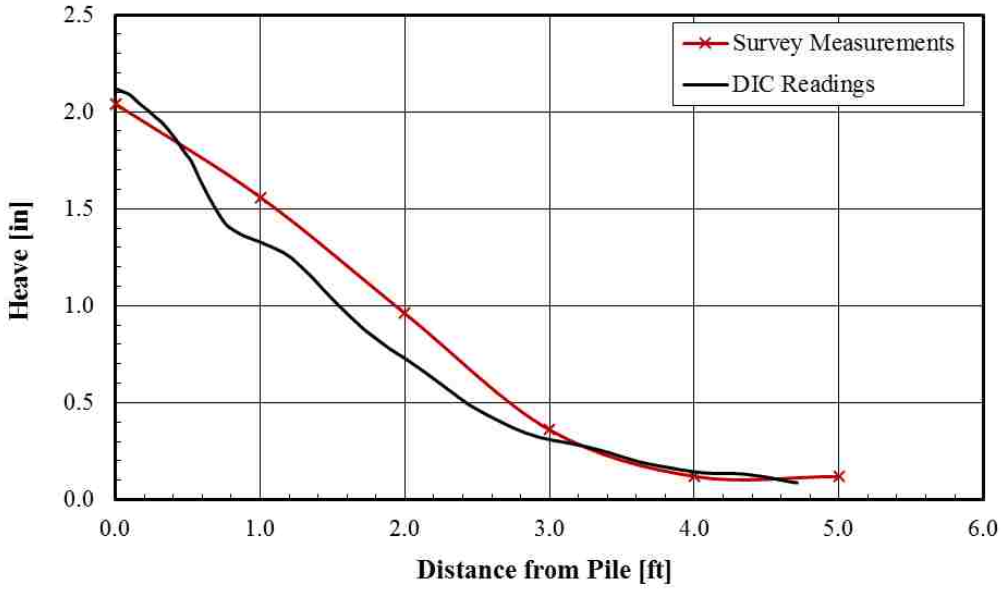

Figure 5-31: Heave Measurements for an H Pile

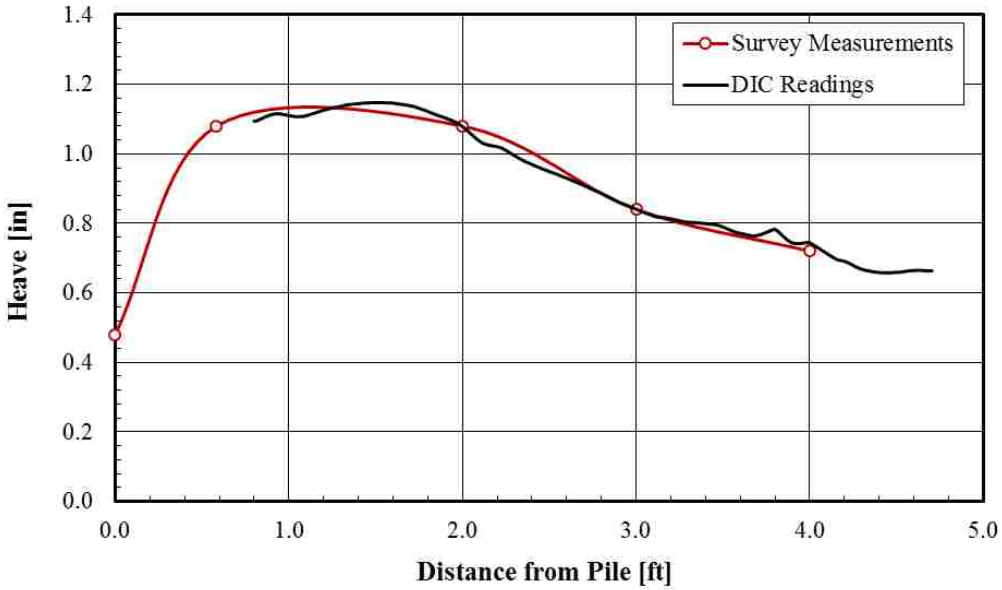

Figure 5-32: Heave Measurements for a Round pile in a CMS

Combining the heave data from the DIC and survey measurements into one will allow further comparisons concerning pile type and heave effect. A fair comparison between pile types must consider the diameter or width of the effective pile as well as the overall heave. Figure 5-33 presents this comparison as normalized heave (heave at any distance divided by heave at the pile face) plotted against normalized distance (distance from the pile face divided by pile width or diameter). In this plot, survey measurements for the round and H pile data are matched with the DIC readings of the CMS and square piles which a provide more detailed heave profile for these shapes. The H pile was oriented about its weak axis therefore flange ends where considered as the effective pile face. In the case of the CMS data, starting at the face of the CMS the distance was divided by the diameter of 24", this explains the shortness of the curve compared to the other piles. From the round, square and H pile heave data, it appears that at a distance of four diameters from the pile face the effect of the pile on the soil isn't as strong. A heave of 25% can

be expected at this distance. It could be assumed that four pile diameters is the size of the zone of influence of the square and H piles on the surrounding soil. Unfortunately, not enough measurements were taken away from the CMS to indicate an edge of the zone of influence but it would be appropriate to postulate a similar trend.

Measurements from a heave analysis of a round pile in over-consolidated clay can also be used as a comparison. The round pile of 641 mm (25 inches) was tested by Reese et al (1968). A load of 596 kN (134 kips) was applied with deflection measurements taken 13 ft away from the pile. The data in this experiment has been normalized and provided in Figure 5-33. The heave matches that of the square and CMS piles closely despite the difference in soil material. These results also show that at four pile diameters the heave is near 25% of the heave at the pile face.

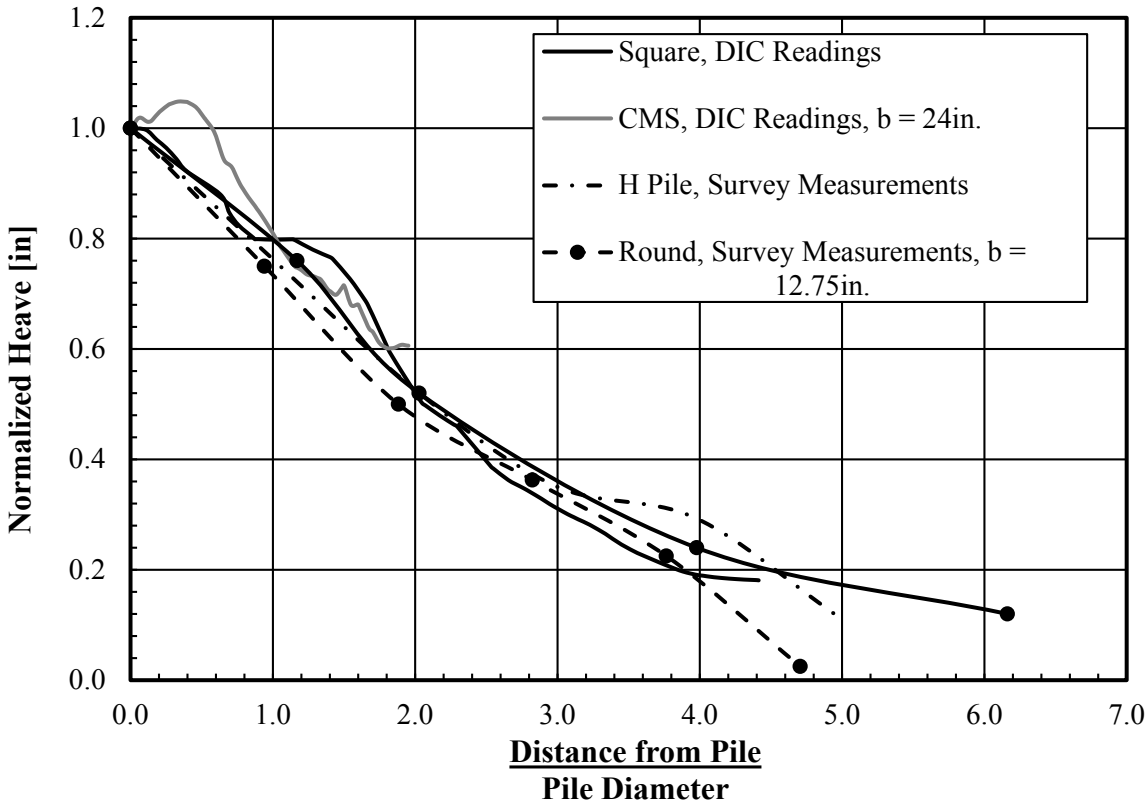

Figure 5-33: The Effect of Pile Shape and Sleeve on Ground Heave

Apart from heave measurements, quantitative observations can be made from DIC contour plots created through the data analysis package, Istra-4D Q-400 (2014). Figure 5-34 was created by assigning colors to various levels of displacement. The contour gradient ranges from cool to hot colors as initial displacements increase in magnitude. This image presents a representation of soil heave that could not be visually observed during testing. The color contours present the progression of the heave within the failure "wedge" or "bulb" surrounding the loaded pile. An analysis, similar to the heave plots shown previously, but in multiple directions from the pile allow further definition of the size of the stress bulb. Similar images have been produced for the square and H piles shown in Figure 5-35 and Figure 5-36. DIC images were not available for the round pile.

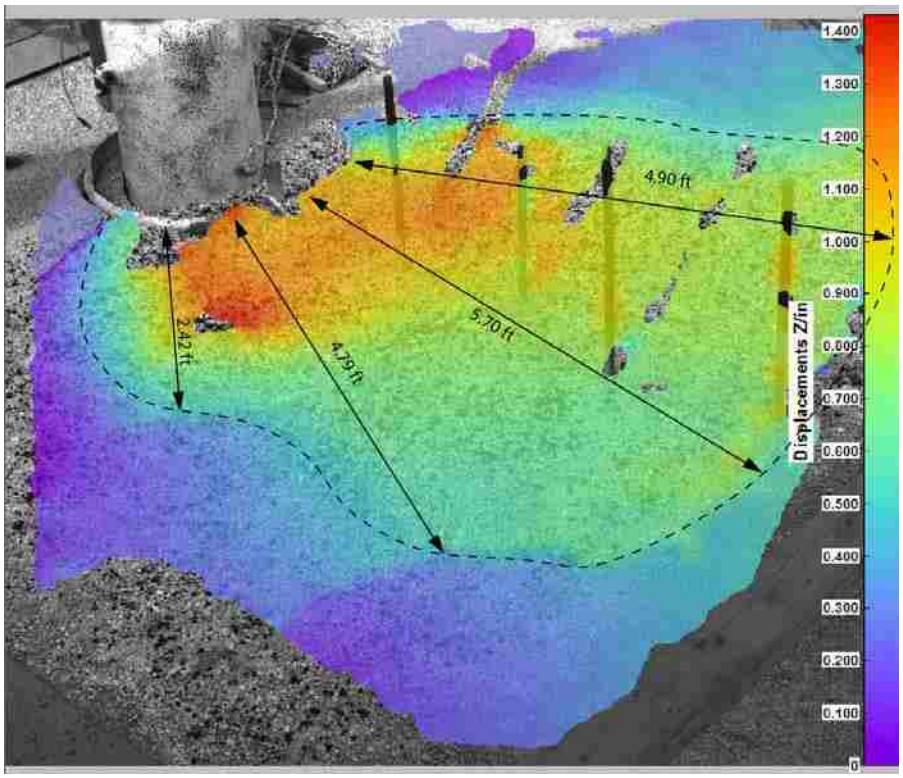

Figure 5-34: Vertical Displacement Contour Plot for a Round Pile in a CMS

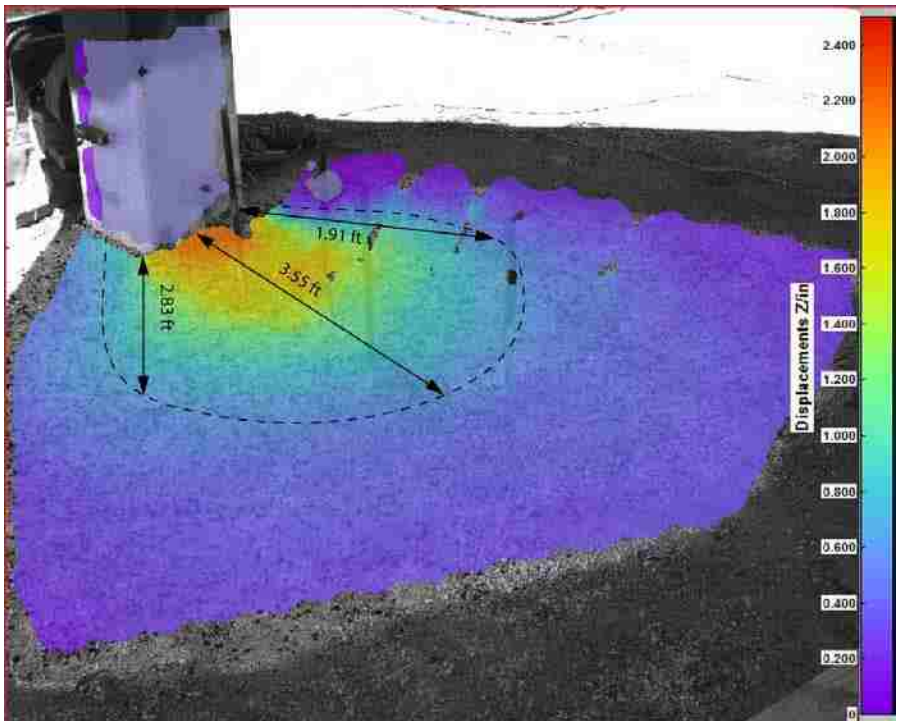

Figure 5-35: Vertical Displacement Contour Plot for a Square Pile

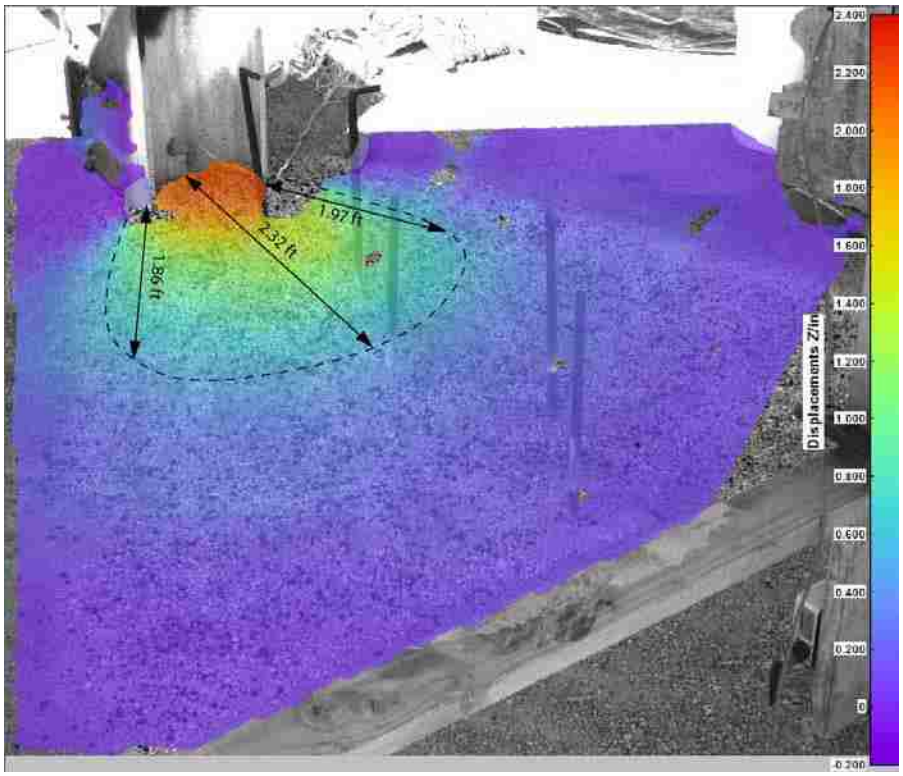

Figure 5-36: Vertical Displacement Contour Plot for an H Pile

Idealized stress bulbs have been shown on these images representing the boundary of 0.5 inches of vertical deflection. It is easy to see that the CMS has a larger radius of influence due to the larger diameter of the pile. The stress bulb of the CMS reaches 5.7 ft from the face of the sleeve while the square and H pile reach 3.55 ft and 2.32 ft out respectively. The magnitude of heave is shown on the right side of these figures as the hotter colors represent greater heave and cooler colors represent lower levels of heave. Going further from the pile the heave values eventually reach zero indicated by a purple color. Three-dimensional relationships such as these can be more helpful in creating a realistic model than relationships presented by the failure wedge method (Reese and Van Impe, 2001).

6 LATERAL LOAD ANALYSIS

The purpose of this lateral load analysis is to create a design approach or a model that accurately describes the lateral load contribution of square or H shaped piles as well as CMS piles. The accuracy of the approach can easily be evaluated by comparing the computed load-deflection curves with those measured during the lateral load tests. Close agreement between the two curves will indicate that the model produces the same resistance as observed in the load test. Another means for verifying the accuracy of the model will be a direct comparison between the moment diagrams produced by the design model and the diagrams measured in load tests.

The widely used computer program LPile (version 2015.8.03), created by Ensoft, Inc., was heavily used in this analysis. As indicated previously, LPile computes deflections and moments for individual piles under lateral loads. The versatility of the program in terms of pile behavior, soil behavior, and output options qualify LPile as an appropriate program for this analysis.

This section starts by defining the LPile program input parameters including, pile properties, soil properties, and load sets. Initially, soil properties were adjusted to match the measured load-deflection curves for the round piles. These same soil properties were then used to analyze the companion square and H shaped piles to confirm that lateral resistance was underestimated by neglecting shape effects. To better account for the apparent shape effects, three different approaches were evaluated, namely: (1) the Equivalent diameter method proposed by Reese and Van Impe, (2001) (2) the F-y/Q-y Mechanism proposed by Briaud and Smith,

(1987), and (3) a simple P-multiplier approach proposed by Rollins and Bustamante (2015). The results from the LPile model for each approach are compared with the load test results to determine the effectiveness of the model in accurately describing the pile response to lateral loading. Lastly, the moment diagrams of the model with a p-multiplier are compared to the moment diagrams of the load tests to verify that the model properly explains the pile's response to a lateral load along the depth of the piles.

6.1 Pile Material Properties

A thorough description of the pile properties has been provided to explain the input properties used in the LPile model. Following this description a similarly accurate model may be reproduced if desired. The piles used for the load tests were selected according to the shape and comparable width or diameter as shown in Figure 6-1. Each pile came from the same grade of steel having a modulus of elasticity (E) of 29,000 ksi with a yield stress (F_y) of 57 ksi for the round pile, 50 ksi for the H pile, and 56 ksi for the square pile. A diameter or width close to 12 inches was chosen for consistency with proportions standard to structural grade steel. Table 6-1 details these pile properties. The moments of inertia of the round and square HSS piles are similar while the H pile is considerably lower, oriented about its weak axis. Angle irons were added previous to pile driving to protect the strain gauges placed on the exterior of the piles from damage. The added stiffness of the angle irons was taken into consideration for an increased moment of inertia as shown in Table 6-1 in parentheses. The angle irons, attached near the neutral axis, had little effect on the H pile.

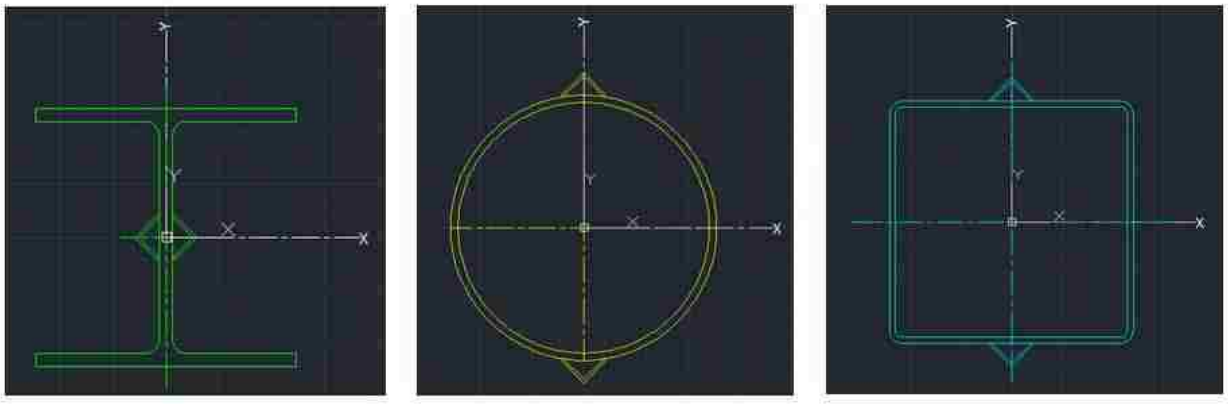

Figure 6-1: H, Round, and Square Pile Shape

Table 6-1: Pile Properties

Type	Diameter/ Depth (in)		Wall Thickness (in)		Moment of Inertia (with angle iron) (in^4)	E (ksi)	F_y (ksi)
Round 12.75X3/8	12.75		0.349		279 (314)	29,000	57
CMP	24		0.064		0.454	29,000	57
HSS 12x12X1/4	12		0.233		248 (335)	29,000	57
HP 12X74	12.1	12.2	0.605	0.61	186 (186)	29,000	57
	Flange Depth	Flange Width	Web Thickness	Flange Thickness			

Each pile was tested to a maximum pile head deflection of 3 inches or until signs of initial yielding were apparent. This ensured that each pile behaved as a linear elastic material allowing the model to neglect post yielding effects. Each pile measured 40 ft long with 2 ft of the pile left above ground after driving and Phase 2 backfill. The load point was one foot above the ground surface or at a distance of 39 ft above the toe. For purposes of analysis the pile was considered to be hollow. A plug did form during pile driving in the bottom 10 feet but this is below the depth of influence for lateral loading. It is unlikely that the plug contributed to the lateral resistance of the pile therefore there was no need to consider a composite elastic modulus or alter the moment of inertia of the pile. A pile properties window for LPile 2015 is presented in Figure 6-2 showing typical input for the analysis of the round pile.

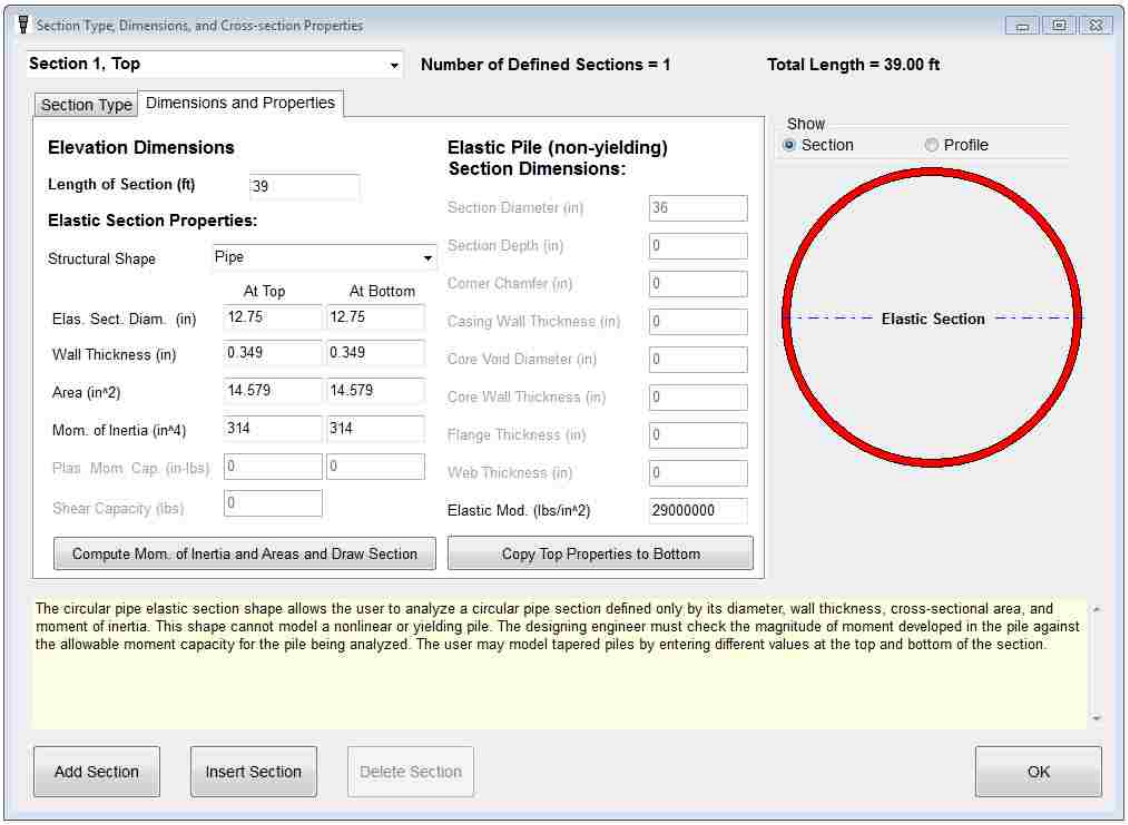

Figure 6-2: LPile Input Property Window for a Round Pile

6.2 Pile Load Model

For practical purposes the piles were modeled as 39 ft long piles with loading applied at the head of the pile. The load condition can be defined as a shear force at the pile head in the positive direction. Loading for the full scale tests was deflection controlled in increments of 0.25 inches. Increasing load was applied until the pile reached the next increment of deflection. As a result, different load sets were used for each analysis as the load that caused an inch of deflection for a square pile was different than the load for a circular pile. Axial forces and moment about the pile head were set equal to zero to match the testing conditions.

6.3 Soil Properties Model

The soil properties required for an LPile analysis are the effective unit weight, γ; the friction angle, ϕ; and the lateral soil stiffness or subgrade modulus, k. Soil properties were entered into the model to represent the soil conditions at the test site including all phases of soil compaction. As mentioned in Section 3.3, the soil model can be described in three layers from the pile toe to the head; 18 feet of native soil, 15 feet of phase 1 soil compaction, and 5 feet of compacted material from phase 2 or phase 3. The native soil and the backfill material, being cohesionless sand, were modeled using the API Sand (O'Neill) p-y curve model. The effective unit weights for each layer can be found in Table 3-3, these values were based on average nuclear density gauge measurements. Measurements for the ϕ and k were not made during testing and were derived by back-calculation as described below.

API suggests that values for ϕ and k can be determined using charts shown in Figure 2-6 (Isenhower & Wang, 2015) that consider the relative density of the soil. Generally, for each iteration, a ϕ was chosen with a corresponding k value, calculated using the equation,

$$\boldsymbol{k = 0.4168\phi^2 - 8.1254\phi - 83.664} \qquad \textbf{(6-1)}$$

which represents the curve presented in Figure 2-6 as defined by API for sand above the water table.

Initially, LPile analyses were performed using a friction angle of 38° which is approximately equal to the value used in the design of a nearby MSE wall using the same backfill material (Besendorfer, 2015; Budd, 2016; Luna, 2016). However, the friction angle produced a force-deflection curve which was considerably lower than the measured curves for either phase 2 or phase 3 of compaction as shown in Figure 6-3. Additional analyses were subsequently performed with progressively higher friction angles until the load-deflection curve

for the model matched that of the round load tests. As shown in Figure 6-3, using a friction angle of 45° in LPile produced a load-deflection curve that matches the measured curve for the round test most closely for soil compaction in phase 2. A corresponding k value of 394 pci was determined using Equation (6-1). Likewise, using a friction angle of 51° produced a load-deflection curve most closely matching the (2) round pile with HDPE in phase 3. While this ϕ value is relatively high, a number of researchers have back-calculated similar values for well compacted sand for lateral load tests (Brown et al., 1988; Rollins et al., 2005; Rollins et al., 2011). At this point it is unclear whether the discrepancy lies in the correlation between relative density and friction angle employed by API or the passive force model used by API which is based on Rankine theory rather than the log-spiral theory. Both of these factors would lead to conservative estimates of lateral pile resistance. The k vs ϕ correlations in Figure 2-6 do not extend to a ϕ of 51° and experience indicates that k values for this friction angle range can differ from values given by Equation (6-1) (Brown et al., 1988; Rollins et al., 2005; Rollins et al., 2011). A k value of 394 pci was found to produce the best agreement with the agreement with the load test results. A summary of the soil properties considered in iterations of the LPile model for a round pile is shown in Table 6-2.

Soil properties for phase 1 were also back-calculated from lateral load tests performed at the 15 ft compacted backfill level. That analysis was performed by Bustamante (2014) who found a friction angle of 45° and a k value of 250 pci to produce the best agreement with the test data. The friction angle is exactly the same as the results obtained for this study for the phase 2 compaction at the 20 ft level.

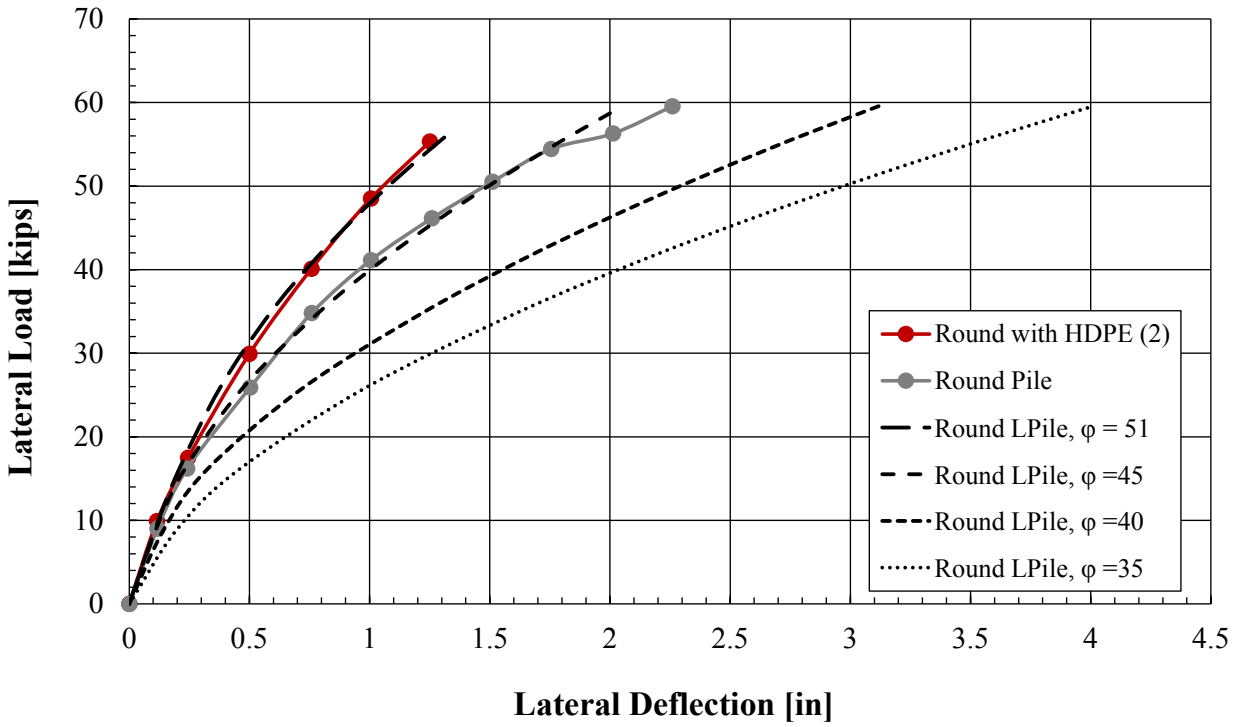

Figure 6-3: Measured Load-Deflection Curve Along with Curves Computed with LPile Using a Range of Friction Angles

Table 6-2: Final Soil Properties Used for LPile Analysis

Soil Layer	Effective Unit Weight [pcf]	Friction Angle [degrees]	k [pci]
Native Soil	125	34	100
Phase 1	129	45	250
Phase 2	131	45	394
Phase 3	131	45	394

Apart from comparing the load verse deflection of the pile face, a comparison for the round pile was made of the LPile p-y curve output with the API method for creating a p-y curve for a

pile in sand. The API method, explained in Section 2.2, considers effective unit weight, friction angle, pile width, modulus of subgrade reaction, loading condition, and depth. Coefficients for passive, active, and at rest soil pressures are intermediate factors used to quantify the lateral bearing capacity for sand at shallow or deep levels. The lesser of the two lateral bearing capacities is chosen as the ultimate soil resistance which is then multiplied by a loading factor, subgrade modulus, depth, and deflection. A sample calculation of this process shown in five steps is given in Appendix A. The method presented by API gave a soil resistance of p = 453 lb/in with a deflection of 1.33 inches at a depth of 16 inches. This is very similar to the values given by the LPile model, p = 457 lb/in at similar deflection and depth. This agreement in results gives verification that the LPile soil model has been entered and calculated correctly.

6.4 Results of the LPile Analysis for Other Pile Shapes

Using the pile material properties, applied loads, and soil properties back-calculated for the round piles, analyses were performed in LPile to calculate pile head load-deflection curves for each pile shape. If pile shape is unimportant, then the computed load-deflection curves should be in good agreement with the measured curves after adjusting for differences in pile width and moment of inertia. Likewise, if H and square piles actually have higher soil resistance than for round piles as anticipated, then the computed load-deflection curves should be softer than measured in the field.

6.4.1 LPile Model for H Piles

Figure 6-4 shows the load-deflection curve computed by LPile along with the average load-deflection curve for the H pile in the soil compacted during phase 2. The computed curve matches the measured curve for the first 0.75 inches of deflection but underestimates the

measured resistance of the H pile at greater deflections. A maximum difference of 5 kips develops at 2.75 inches of deflection, that amounts to a 9% difference from the measured resistance. These results suggest that the lateral resistance may be somewhat underestimated for the H pile if shape effects are ignored. This model could potentially be improved by considering shape effects on the soil resistance.

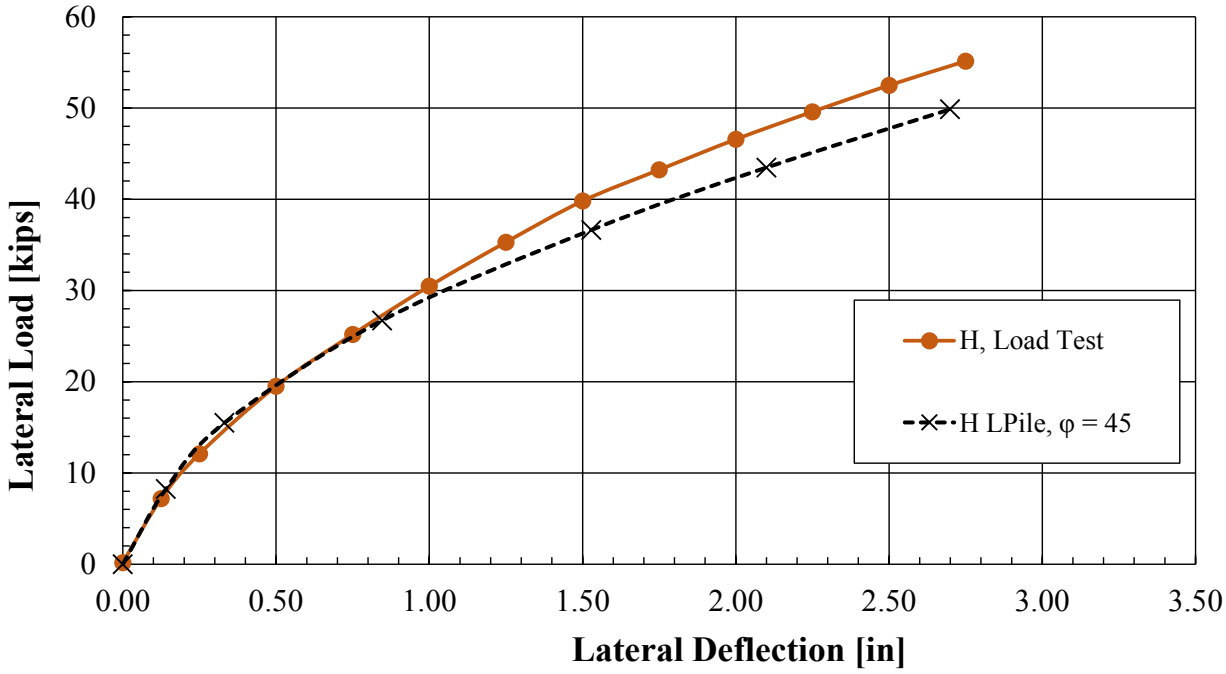

Figure 6-4: H Shaped LPile Analysis Compared to H Pile Load Test Results

6.4.2 LPile Model for Square Piles

The load vs deflection curve computed by LPile for a square pile is compared with the measured curves for the two square pile load tests in Figure 6-5. In this plot the computed curve is consistently lower than the two measured curves. The increasing gap between computed and

measured curves reaches a difference of nearly 9 kips at 1.75 inches of deflection. This difference amounts to a 12% increase in lateral resistance relative to the computed value.

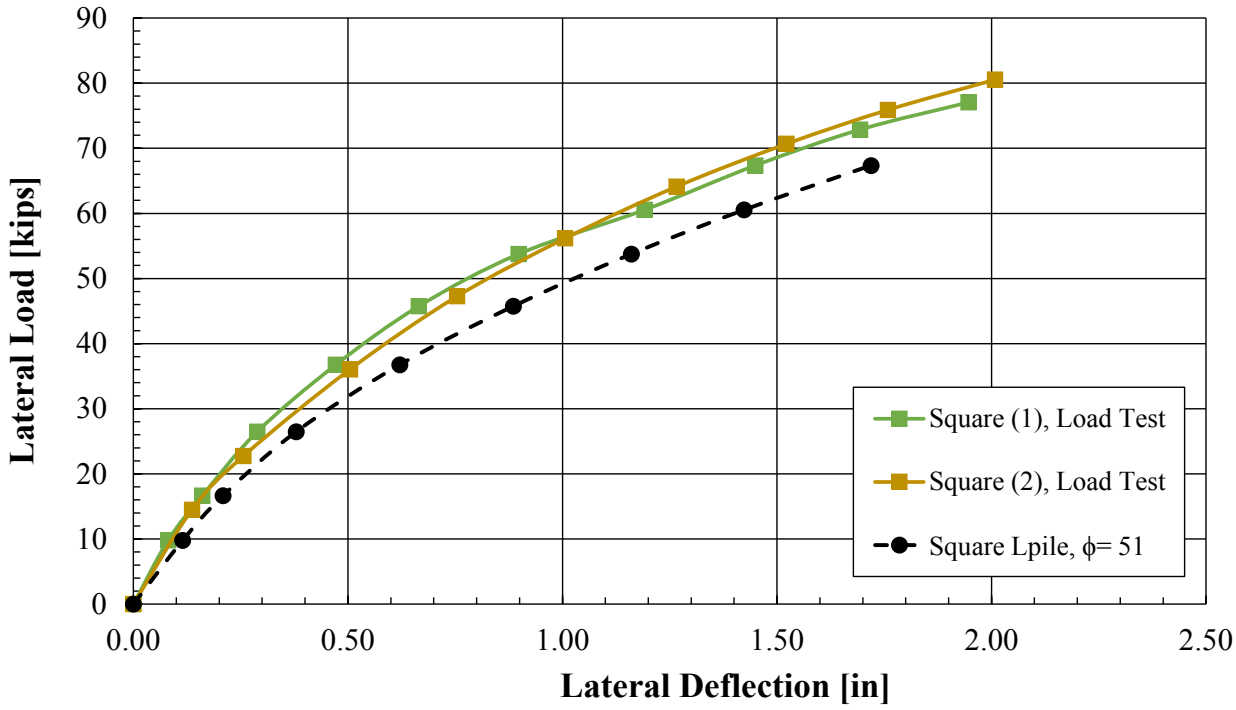

Figure 6-5: Square LPile Analysis Compared to Square Load Test Results

The fact that the computed resistance is consistently lower than the measured curves suggests that the square pile shape is producing greater than expected lateral resistance. Pile shape is not considered in the API method for estimating lateral resistance. To more accurately estimate the lateral resistance of square shaped piles there should be a method to quantify the effect that pile shape has on soil pile interaction. Approaches to better account for this shape effect will be explored subsequently.

6.5 Investigation of Approaches to Account for Pile Shape on Lateral Pile Resistance

After exploring laterally loaded pile models without shape effects an investigation of pile shape effect leads to three separate approaches: (1) the Equivalent diameter method proposed by Reese and Van Impe, (2001) (2) the F-y/Q-y Mechanism proposed by Briaud and Smith, (1987), and (3) a simple P-multiplier approach proposed by Rollins and Bustamante (2014). Each method will be used to produce load-deflection curves for each pile shape. These plots will individually be compared to the load tests then collectively to determine which method best describes the response of the pile to lateral load.

6.5.1 Reese and Van Impe Equivalent Diameter

As described in Section 2.3, Reese and Van Impe (2001) propose the use of an equivalent diameter to account for the increased lateral resistance on the sides of non-circular pile shapes. The equivalent diameter method uses the width and depth dimensions of the non-circular pile to produce an equivalent round shaped pile. For example, square or H shaped piles with dimensions matching that of an equivalent round pile will result in an increased equivalent diameter, b_{eq}, which will lead to an increase in lateral resistance. This method considers soil properties as well as the pile dimensions of width and depth.

Calculations involved in finding the equivalent diameter of the piles in this study are provided in Appendix D whereas a description of the procedure implemented in this analysis is provided in this section.

The equivalent diameter method is similar to the API method for finding ultimate resistance of a circular section. Like the API method, soil property coefficients C_1, C_2, and C_3 can be found by using Equation (2-9), Equation (2-10) and Equation (2-11). These coefficients

along with the effective vertical soil stress at depth x, pile width b, and depth can be used to find the ultimate resistance at shallow depths, p_{us}, Equation (2-2), or deep depths, p_{ud}, Equation (2-3). The minimum of these two values is considered the ultimate soil resistance. Unlike the API method, the equivalent diameter method labels this ultimate resistance as p_{uc}. This value is then used in the equivalent diameter Equation (2-21) along with the pile width and shearing resistance, f_z. Calculating the f_z along the sides of the pile requires the vertical effective soil stress at the specified depth, the interface friction angle which has been taken as two-thirds of the friction angle of the soil, and the lateral earth pressure coefficient, K, as outlined in Equation (2-12). A lateral earth pressure coefficient was assumed to be 1.0 in this analysis which is consistent with API recommendations for axial loading. Once the p_{uc} and f_z have been determined the equivalent diameter can be found with Equation (2-21). With the vertical effective stress varying with depth, a unique equivalent diameter can be calculated at each depth. It is suggested that the average equivalent diameter along a determined depth be used in the final analysis (Reese & Van Impe, 2001). A depth of 5 feet was considered for the bounds of the average equivalent pile diameter, see Table 6-3. Averaging the equivalent pile diameter over a greater length would result in a smaller value since the equivalent diameter is a ratio of the added contribution of side shear to the ultimate resistance, which increases greatly with depth. The square shape pile gives an average equivalent diameter of 12.3 which is a 2.5% increase in pile width while the H pile has an average equivalent diameter of 12.5 which is a 3.3% increase. Although these numbers indicate that the square and H shapes should provide extra resistance relative to an equivalently shaped round pile, the difference is quite small.

Table 6-3: Average Equivalent Diameter for Square and H Piles

	Actual Width	b_{eq}	Percent Increase
Square	12	12.3	2.49%
H	12.2	12.5	2.48%

The effectiveness of the equivalent diameter method in accurately predicting the lateral resistance can best be seen through a comparison of the measured and computed load-deflection curves as was done previously in Section 6.4. In that section the comparisons showed a deficit in the computed lateral resistance relative to the measured resistance from the lateral load tests. Higher equivalent diameter values should minimize the deficit and improve accuracy in estimating lateral resistance. The equivalent diameter replaces the width dimension and models the pile as a round shape while maintaining the moment of inertia and modulus of elasticity values (*E* and *I*) for the non-circular shape. Load-deflection curves obtained using this method are compared to the measured curves from load tests in Figure 6-6 and Figure 6-7 for the H and Square piles, respectively.

The approach suggested by Reese and Van Impe (2001) for calculating an equivalent diameter for non-circular piles still provides a lower estimate for lateral resistance relative to the measured curves, as shown in both Figure 6-6 and Figure 6-7. In fact, the load-deflection curves computed with the increased equivalent diameters are nearly identical to the curves computed previously for the original pile widths. For the equivalent diameter method to match the measured load-deflection curve for the H pile, a diameter closer to 15.5 inches would need to be used. Although the equivalent width approach proves to be slightly less conservative than using the original pile width it still fails to closely match the measured load test curves.

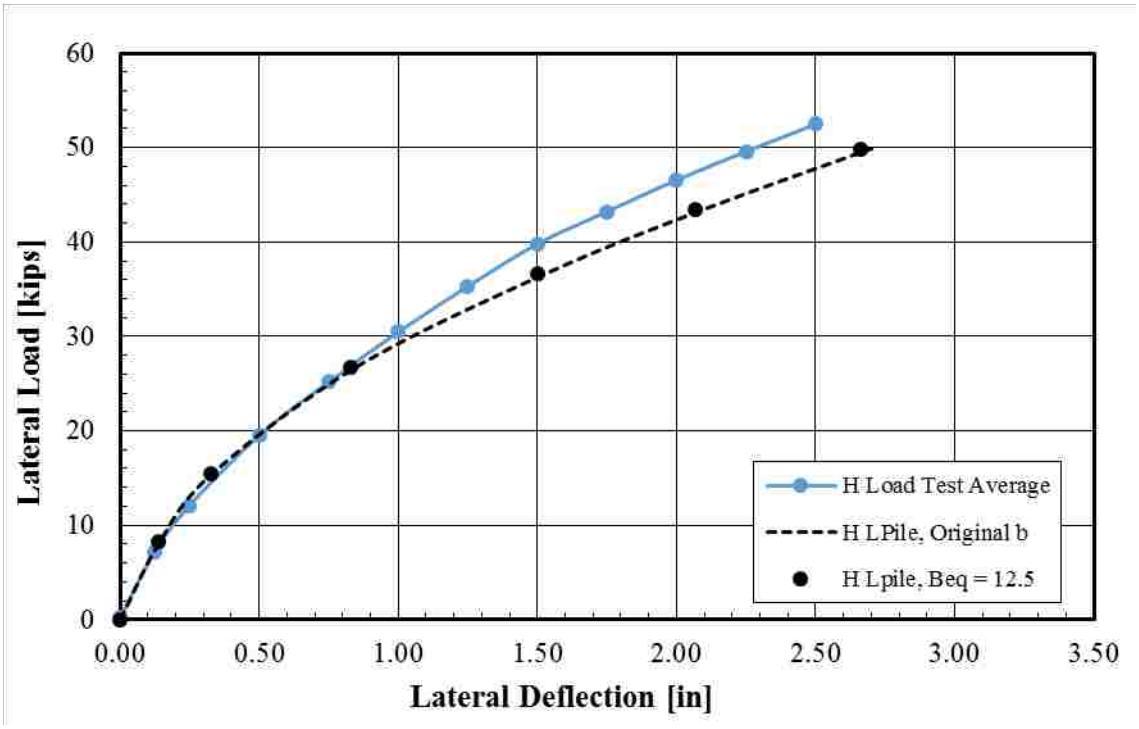

Figure 6-6: Load vs. Deflection Curve for Equivalent Diameter Approach for an H Pile

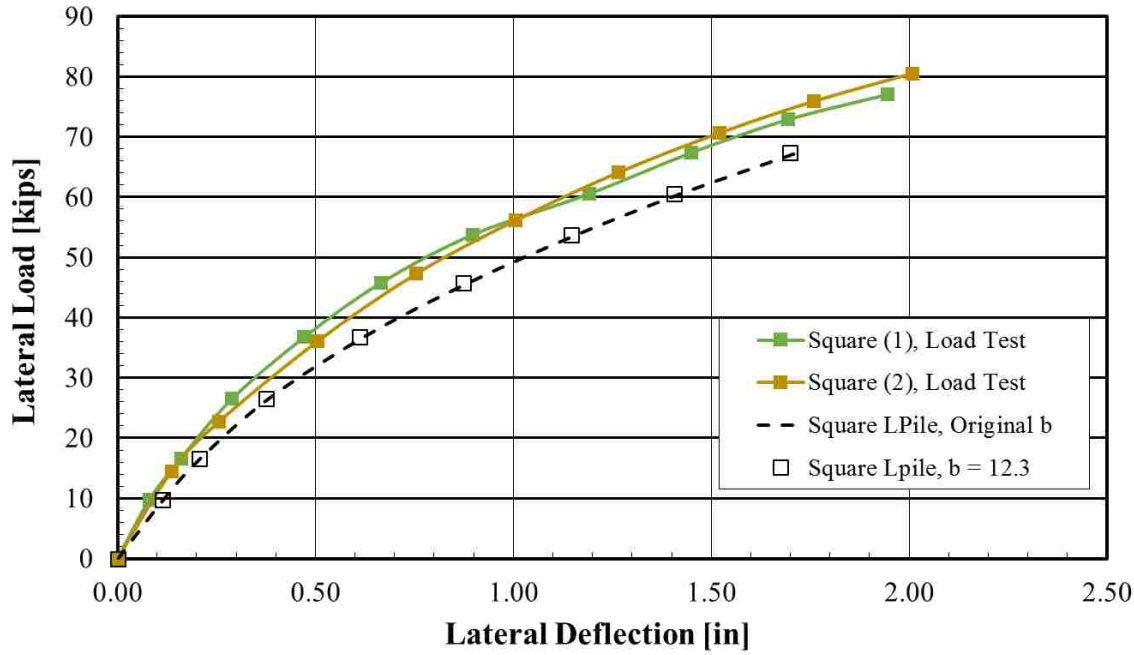

Figure 6-7: Load vs. Deflection Curve for Square Load Tests Compared with Equivalent Diameter Approach for a Square Pile

The greatest increase resulting from the increased equivalent width is shown in Figure 6-7. The square shape with a b_{eq} of 12.3 presents a slight increase from the LPile model with the actual square pile width; however, resistance is still about 8 kips lower than the measured resistance at the largest deflection. An equivalent diameter of about 17 inches would need to be used in the analysis to match the measured load-deflection curve from the load test. Bustamante's (2014) study of this approach in relation to the measured load test data also indicated short comings in the methods estimation of pile shape resistance.

6.5.2 Briaud and Smith F-y/Q-y Mechanism

As mentioned in Section 2.2, the pressuremeter test can be used to explain the lateral resistance of the soil on a pile foundation. Briaud et al. (1983) developed a system of analysis using pressuremeter data to produce Q-y and F-y curves at any depth. These two components were then combined to result in a p-y curve that explains the overall resistance of the pile. This process is demonstrated in Figure 2-2 as resistance values from Q-y and F-y curves are superimposed to produce the p-y curve. Although a pressuremeter was not used during these tests, a similar analysis implemented in reverse may be used to determine if this Q-y/F-y approach could explain the observed increase in soil-pile interaction for square and H shape piles.

Generating p-y curves at user specified depths is an output option of the LPile program. Using the round LPile model created in Section 6.4, p-y curves at specific depths were generated as the starting point of this analysis. At the selected depths of 1, 2, 4, 6, 9, 12, 15, 18, and 39 ft, p-y curves were created as a result of the lateral analysis are shown in Figure 6-8. The plot demonstrates how the soil resistance in units of kip/in of pile length increases as the pile deflects

laterally and engages the soil. Each curve initially shows a linear stiffness with eventual yielding in the soil with increased deflection. At a certain load the soil yields completely as deflection increases at a constant resistance. It should also be noted that greater depths yield p-y curves of increased resistance as a result of increased stiffness and shear strength resulting from higher confining pressures. According to Equation (2-1) the p-y curve is a combination of the Q-y curve and the F-y curve or the passive resistance and side shear resistance. Once the shear contribution has been defined the front facing passive resistance can also be obtained by subtracting the F-y curve from the Q-y curve.

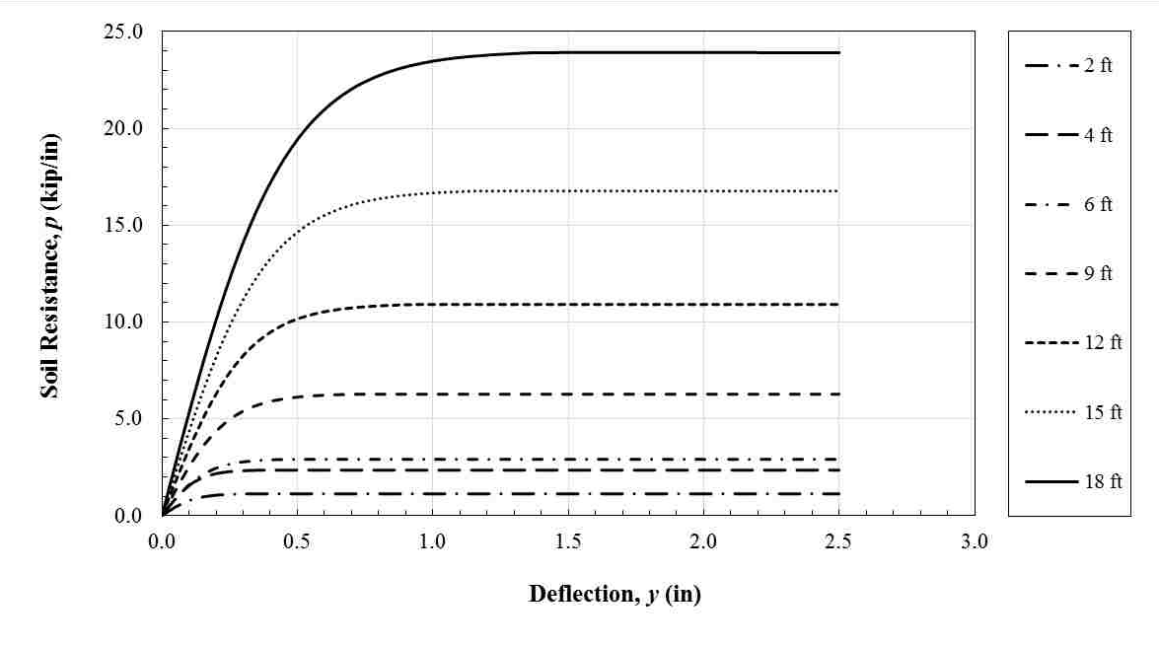

Figure 6-8: P-y Curves at a Specified Depth for a Round Pile

Using a method similar to that explained by Briaud et al. (1983), the side shear resistance F can be calculated at a specific depth using Equation (6-2).

$$F = k\,\gamma\,z\,\tan(\delta)\,D\,(SF) \qquad \textbf{(6-2)}$$

Where:

K = lateral pressure coefficient, or 1.00 for API sands

γ = unit weight of the soil

z = depth

δ = interface friction angle between soil and wall of the pile, $taken\ as\ \frac{2}{3}\phi$

D = diameter of the pile or width of the non-circular pile

SF = shape factor for square piles = 1.76
shape factor for round piles = 0.79

Using Equation (6-2), the maximum shear contribution can be calculated at any depth knowing the properties of the soil: lateral earth pressure coefficient, unit weight, and interface friction angle, along with the diameter of the pile. As the soil is engaged by the pile the shear force increases from zero to the maximum shear resistance. It was assumed that the shear force would require 0.1 inches of deflection to reach maximum resistance (Smith, 1987). With this in mind, shear components were calculated using shape factors in accordance with research by Smith (1987) on friction mobilization curves for laterally loaded square and round piles. A shape factor of 0.79 was used for the round pile while a shape factor of 1.76 was used for the square pile primarily because of greater contact along the side of the square pile. (Smith, 1987). Sample calculations of these F-y curves are provided in Appendix D. The computed F-y curves at a depth of 1 ft are plotted in Figure 6-9Figure 6-9: F-y Curves for Round and Square Piles at Depth of 1 ft, where the shear resistance around the square pile is more than twice that around the round pile.

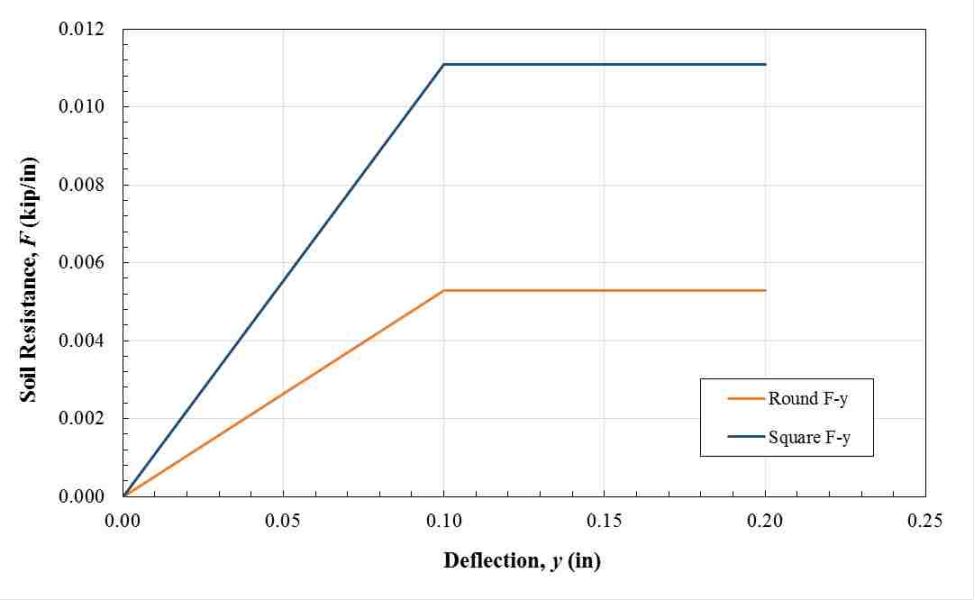

Figure 6-9: F-y Curves for Round and Square Piles at Depth of 1 ft

After calculating the shear contribution, the passive resistance of the round pile was found by subtracting this shear component from the overall resistance as a function of displacement. Smith (1987) suggested that passive resistance of the square pile can be found by applying a factor of 1.33 to the passive resistance for the round pile. This is a revision from the shape factor (SF) of 1.25 suggested earlier by Briaud et al. (1983). Applying this factor to the passive resistance of the round pile and using the shear contribution calculated earlier, a p-y curve was computed for each depth formed for a square pile. An example of the calculated F-y, Q-y and P-y curve for a round and square pile at 1 ft of depth is presented in Figure 6-10. Relative to the round pile, the square pile develops greater resistance for passive resistance and side shear which results in a greater p-y curve. According to Figure 6-10 it appears that the shear contribution is minor in comparison to the passive resistance developed by the front face of the pile. At 1 ft of depth the side shear of a square pile only contributes, at maximum, 2.5% of the overall

resistance. This percent contribution is smaller when looking at a round pile and decreases with depth for both pile types as the magnitude of passive resistance increases.

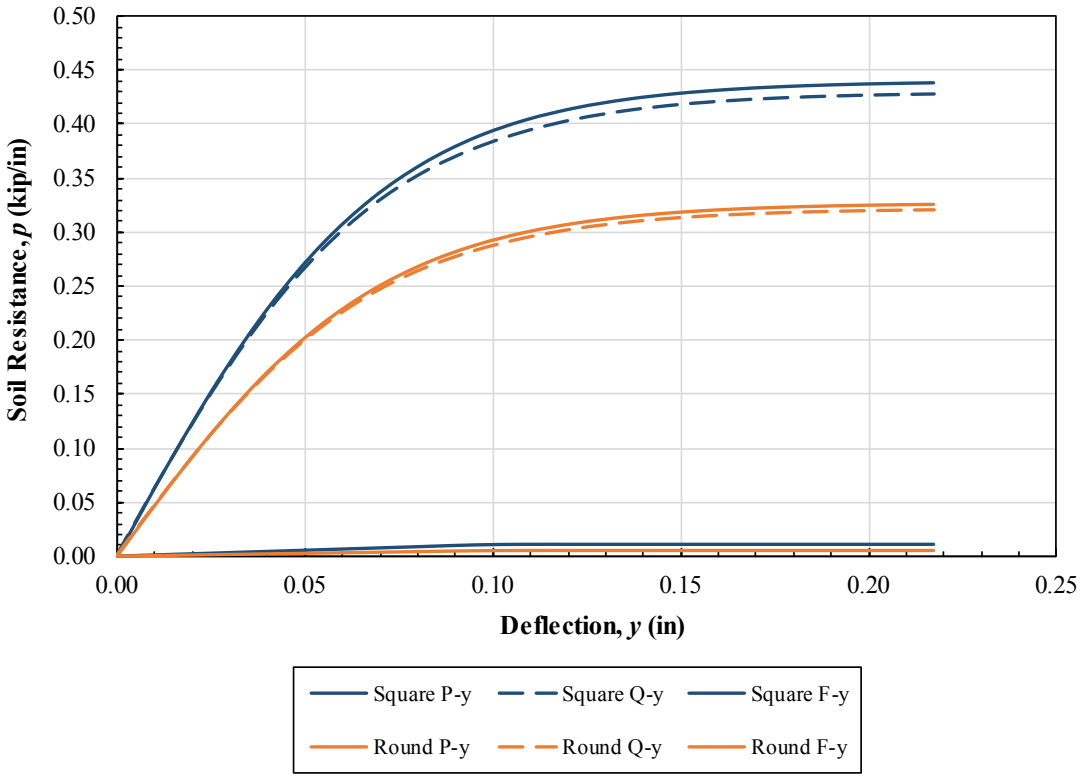

Figure 6-10: P-y Curves and Components for a Square and Round Pile at 1 ft Depth

Once p-y curves were calculated at a number of depths they could be used as manually input p-y curves in the LPile analysis. P-y curves were calculated at depths of 0, 1, 2, 4, 6, 9, 12, 15, 18, and 39 ft to provide a full description of the soil resistance as a function of depth. Using the pile properties of a square pile, namely pile width, I, and E, an analysis was run in LPile to compute a load versus deflection curve as shown in Figure 6-11 in comparison with to the measured curve. The same procedure was completed for an H pile as and the computed load-deflection curve is presented in Figure 6-12 along with the measured curves. These computed

curves can be compared to the load-deflection curves for the measured load test results to determine accuracy in predicting the pile resistance.

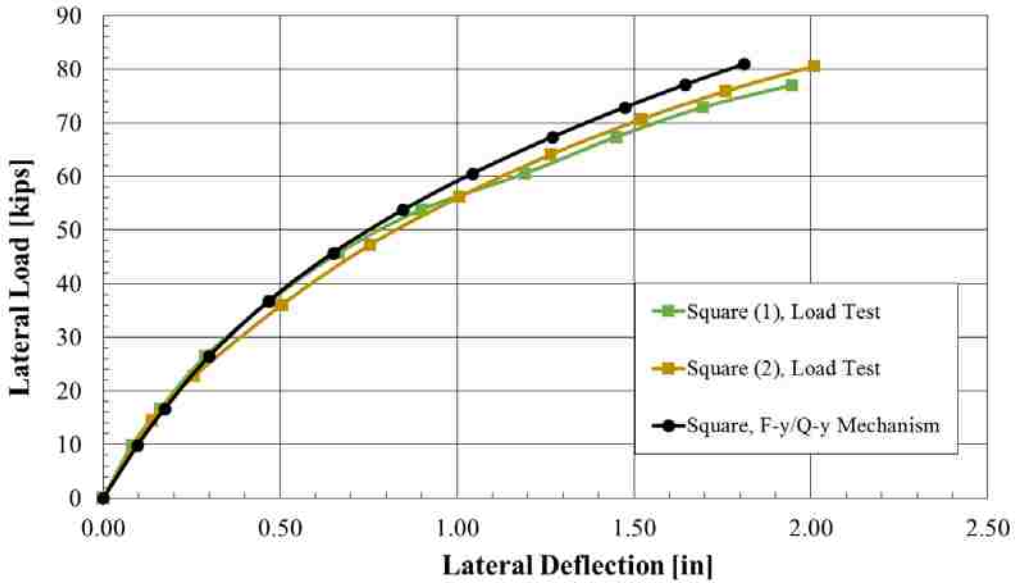

Figure 6-11: Comparison of Measured Load-Deflection Curve in Comparison with Curve Computed Using F-y/Q-y Mechanism for a Square Pile

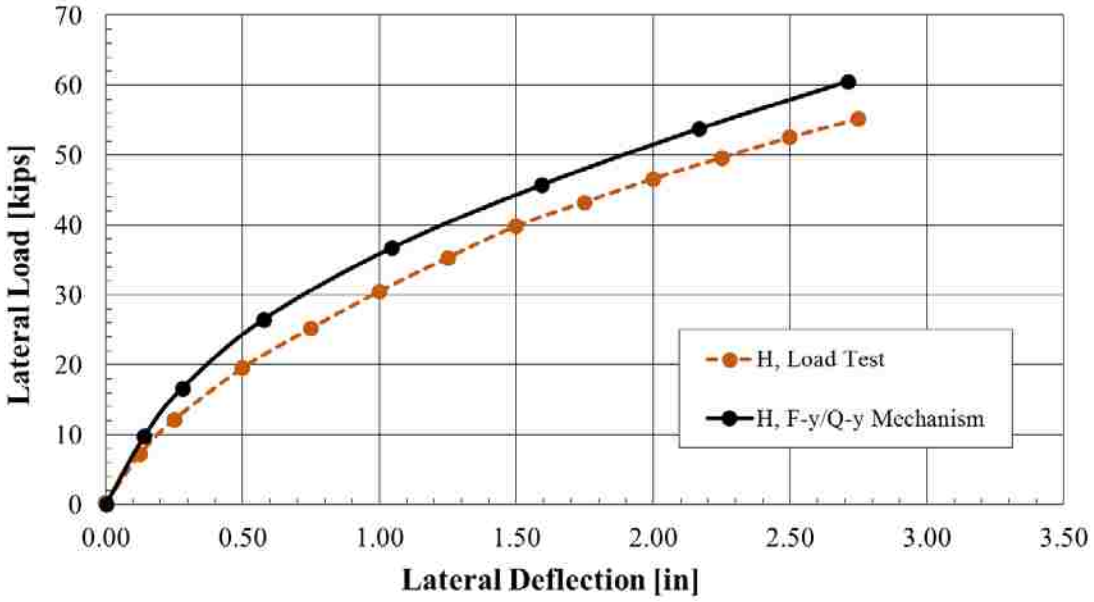

Figure 6-12: Comparison of Measured Load-Deflection Curve in Comparison with Curve Computed Using the F-y/Q-y Mechanism for an H Pile

Initially, the computed load-deflection curves are very close to the curve measured in the load test for the square pile but at larger deflections the computed curve shows slightly more resistance than measured. Nevertheless, the procedure does provide a reasonable estimate of the measured response overall even though the final load it assumes greater capacity for the soil-pile interaction. The Briaud and Smith (1987) approach computes a load-deflection curve for the H pile with a resistance nearly 5 kips greater than that for the actual load test. This method provides a much better approximation of the response of the square pile than the equivalent diameter method yet it over predicts the maximum resistance for the H pile. Perhaps, the shape factors suggested by this method are a little too high and overestimate the shape effect on the lateral resistance. Similar findings were obtained in Bustamante's (2014) study except there was greater agreement between the measured H pile load-deflection curve and the F-y/Q-y mechanism results rather than the square pile.

6.5.3 P-multiplier Approach

The p-multiplier approach is a simple and convenient method for adjusting the expected lateral soil resistance by a modification factor. Uses of the p-multiplier approach include providing a reduction to lateral resistance in liquefied sand or reducing the lateral soil resistance to account for pile group interaction from multiple rows of piles (Isenhower & Wang, 2015). Varying p-multipliers may be applied at any depth along the pile to account for stratified soil layers of fluctuating strength. In this instance, a constant p-multiplier can be used along the entire pile length to account for the pile shape of the entire pile. The LPile models created in Section 6.4 can be used as a base from which to apply the p-multipliers.

After applying p-multipliers to the square and H LPile soil models, load vs. deflection curves were computed and plotted against the measured load vs. deflection curves from the load tests. Through multiple iterations a computed load-deflection curve was developed that was very similar to the measured load-deflection curves for both the H and Square piles. The back-calculated p-multipliers for the H and square piles, summarized in Table 6-4, are constant for the entire pile length. As indicated in Table 6-4, applying a p-multiplier of 1.25 to the square model and 1.2 to the H model produced the load vs. deflection curves shown in Figure 6-13 and Figure 6-14, respectively.

Table 6-4: P-Multipliers for Square and H Piles

Square	H
1.25	1.2

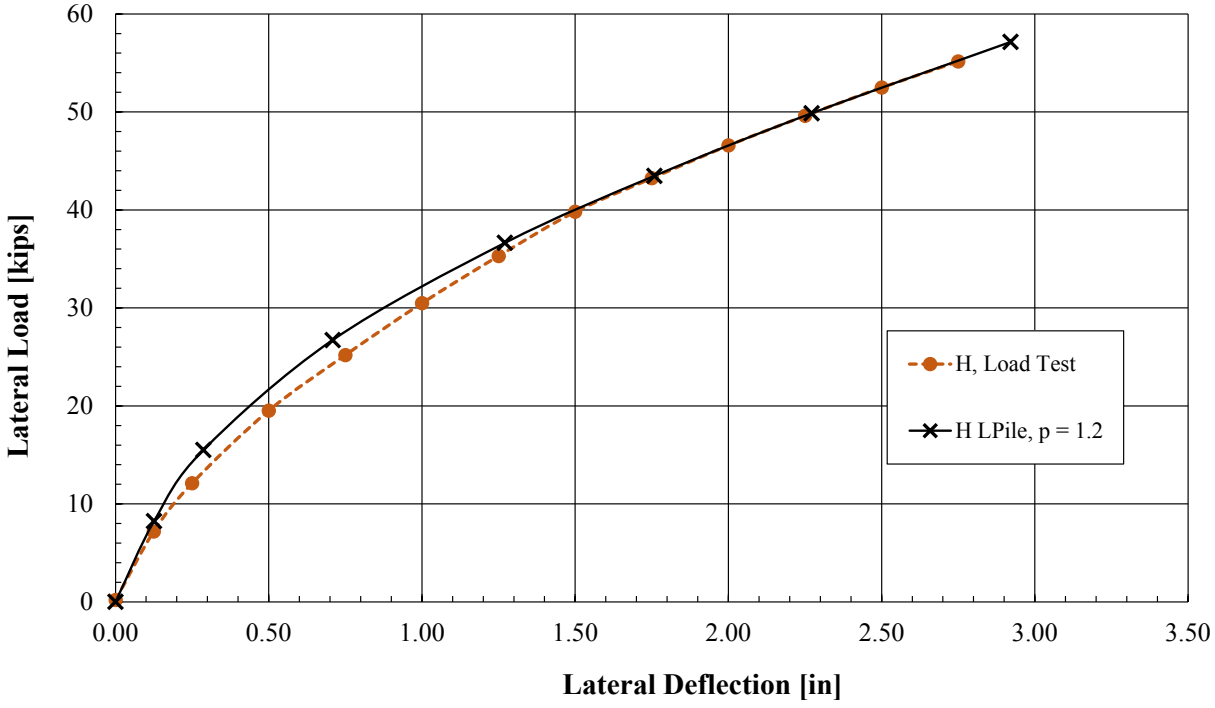

Figure 6-13: P-multiplier Approach for H Piles

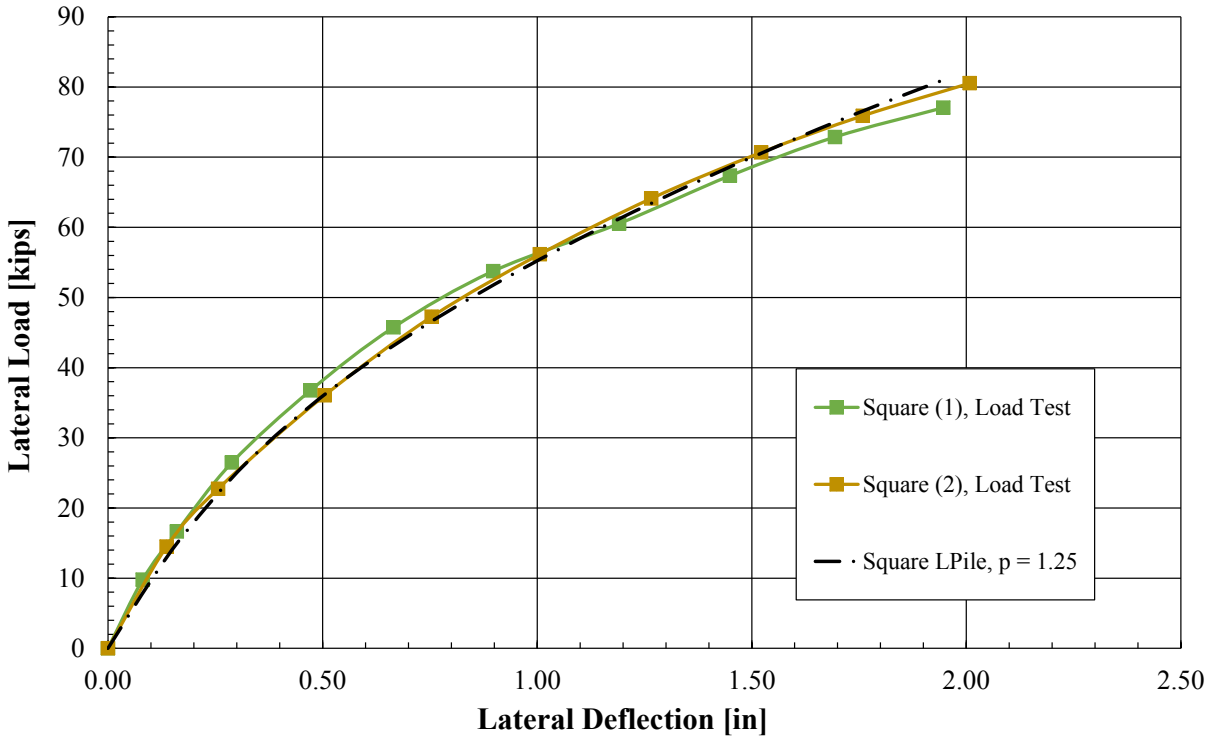

Figure 6-14 P-multiplier Approach for Square Piles.

The lateral resistance of the two square load tests is analogous to the estimated resistance of the LPile model with a modification factor of 1.25. The precision of the match from 0 inches of deflection to the ultimate resistance is significant. The match for the H Pile analysis is also close to the measured load test results. The period of the curve from 0.25 inches to 1.25 inches varies by no more than 0.1 inches for a given load. All other sections of the curves correlate remarkably well with each other.

The p-multipliers of this research can also be compared to those suggested by Bustamante (2014) based on tests conducted on round, square and H piles for the 15 ft thick fill. For the square pile Bustamante recorded a p-multiplier of 1.2 which is rather close to the 1.25 suggested

by this analysis. It is recommended that a p-multiplier between this range be used for further design of square piles using the LPile program. This modification would account for the extra passive and side shear forces that a square pile provides. This would be an advantage in using square piles in the design of deep foundations. The p-multiplier suggested by Bustamante for the H pile was 1.35, which is higher than the 1.2 recorded in this research. It appeared that the H pile test results in that research was somewhat higher than expected. Using a p-multiplier of 1.2 for H piles would account for the added side shear and front facing pressures of an H pile while still remaining within the conservative bounds of the test results.

As an overall comparison, the computed load-deflection curves for all of the analytical methods have been plotted in Figure 6-15 for the square pile and Figure 6-16 for the H pile. A review of the plots indicates that the p-multiplier method provides the closest agreement to the measured curves from the load tests. In both cases the LPile model which neglects pile shape effects predicts lower resistance than that measured in the load tests. This is expected on account of the moment of inertia providing the only distinguishing factor in accounting for the difference in the performance of each pile. The Reese and Van Impe (2001) equivalent diameter approach suggests using a higher effective width for square and H piles but this adjustment is so small that it does not markedly change the resistance in comparison with analyses that neglect shape effects. This result also suggests that the increased lateral resistance may develop owing to increased passive force on the pile face more than increased resistance on the side of the pile. The shape factors suggested by Briaud and Smith (1987) applied to the F-y/Q-y mechanism show promise in accounting for the increased lateral resistance owing to pile shape effects. However, in the case of the H pile this approach overestimated the resistance of the pile resulting in a non-conservative prediction. The close agreement between the square and H pile load tests

and the calculated LPile model with p-multipliers is visually observable. According to these results the p-multiplier approach provides the simplest and most reasonable approach to account for pile shape effects.

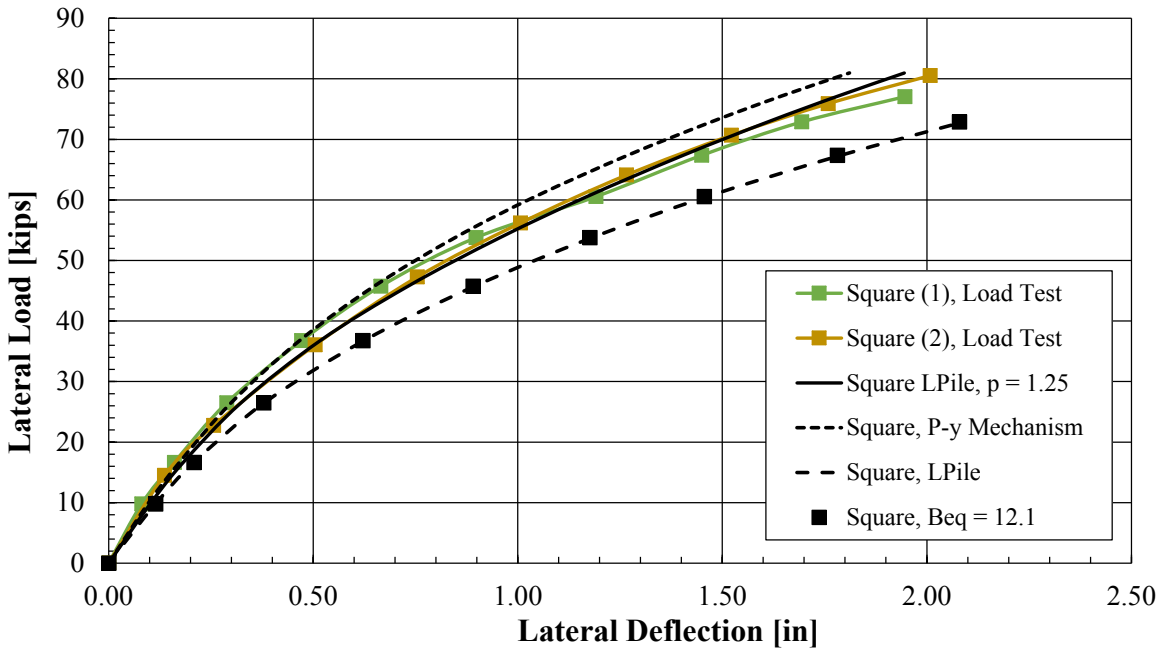

Figure 6-15: Comparison of Analytical Methods for a Square Pile

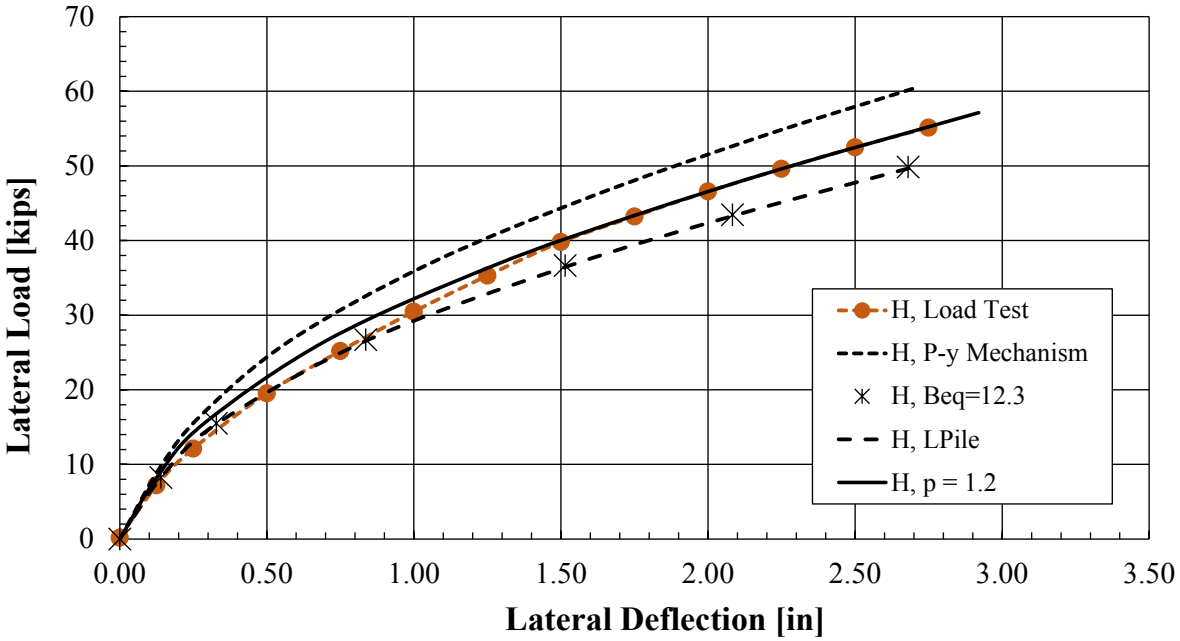

Figure 6-16: Comparison of Analytical Methods for an H Pile

6.6 Bending Moment vs. Depth Curves

Comparisons up until this point have generally looked at the pile head load-deflection curves. Another perspective can be attained by plotting the measured bending moment vs. depth curves with those computed using LPile with the p-multiplier approach for account for shape effects. As discussed in Section 6.5.3, p-multipliers have been utilized in the LPile model to better fit the pile model to the load test results in terms of lateral load vs. deflection. This section will compare the moment vs. depth output results of the LPile models to ensure that the p-multiplier approach provides a good description of the moments along the length of the pile.

The measured moment vs. depth plot for the load test on the square pile is shown in Figure 6-17 and Figure 6-19 for loads of 37 and 50 kips respectively. The computed bending moment vs. depth curves for a square pile with no p-multiplier as well as one with a multiplier of p = 1.25 have also been plotted for comparison. Points of interest include the magnitude of the maximum moment in the pile as well as the depth that the maximum moment occurs. The measured pile moment has been calculated using strain gauge data which recorded the strain at the top 18 ft of each pile. It is easy to see that the LPile model with the p-multiplier gives a closer approximation of the maximum moment in magnitude and depth to that measured during the tests on the square pile. The same comparison is shown for an H pile in Figure 6-18 and Figure 6-20 for loads of 37 kips and 50 kips respectively. The measured moment on the H pile occurred at a depth of six feet whereas both LPile models had a maximum moment occur at about five feet. The bending moment for the LPile model with a p-multiplier did show a magnitude nearer to the measured maximum moment of 2000 kip-in that without a p-multiplier. In both cases the LPile model with the p-multiplier displayed a moment versus depth curve closer to the measured load test data.

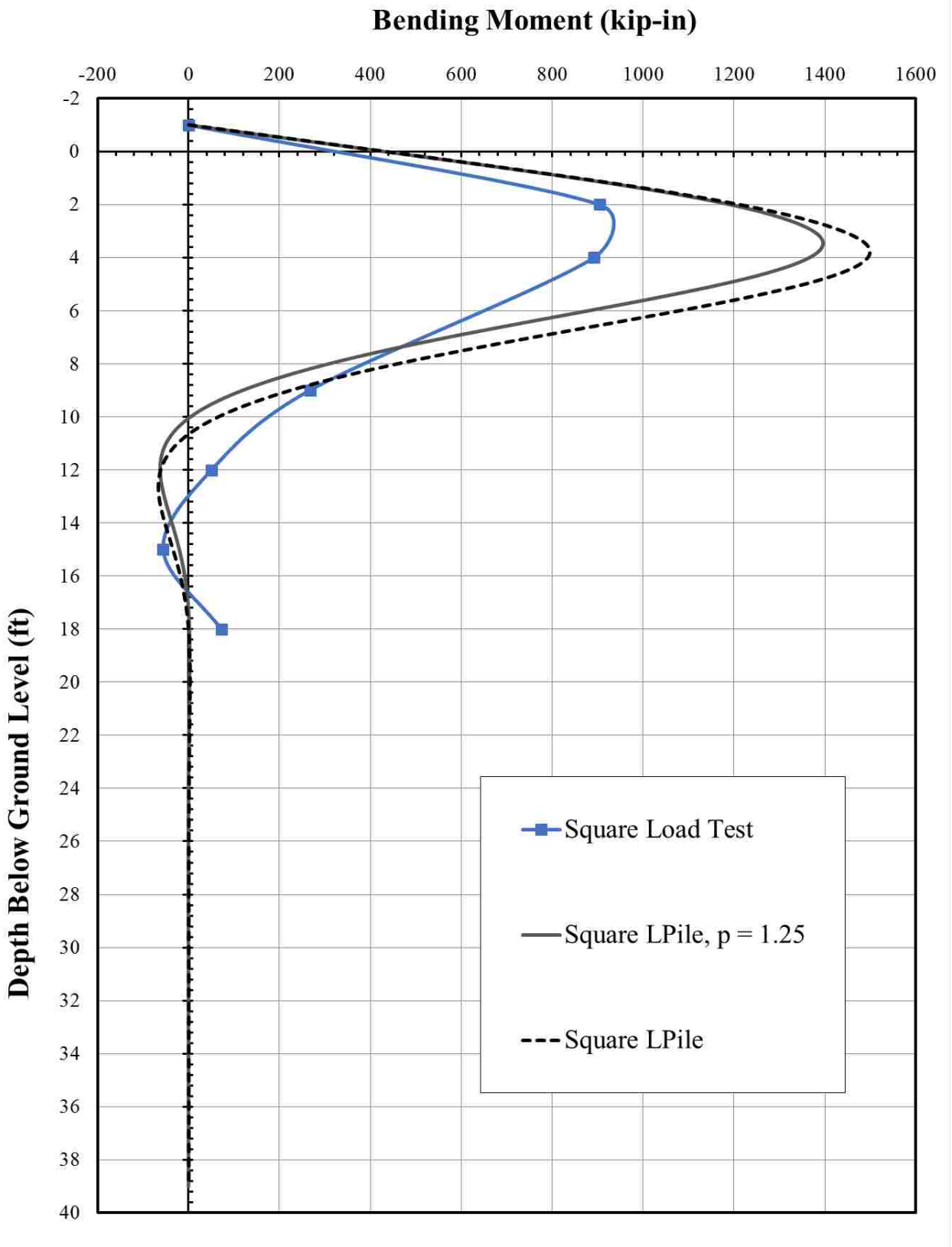

Figure 6-17: Bending Moment versus Depth for a Square Pile at 37 Kips of Load

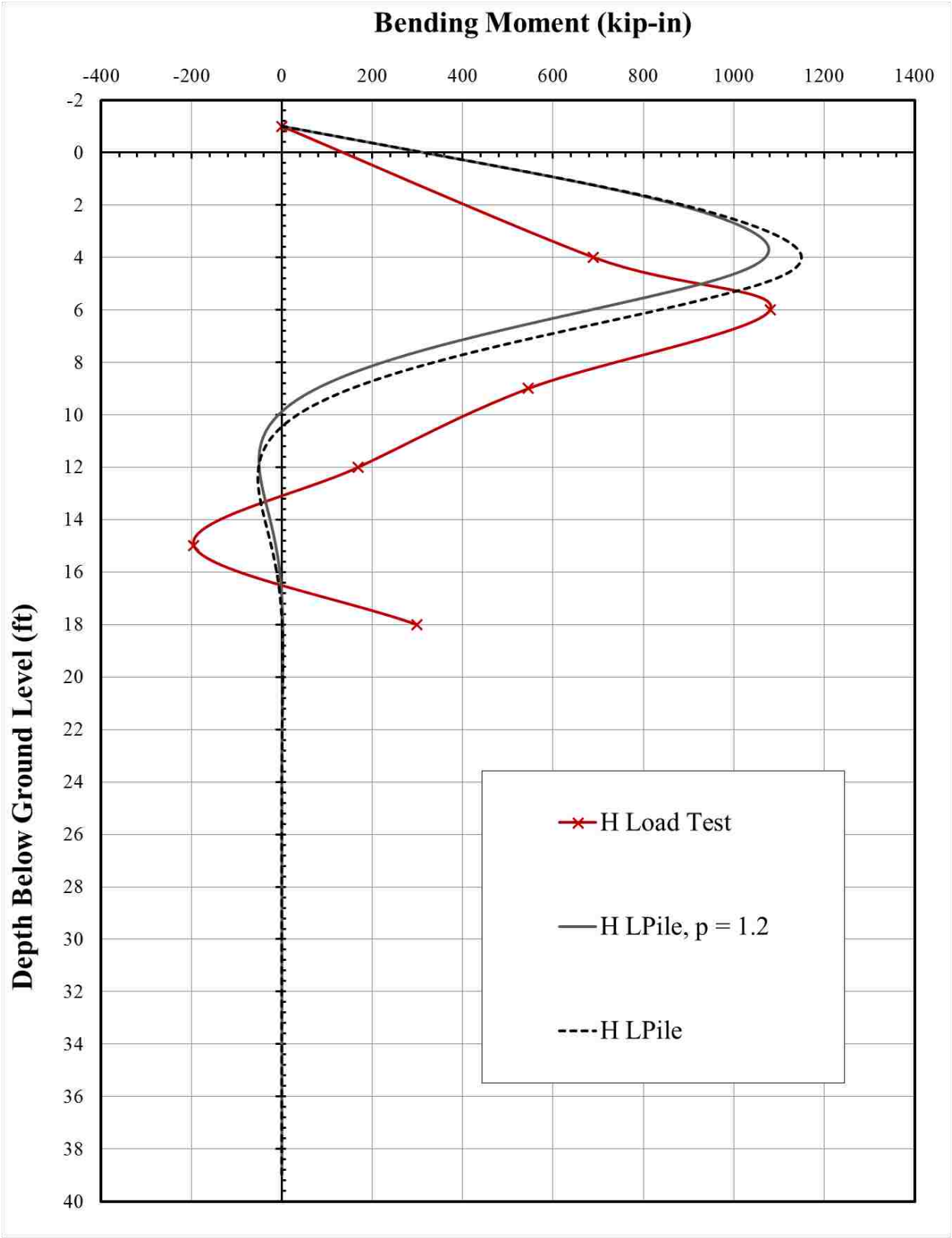

Figure 6-18: Bending Moment versus Depth for an H Pile at 37 Kips of Load

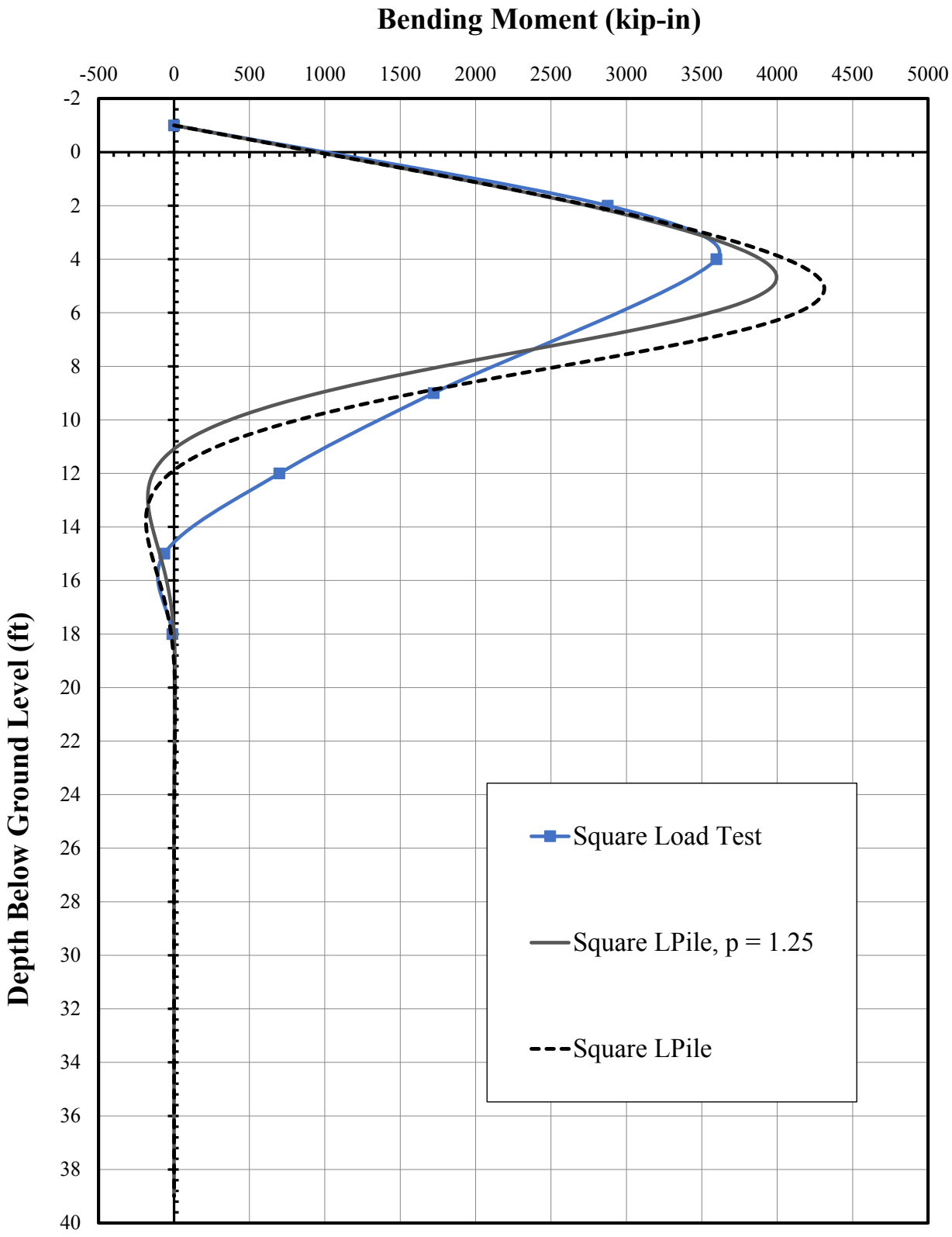

Figure 6-19: Bending Moment vs. Depth for a Square Pile at 50 Kips of Load

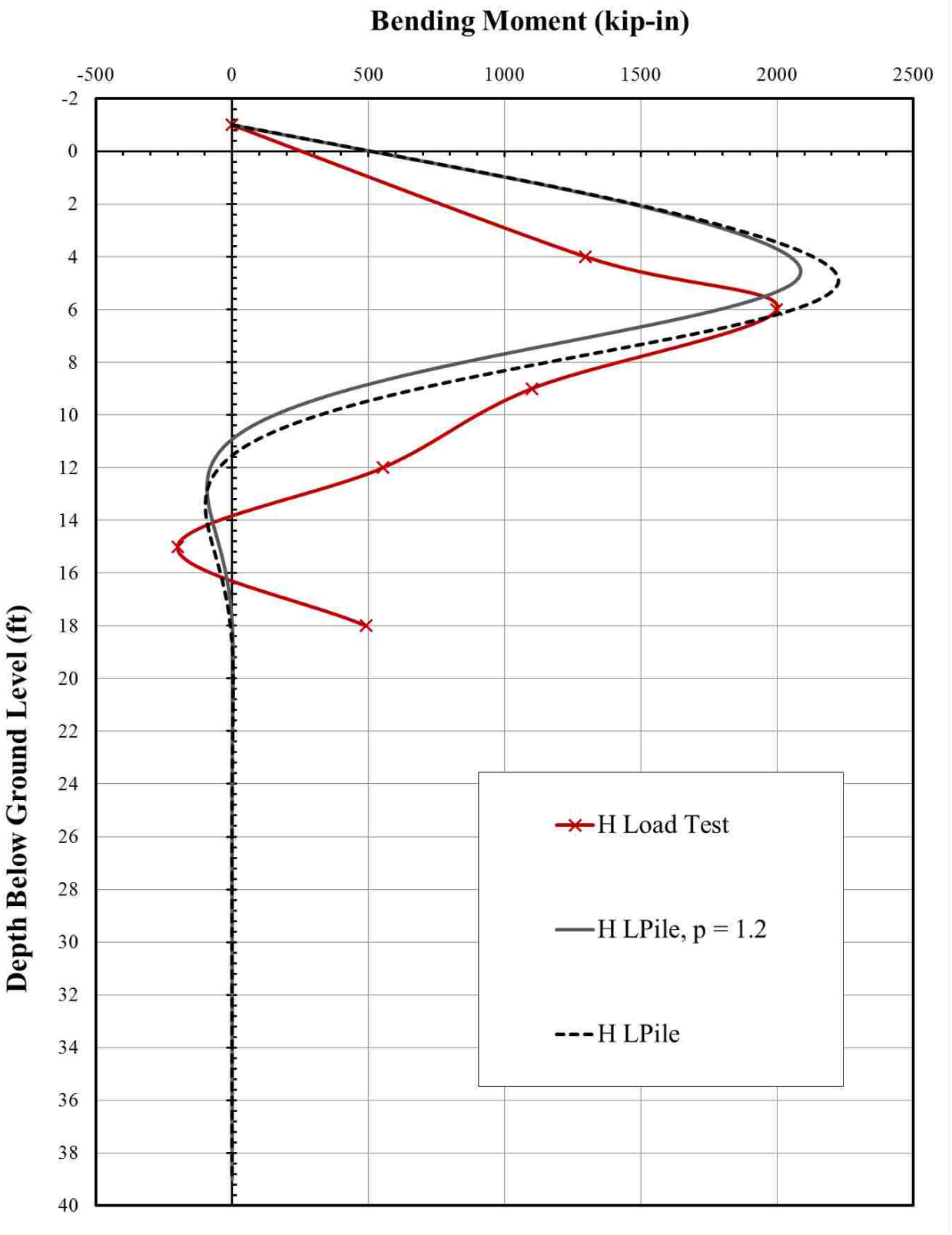

Figure 6-20: Bending Moment versus Depth for an H Pile at 50 Kips of Load

6.7 The Influence of Pile Shape on Lateral Load Resistance

Does pile shape make a difference in the lateral resistance of a pile? The test results from Section 5 presents comparisons of lateral resistance of round, square and H pile shapes with similar widths and with similar backfill soils. A noticeably higher difference was observed from the ultimate resistance of the square piles, a difference of nearly 14% than that of the round pile. This ultimate resistance is a combination of the structural stiffness of the pile and the resistance provided by the soil. With both piles having nearly the same moment of inertia this difference can be attributed to the influence of pile shape on the soil resistance. The suggested p-multiplier for a square pile is 1.25 which indicates that the resistance in the soil for a square pile is actually 25% greater than a similar round pile. The H pile demonstrated a resistance of 85% compared to that for the round pile, the moment of inertia of the H pile was only 59% in comparison to the same round pile. This suggests that given equal moments of inertia, the H pile may have greater resistance than the round. The p-multiplier for an H pile is 1.2 which indicates a 20% increase in the resistance in the soil around an H pile. Similar results for the same pile shapes were observed by Bustamante (2014). These observations suggest that pile shape can have an influential role in the lateral resistance of a pile. Lateral analysis using three different methods indicates that the p-multiplier approach is a simple, intuitive, and more effective approach to estimating the resistance of such pile shapes.

This being said, pile shape is not the only influence on lateral resistance nor should it the most important. Pile properties such as, the modulus of elasticity and moment of inertia, as well as soil properties including, unit weight, friction angle, and soil type, are known to have greater influence on lateral pile design. The degree of certainty of values such as relative compaction should also be considered before a specific p-multiplier is applied. There are also constructability

factors such as availability and cost to consider although shape can influence the economics of deep foundation design.

A basic cost analysis can also provide insight on the whether or not the pile shape should be changed from a round to square pile shape for a given project.. Apart from considering pile driving cost, the price of each pile can be correlated to its weight in steel. If each pile has similar material properties, then price per foot of pile is a ratio of the cross sectional area. This study utilized piles of comparable width and diameter. Although this similarity also extends to the cross sectional area of the square and the round piles, 14.8 in^2 and 14.57 in^2 respectively, the same cannot be said about the H pile, 22.5 in^2. Using these factors as the basis of comparison, the square pile would cost 2% more than the round pile while the H pile, orientated about its weak axis, would cost 55% more than the round pile. This price can be reduced by using an H pile with a smaller section, such as a non-compact W12x53 shape, if bending capacity is not a large concern. As the price of steel is constantly fluctuating, these ratios will hold true in any market and other pile sizes with similar width/diameter and areas.

As demonstrated in this study, pile shape does have an influence on the lateral resistance of a pile. It has been shown that a square pile with a similar width, moment of inertia and cross sectional area as a round pile will provide more lateral resistance with nearly the same cost. An H pile on the other hand, oriented about the weak axis, will provide less resistance and possibly cost 55% more than a comparable round pile. Although pile shape is usually not the most important consideration in design, to the attentive engineer the use of pile shape factors can be a secondary consideration that should be considered in the design of deep foundations.

6.8 LPile Model for Round Piles with a CMS

When using a round pile in a CMS it is generally assumed that a reduction in lateral resistance would be expected. Contrary to this belief, the numerical model performed by Filtz et al. (2013) suggests that stiffening of the loose infill soil in the annular space may cause an increase in lateral resistance. The results of the load test shown in Section 5.2.4 also demonstrate an increase in lateral resistance from the CMS particularly at larger deflections. With these contradictions in view, it is important to investigate how the pile, loose infill, and CMS interact to produce increased lateral resistance. Models created using LPile will be a critical component in this investigation. Various models have been tried in order to explain this unexpected phenomena until a model producing reasonable agreement with the measured response was found.

A reasonable model will allow further understanding of how the pile structure acts under lateral loads and can be used to further predict how this pile structure will react under different loads. A round pile with a CMS is not a pile option in the standard section type and shape category in LPile. Initial endeavors were spent finding existing pile types that resembled a round pile in a CMS. An initial model was produced as a round shaft with permanent casing and core using the CMS properties for the casing, round pile properties as the shaft core and the soil infill as the concrete fill. Results proved that this was an inappropriate model that yielded resistance far greater than what was observed in the load test. It is possible that the model would match observed response if lower values for the compressive strength of sand fill could be introduced but this exceeded the lower bounds set by the LPile program.

Eventually, the endeavor of modelling the round pile in a CMS as a round shaft with casing was discarded because it suggests that the element acts entirely as a composite member

which further discussion suggests is not true. The next step was to decide on an appropriate moment of inertia that would describe the behavior of the combined pile-infill-CMP structure.

Much deliberation went into formulating an appropriate moment of inertia that represents the stiffness of the seemingly composite pile and sleeve combination. Tables for sectional properties for corrugated steel pipe products provided by Contech Engineered Solutions provided insight on the CMS contribution to a composite moment of inertia. Although the CMS has twice the diameter of the round pile, the thin wall and corrugated nature of the pipe provide values for moments of inertia of around 1.892×10^{-3} in^4/in. That quantity is minute in comparison to that of the steel pipe pile itself. In the design of a round shaft with permanent casing, the properties of the core, case, and fill material would be weighted to create a composite moment of inertia and modulus of elasticity. These stiffness properties can be calculated for a round shaft with permanent casing assuming that the concrete has sufficiently bonded to the case and core, acting as one amalgamated member. However, the same procedure cannot be used for the CMS with cohesionless infill because unlike the round shaft with permanent casing, the member does not act as a uniformly composite material. As the member is loaded, the cohesionless infill provides no contribution in tension and it is difficult to quantify the contribution in compression as the material continuously compacts with increased load. The only sure contribution in flexural stiffness for the member was that of the central round pile. This moment of inertia was used for further models.

One of the models was created using the moment of inertia of the pipe pile alone and assuming that no resistance is provided by the infill or the CMS. This assumption idealized the annular material as being very loose and allowing for large deflections within the CMS. The computed load-deflection curve for this model is plotted in Figure 6-21. Because the load is

applied with a moment arm 21ft above the native soil very little lateral resistance is developed with deflection and the maximum load only reaches 2.5 kips at 3.2 inches of deflection. Although designers often assume that this model applies to sleeved piles it does not appear to be realistic. As an attempt to replicate the load tests, this theory can immediately be dismissed on account of the extremely low load-deflection curve in comparison with the measured results as shown in Figure 6-21. The failure of this model to match measured response proves that the annular fill, although loose, provides a significant amount of lateral resistance to the pile structure.

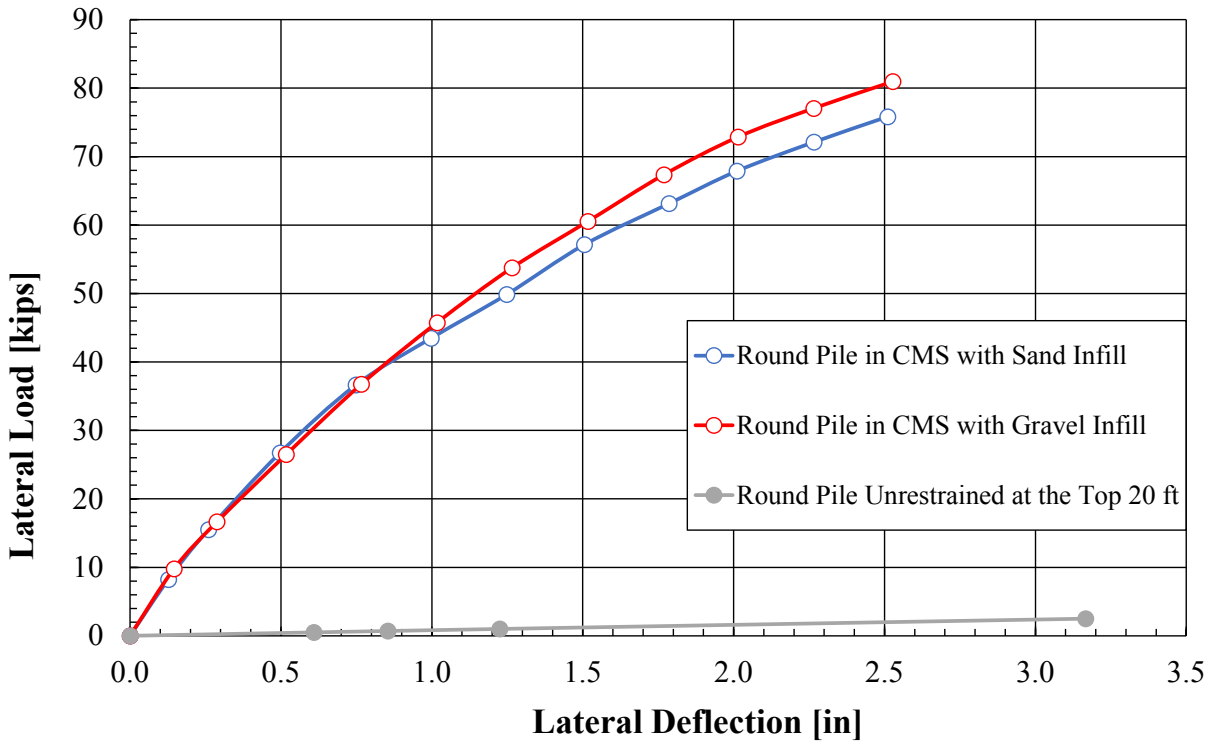

Figure 6-21: Round Pile Unrestrained at Top 20 feet Compared to Round Piles with CMS Load Test Results

While testing the round piles in the CMS it was observed that initially the round pile deflected in response to the load. As a way of replicating at least the initial stages of loading, the LPile model for the round pile was plotted against the CMS test data. This comparison between the CMS load tests and an individual round pile modeled in LPile assuming soil with a ϕ of 45° and a k of 394 pci is provided in Figure 6-22. Keeping in mind that the annulus was filled with loose, non-compacted infill, it is expected that this inner round pile will initially deflect more than the individual round pile in compacted backfill. Initially, the round pile inside the CMS does deflect a little more than the solo round pile but this isn't as large of a difference as was expected. The deflection difference between the load tests and the model is only 0.03 inches at a load of 26.4 kips. For the most part, the shape of the measured and computed load-deflection curves fit quite closely together for the first 0.5 inches. This suggests that as the round pile inside the CMS is loaded, it responds to the load like an independent round pile in compacted backfill. The confinement provided by the CMS is apparently sufficient to provide significant lateral resistance even with loose infill material.

As the load increases the measured load-deflection curves for the round piles in the CMS exceeds the computed curve for the round pile model. The effect of the CMS begins to show in the load-deflection curve as the slope becomes steeper at about 0.5 inches of deflection as it crosses over the curve predicted by the individual round pile model. It appears as though the loose annular material compacts as the load-deflection curve reaches 0.5 inches of deflection. As the infill material is loaded by the pile it compacts and transfers the load to the CMS. Up until one inch of deflection the CMS with sand infill and the CMS with gravel infill have identical load-deflection curves. This validates the consistency in the test results as well as the interaction of the infill between the round pile and CMS.

As the two load-deflection curves in Figure 6-22 separate, the difference that the infill material makes in the pile resistance becomes apparent. Between 1.0 inch of deflection and 1.75 inches of deflection there is a transition in the slopes for the load-deflection curves. The relatively linear midsection of the slopes begin to flatten out indicating yielding in the soil. This yielding is more dramatic in the sand infill as the p-y curve drops below that of the gravel infill. The gravel infill provides more resistance as it is able to handle increased load without deflecting as much as the sand infill. At 1.75 inches of deflection the CMS appears to have fully engaged the surrounding soil material.

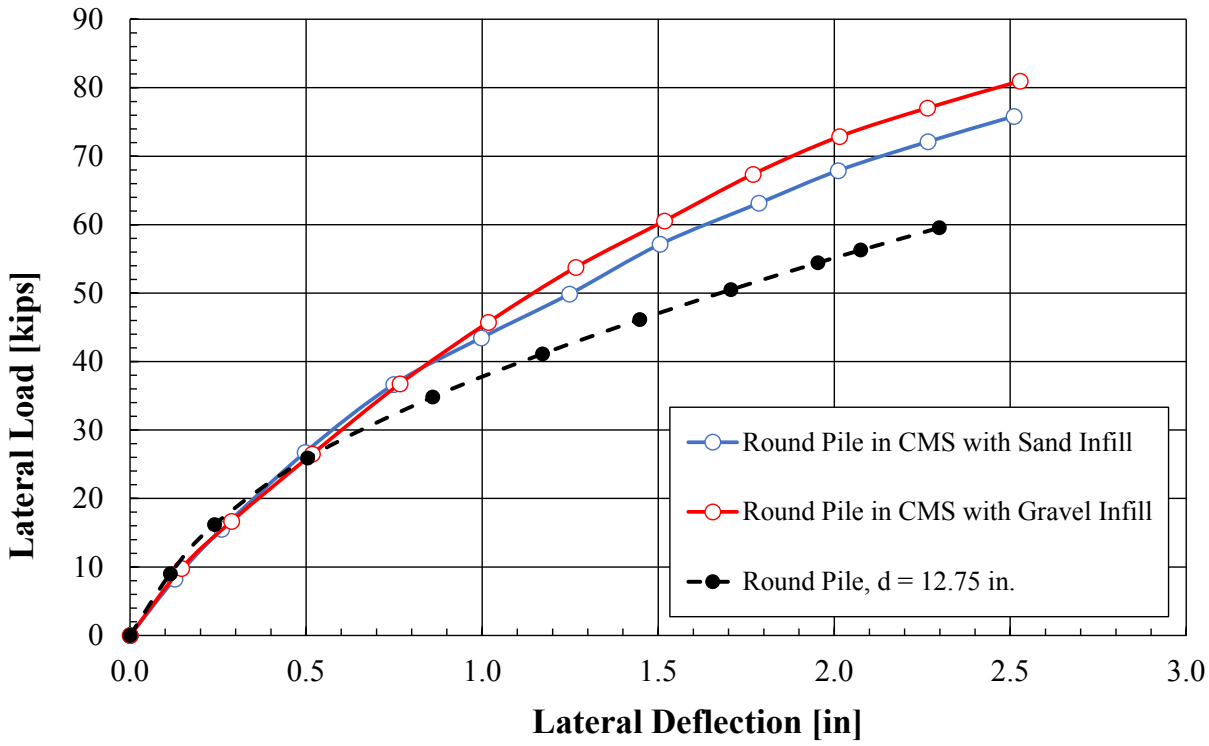

Figure 6-22: Round 12.75" Diameter LPile Analysis Compared to Round Piles with CMS Load Test Results

As shown in Figure 6-22, both p-y curves are parallel at the maximum loads shown by the last four data points. The points for the CMS with sand infill are offset by only 5 kips less than the CMS with gravel infill which is a difference of about 6% of the ultimate load. This indicates that at this stage of loading the piles engage the soil outside the CMS at about the same rate and that the soil provides the same rate of resistance. It was demonstrated in Figure 6-22 that an LPile model of a round pile with a diameter of 12.75 inches matches the load vs. deflection curve of the Round/CMS piles up to 0.5 inches of deflection. This model sets the lower bound of what resistance to expect from this pile structure. Another model needed to be created to match the upper limit of the load vs. deflection curves. For the model to be comparable a member with similar stiffness properties would need to be defined.

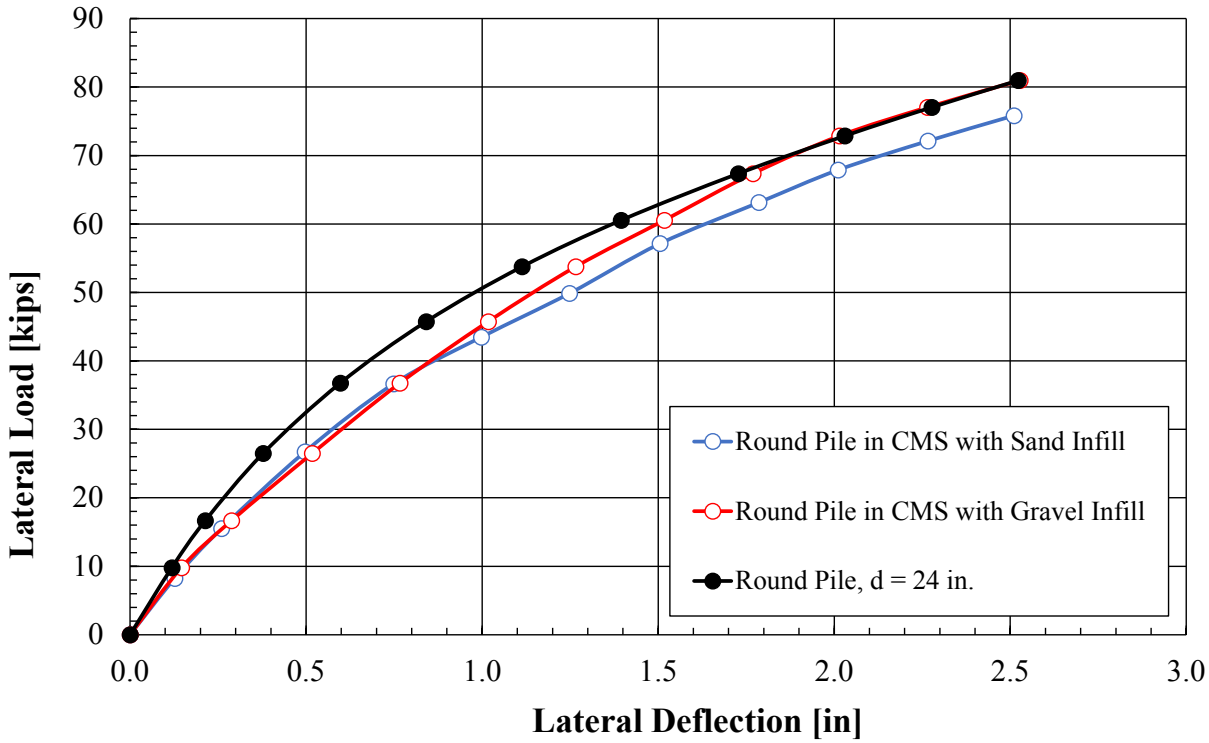

Figure 6-23: Round 24" Diameter LPile Analysis Compared to Round Piles with CMS Load Test Results

A load vs. deflection curve was produced with the moment of inertia and modulus of elasticity of a 12.75 inch diameter round pile but with the diameter of the 24 inch diameter corrugated metal pipe pile. As shown in Figure 6-23, the load–deflection curve computed by LPile with this model matched with the round pile in the CMS with gravel infill curve from the load test at deflections greater than about 1.75 inches. At deflections less than 1.75 inches the 24 inch round pile model overestimates the resistance. From this model it seems that after a certain amount of deflection and loading the CMS engages the surrounding soil as a round pile of similar diameter.

According to this analysis, the lateral resistance of the round-CMS pile structure can be defined within the bounds of a 12.75 and a 24 inch diameter round pile with the moment of inertia of the 12.75 inch diameter pile as shown in Figure 6-24. Fitting a linear transition between the two models at 0.5 inches of deflection and 1.75 inches of deflection creates a load-deflection curve that fits the CMS gravel infill curve very well as presented in Figure 6-25. This composite curve matches the initial and ultimate deflections and provides a fit for the transition period. This model indicates that initially the pile acts as a regular round pile and eventually receives the benefit of the diameter of the CMS as it deflects into the surrounding compacted sand. As is apparent in Figure 6-25, the gravel infill material provided a higher resistance at ultimate loads when compared to the pile with the sand infill material. This suggests that using a sand infill material with less gravel can cause a reduction in ultimate loads, by 6% in the case of this test.

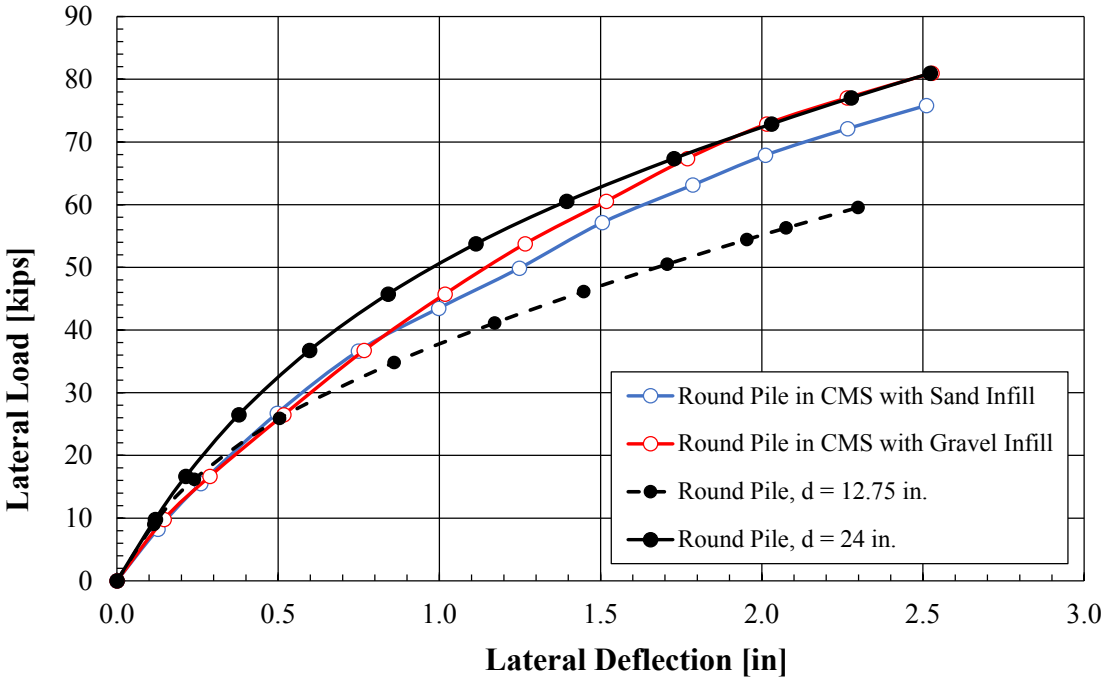

Figure 6-24: Round-CMS Piles with LPile Models for Round Piles of 24 and 12.75 Inch Diameter

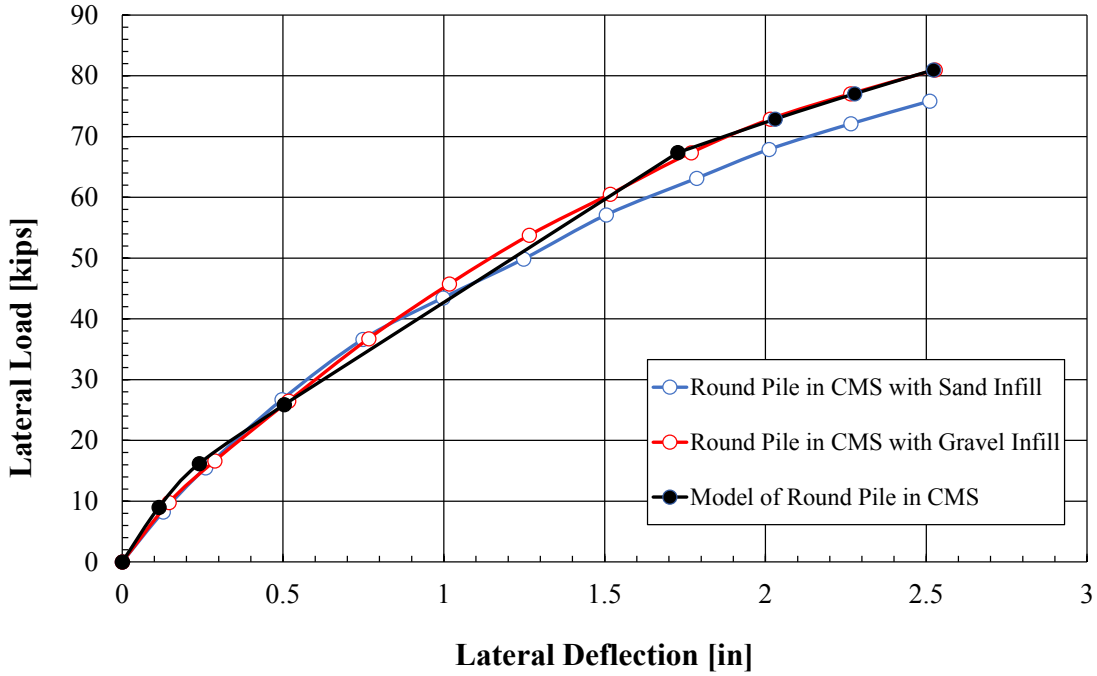

Figure 6-25 Round-CMS Pile Model Matched with a Composite Curve: Lower and Upper Bounds set by Round Piles of 12.75 and 24 Inch Diameter with Linear Transition Between 0.5 and 1.75 Inches of Deflection

7 CONCLUSION

The conclusions of this research have been summarized in two sections, conclusions from the results of the load tests and conclusions derived from the lateral load analysis. Recommendations for further research have also been provided.

7.1 Test Results

1. The square pile showed a 14% increase in resistance when compared to a round pile of comparable width, similar moment of inertia and the same density backfill. This result suggests that square piles develop larger soil resistance than round piles owing to differences in pile shape.
2. The H pile orientated about its weak axis showed considerably less resistance when compared to the round pile of comparable width. It should be noted that the moment of inertia for the H pile about its weak axis is 59% of the moment of inertia for the round.
3. There is no consistent test results to suggest that the use of HDPE sheeting on the round pile will cause a significant reduction in lateral pile resistance. However, the results of these tests were compromised on account of differing levels of compaction around the round piles.
4. The use of a CMS increased the effective width of the round pile creating a larger failure wedge as stresses propagated through the infill and engaged the CMS.

Contrary to current belief, use of the CMS increased the overall lateral resistance of the pile. It was observed that the gravel infill deflected less than the sand infill under similar loads.

5. Failure planes were seen propagating from the pile at angles of 43° from the H pile and a range of 37°-45° from the square pile. The size of the failure planes around the CMS also indicated that the CMS increases the effective width of the pile as it is loaded by the central pile.
6. The maximum bending moment occurred at a depth below the ground surface of four feet for the round and square piles, six feet for the H pile, and eight to nine feet for the round piles with a CMS of larger diameter.
7. According to rotation data of each pile, it was observed that pile rotation is a function of deflection at the head of the pile rather than correlation of pile shape or sleeve.
8. The vertical ground displacement can be recorded with DIC cameras with reasonable accuracy. At a distance from the pile of four pile diameters the soil experiences less than 25% of the vertical heave at the face of the pile. This trend holds true for each pile shape tested and matches testing in stiff clay as well.
9. The horizontal ground displacement with distance from the pile face show similar trends for laterally loaded piles of different shape and sleeve. Normalizing the results showed that at a distance of five pile diameters from the pile face the soil only experienced about 10% of the overall pile deflection.
10. The amount of backfill, whether it be 15 ft, such as in phase 1, or 20 ft, such as in phase 2 or phase 3, did not have a large effect on the lateral resistance. This is

apparent in the test results for the round pile from Bustamante (2014) with 15 ft of constructed backfill when compared to the round test results in this study, both having similar load-deflection curves despite the differences in backfill amount. This suggests that after a pile has reached a certain embedment length, there is no increase in lateral resistance with increased embedment depth.

7.2 Lateral Load Analysis

1. Compactive effort around a pile has a significant effect on the lateral resistance of a pile. Back-calculating the friction angle with LPile showed that the 6" lifts with the jumping jack compactor in phase 3 of compaction resulted in a higher friction than phase 2 of compaction which was placed in 12" lifts.

2. LPile model is lower than the load test results. This is expected on account of the moment of inertia providing the only distinguishing factor in the current method. The Reese and Van Impe equivalent diameter approach suggests using a higher effective width for square and H piles but this amounts to a small adjustment from the LPile analysis, still underestimating the actual resistance of the pile. The shape factors suggested by Briaud and Smith applied to the F-y/Q-y mechanism overestimate the resistance of the piles resulting in a non-conservative estimation.

3. P-multipliers of 1.25 for square piles and 1.2 for H piles were required to provide the closest agreement with the measured load tests. These same p-multipliers more accurately described the bending moment of the pile when compared to the measured bending moment of similar piles.

4. As suggested by this research and Bustamante (2014), it is recommended that design for square piles considers a p-multiplier in the range of 1.2 to 1.25 while design for an H pile should include p-multipliers of 1.2 to 1.35.

7.3 Recommendation for Future Research

1. Further testing with HDPE sheeting is necessary to determine whether using the material as a sleeve greatly influences the lateral resistance. Possible studies could include the use of driven reinforced concrete piles where the contrast between a rougher surface such as concrete and the HDPE sheeting could be better observed.
2. This is the first case of full scale lateral load testing of round piles in a CMS. There are many variations of this pile structure including the use of different infill material, construction techniques and various other pile shapes used as the central pile. Further testing on these variations could introduce new techniques to gain more lateral capacity. For instance, an H pile oriented about its strong axis with a corrugated metal sleeve could take advantage of the stiffness of the H pile along with the added diameter of the CMS.
3. More testing on soil heave and deflection at further distances from the pile could provide valuable data on effective stress distance developed by lateral loading. This research looked at a distance of 5 ft from the pile face, observing a larger area would provide a better view of this phenomena. This information would have implications on pile spacing in groups and near other structures.
4. This research tested H piles oriented about the weak axis. Additional testing on piles about their strong axis would provide a look at the contribution to an increase

moment of inertia as well as the different F-y and Q-y contributions of this orientation. It would be assumed that a flat pile face would provide more passive resistance whereas the side shear would be less along the sides.

REFERENCES

American Petroleum Institute, 2010. *Recommended Practice for Planning, Designing and Constructing Fixed Offshore Platforms - Working Stress Design, API RP 2A-WSD*, 21st Edition, Errata and Supplement, 2010.

Besendorfer, J. (2015). "Lateral Resistance of Pipe Piles Near 20-ft Tall MSE Abutment Wall with Strip Reinforcements" MS Thesis, Department of Civil and Environmental Engineering, Brigham Young University, Provo, UT.

Bowman, E.R. (1958). "Investigation of the Lateral Resistance to Movement of a plate in Cohesionless Soil" Thesis, University of Texas, Austin.

Briaud, J.L., Smith, T.D., and Meyer, B. 1983. "Laterally Loaded Piles and the Pressuremeter: Comparison of Existing Methods", ASTM STP 983.

Brown, D.A., Morrison, C., and Reese, L.C., (1988). "Lateral load behavior of a pile group in sand." J. Geotech. Geoenviron. Eng., ASCE, 114(11), 1261-1276.

Budd, R. (2016). "Lateral Resistance of Pipe Piles Behind a 20-ft Tall MSE Wall with Welded-Wire Reinforcements" MS Thesis, Department of Civil and Environmental Engineering, Brigham Young University, Provo, UT.

Bustamante, G. (2014). "Influence of Pile Shape on Resistance to Lateral Loading" MS Thesis, Department of Civil and Environmental Engineering, Brigham Young University, Provo, UT.

Coduto, D. P. (2001). Foundation Design: Principles and Practices. Prentice Hall, Upper Saddle River, NJ.

Cosentino, P. J., Kalajian, E. H., Stansifer, R., Anderson, J. B., Kattamuri, K., Sundaram, S., Messaoud, F., Misilo, T. J., and Cottingham, M. A. (2006). Standardizing the Pressuremeter Test for Determining P-y Curves for Laterally Loaded Piles, rep., Melbourne, FL.

Duncan, J. M., Evans, L. T., and Ooi, P. S. K. (1994). "Lateral Load Analysis of Single Piles and Drilled Shafts." *Journal of Geotechnical Engineering*, 120(5), 1018–1033.

Filtz, G. M., Arenas, A. E., Cousins, T. E., (2013). "Thermal Response of Inegral Abutment Bridges with Mechanically Stabilized Earth Walls" *VCTIR 13-R7*.

Isenhower, W.M., Wang S. (2015). "Technical Manual for LPile 2015 (Using Data Format Version 8)", Ensoft Inc., Austin, TX.

Isenhower, W.M., Wang S. (2015). "User's Manual for LPile 2015 (Using Data Format Version 8)", Ensoft Inc., Austin, TX.

"Istra-4D Q-400." (2014). computer software, Dantec Dynamics, Skovlunde, Denmark.

Journal of the structural division proceedings of the American society of civil engineers resistance to overturning of single, short piles. Czerniak 1957

Luna, A. I. (2016). "Lateral Resistance of H-Piles and Square Piles behind an MSE Wall with Ribbed Strip and Welded Wire Reinforcements" MS Thesis, Department of Civil and Environmental Engineering, Brigham Young University, Provo, UT.

"Measurement Principles of (DIC)." *Digital Image Correlation (DIC) Measurement Principles*, <http://www.dantecdynamics.com/measurement-principles-of-dic> (Aug. 11, 2015).

Price, J. S. (2012). "Lateral Resistance of Piles Near Vertical MSE Abutment Walls" MS Thesis, Department of Civil and Environmental Engineering, Brigham Young University, Provo, UT.

Reese, L. C., and Van Impe, W. F. (2001), "Single Piles and Pile Group under Lateral Loading", A. A. Balkema, Rotterdam, Netherlands.

Reese, L.C., W.R. Cox & F.D. Koop 1968. Lateral load tests of instrumented piles in stiff clay at Manor, Texas. A report to Shell Development Company, 303 pp. (published).

Robertson, P.K., Hughes, J.M.O., Campenella, R.G., Brown, P. and McKeown, S. 1986, "Design of Laterally Loaded Piles Using the Pressuremeter", The Pressuremeter and Its Marine Application: 2nd Intl. Symposium, ASTM STP 950, ASTM.

Rollins, K.M. and Bustamante, G. (2015). "Influence of Pile Shape on Resistance to Lateral Loading" Procs. XV Pan-American Conference on Soil Mechanics and Geotechnical Engineering, D. Manzanal and A.O. Sfriso (Eds.), Buenos Aires, Argentina, IOS Press, p. 1885-1892.Ch 2 p-y

Rollins, K.M., Lane, J.D., Gerber, T. M. (2005) "Measured and Computed Lateral Response of a Pile Group in Sand." *J. Geotechnical and Geoenvironmental Engrg*., ASCE Vol. 131, No. 1, p. 103-114.

Rollins, K.M., Price, J.S., and Bischoff, J. (2011). "Lateral Resistance of Piles Near Vertical MSE Abutment Walls." Procs. GeoFrontiers 2011 *Advances in Geotechnical Engineering, Geotech*. Special Pub. No. 211, ASCE, p. 3526-3535.

Smith, T. D., (1987), "Side Friction Mobilization F-y Curves for Laterally Loaded Piles from the Pressuremeter," *Prediction and Performance in Geotechnical Engineering: Proceedings of the International Symposium*, p. 89-95, Calgary, June 1987.

Source: "Test Site." 40°27'14.08" N and 111°53'53.60" W. GOOGLE EARTH. June 4, 2013. December 20, 2015.

Tawfiq, K. S., and Caliendo, J. A. (1995). "Bitumen Coating versus Plastic Sheeting for Reducing Negative Skin Friction." *Journal of Materials in Civil Engineering*, 7, 69–81.

Terzaghi, K., 1955. "Evaluation of Coefficients of Subgrade Modulus," *Géotechnique*, Vol. 5, No. 4, pp. 297-326.

APPENDIX A. ADDITIONAL LATERAL LOAD PLOTS

As each separate pile shape was considered in the report it can be informative to see plots comparing all the pile shapes and load sets. The following plots provide such a comparison.

A.1 Load-Deflection

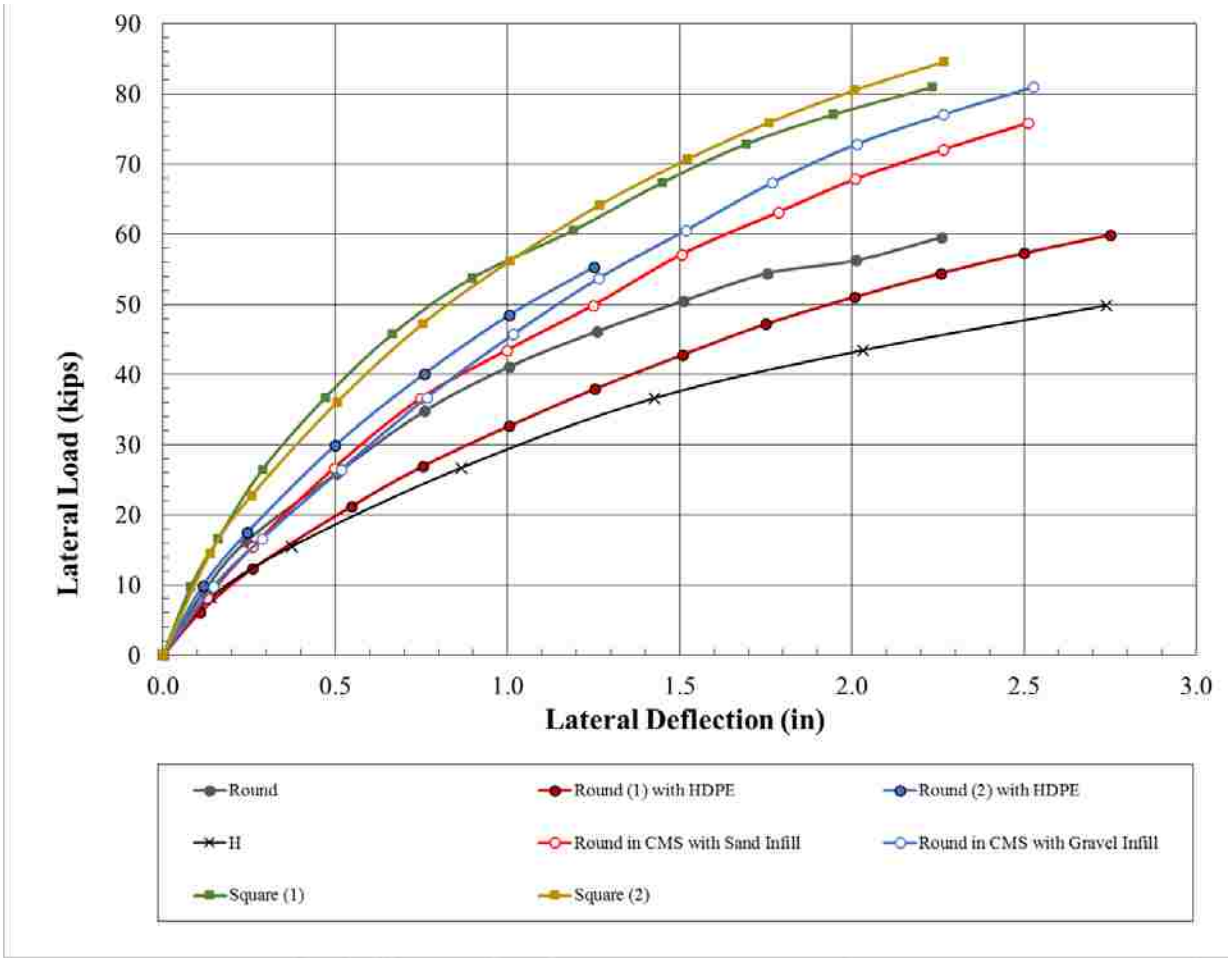

Figure A-1: Load Deflection Curves for all Pile Types

A.2 Pile Rotation with Lateral Load

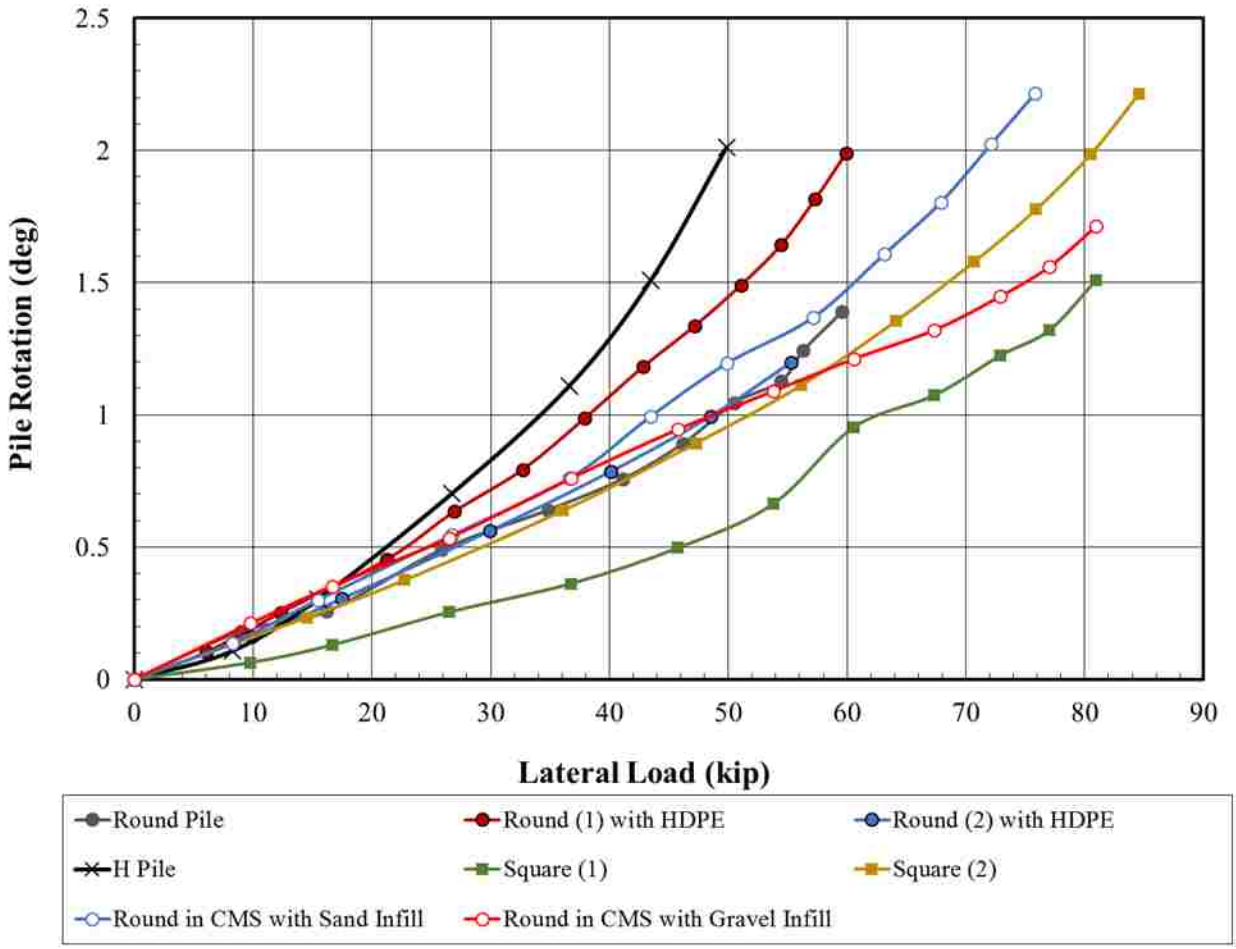

Figure A-2: Pile Rotation Curves for all Pile Types

A.3 Moment versus Depth

Moment versus depth data was not available for the Square (2) or Round (2) with HDPE piles.

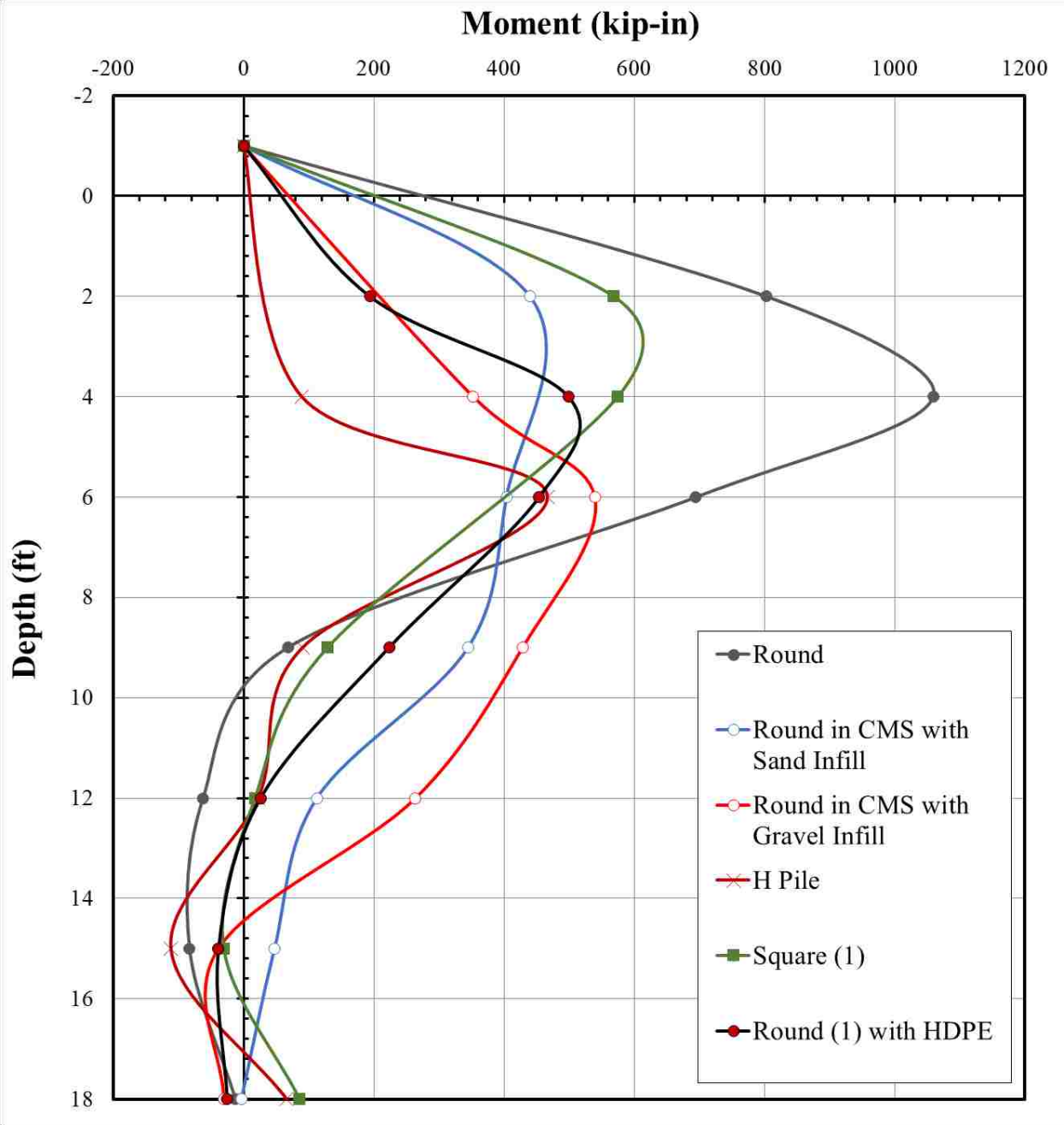

Figure A-3: Moment vs Depth Plot for Pile Types at 0.25" of Deflection

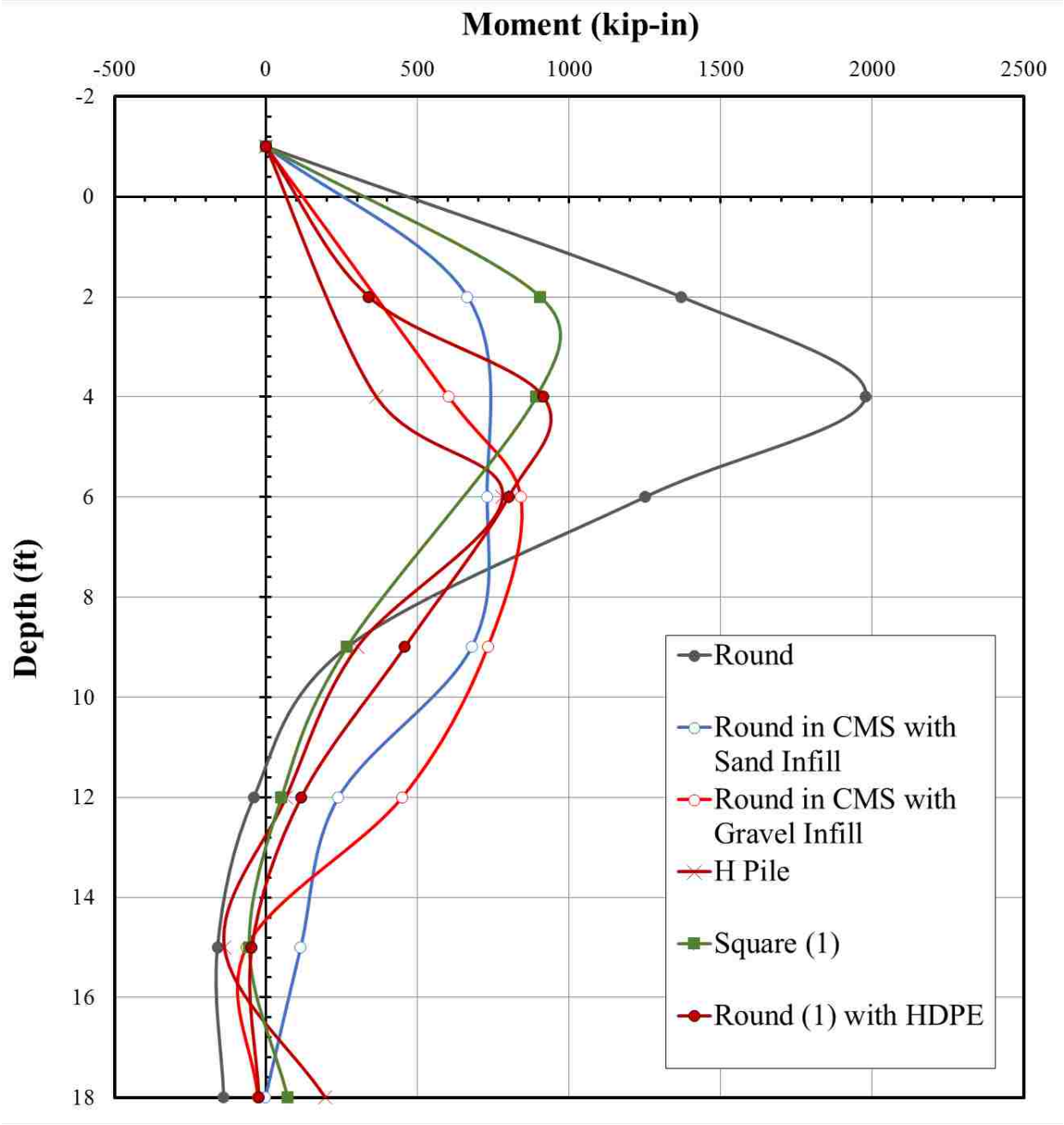

Figure A-4: Moment vs Depth Plot for Pile Types at 0.50" of Deflection

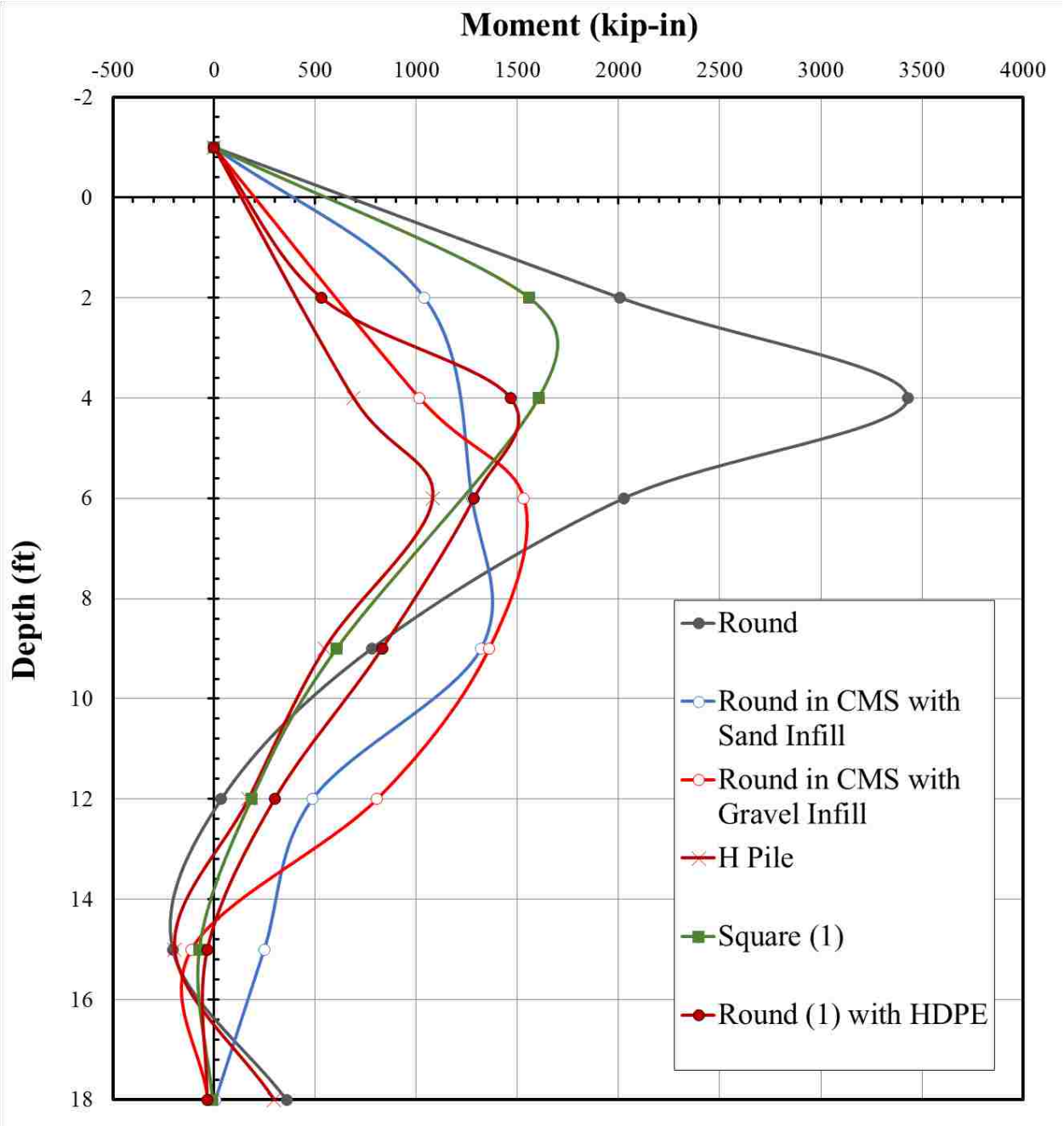

Figure A-5: Moment vs Depth Plot for Pile Types at 1.0" of Deflection

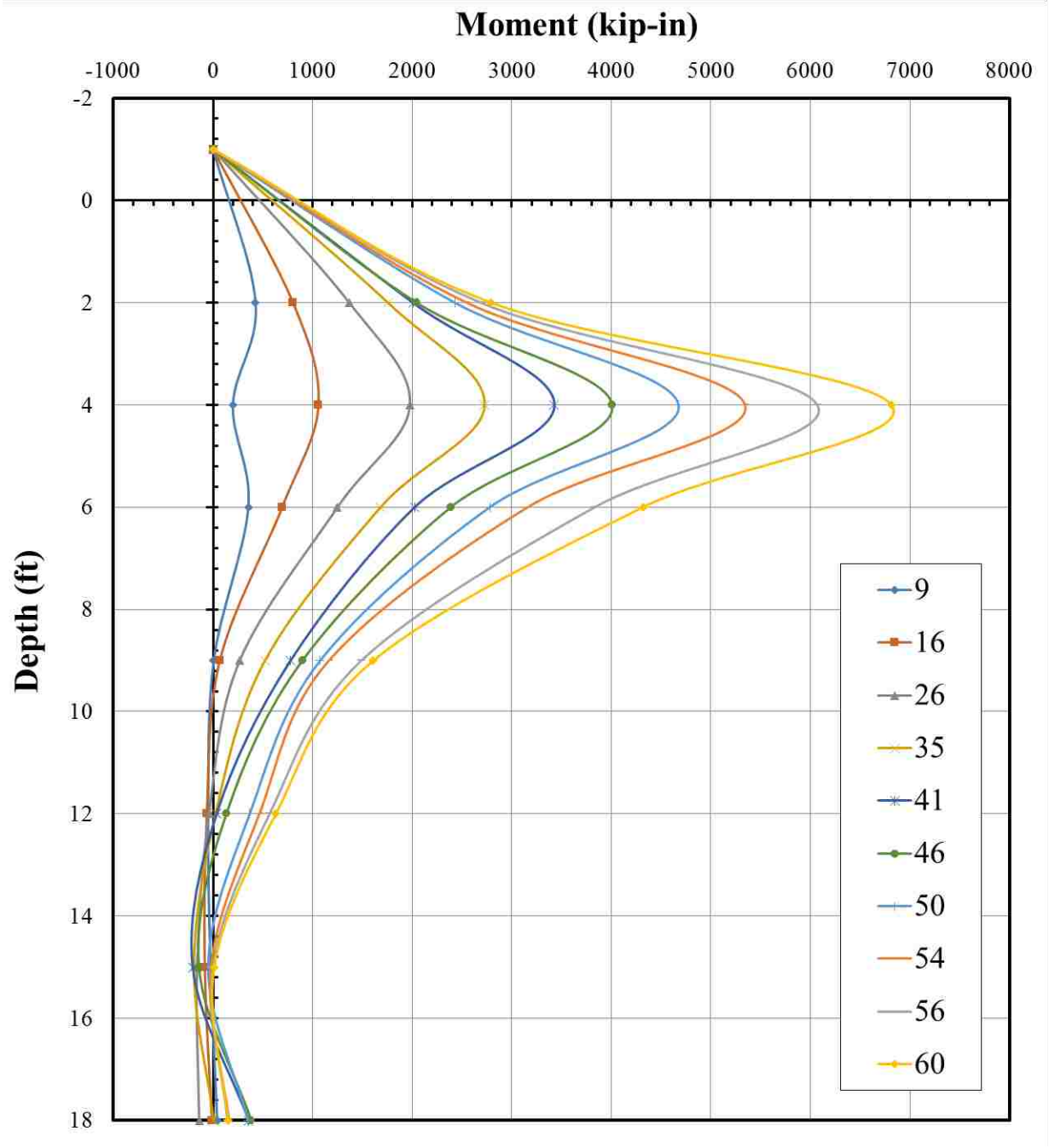

Figure A-6: Moment vs. Depth Curves for a Round Pile at Various Load States

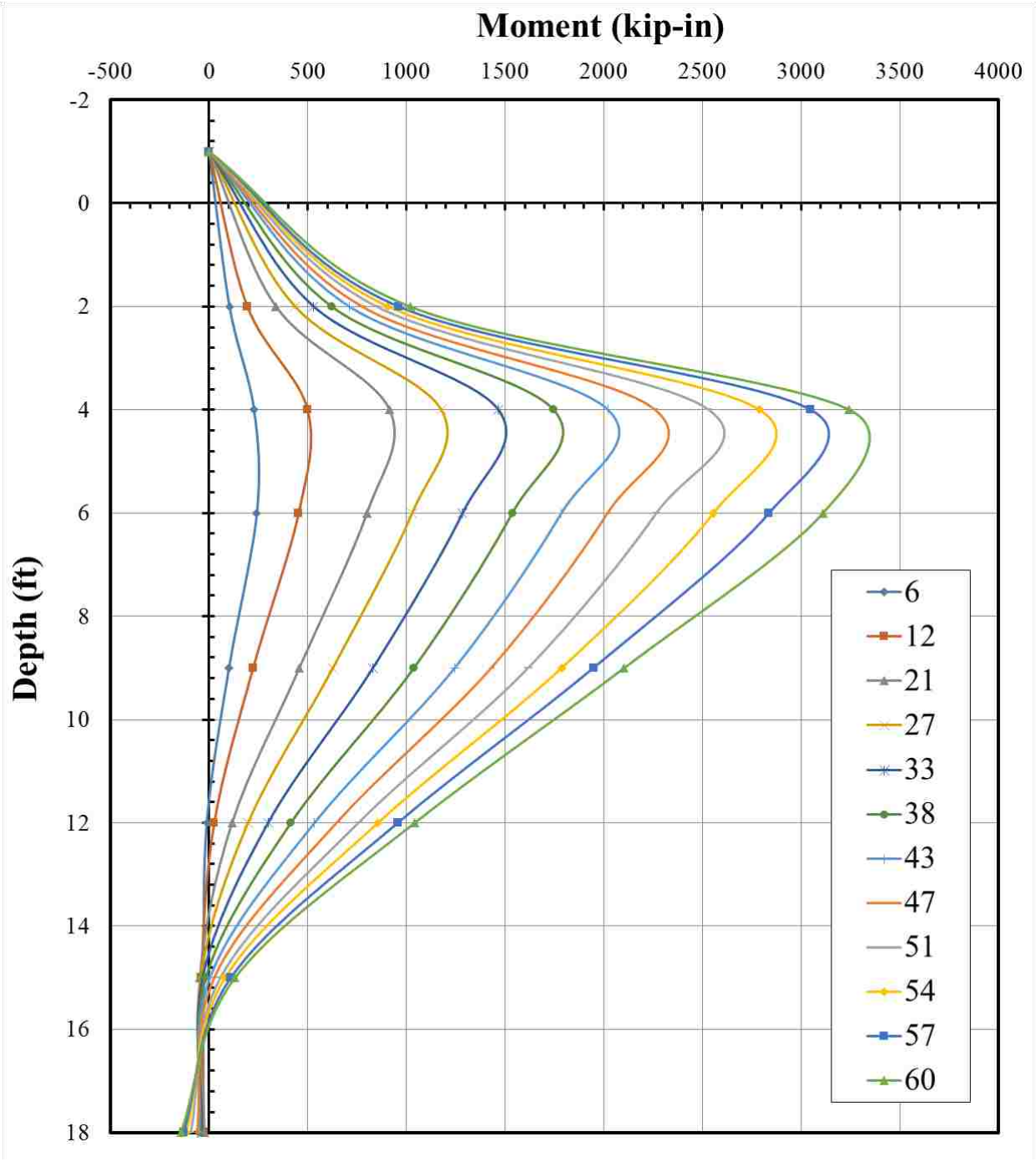

Figure A-7: Moment vs. Depth Curves for a Round Pile with an HDPE Sleeve Pile at Various Load States

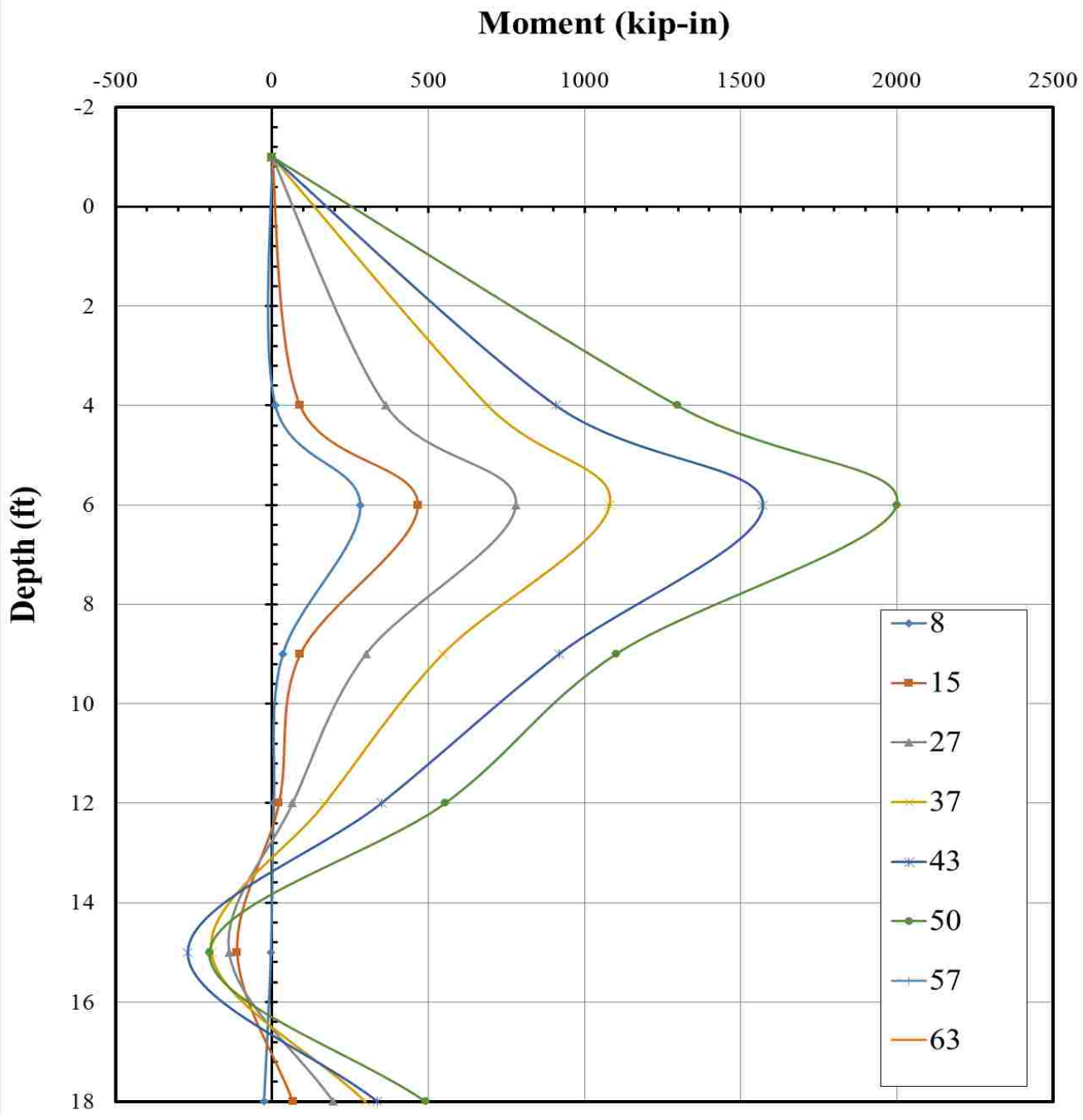

Figure A-8: Moment vs. Depth Curves for an H Pile at Various Load States

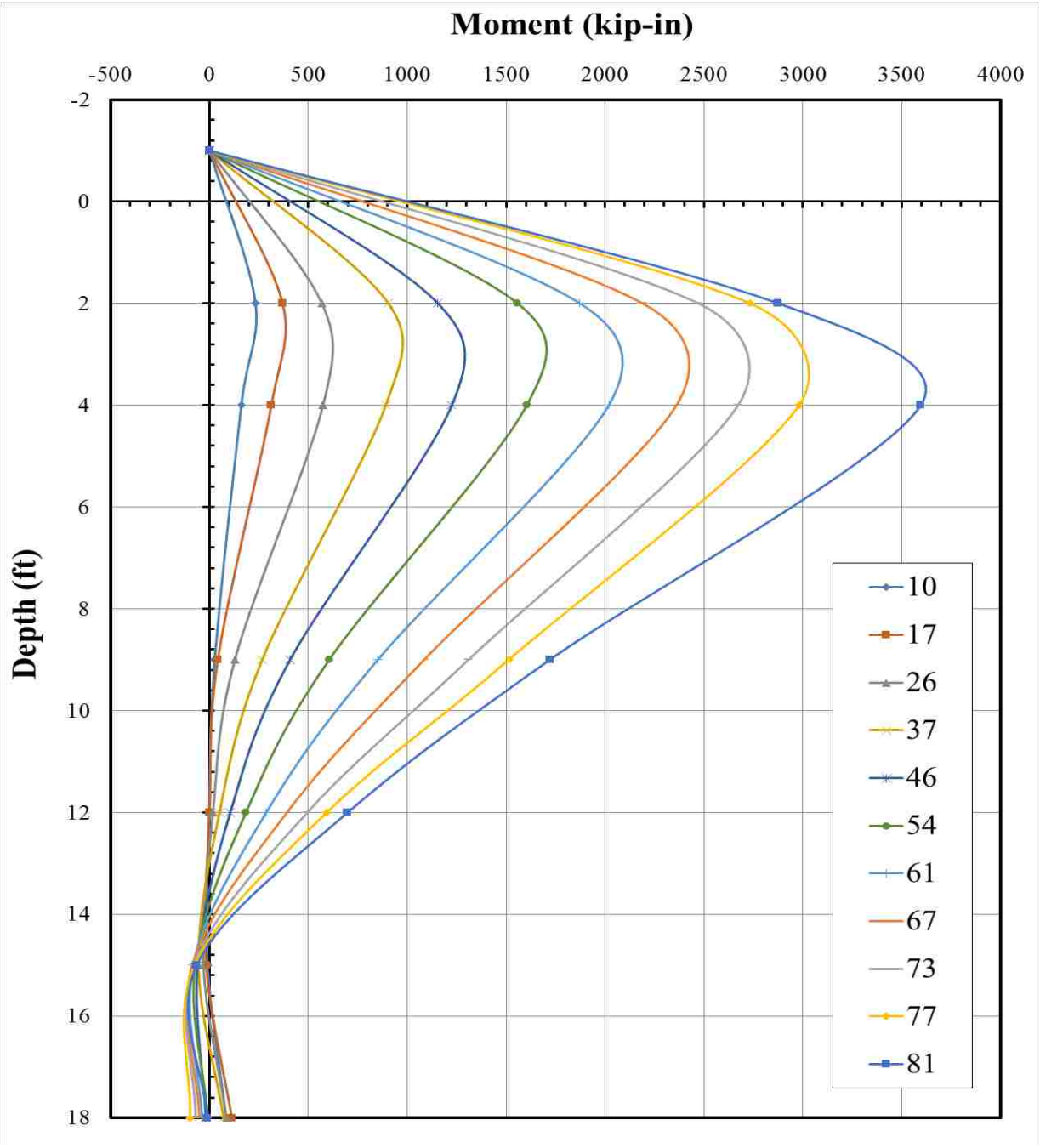

Figure A-9: Moment vs. Depth Curves for a Square Pile at Various Load States

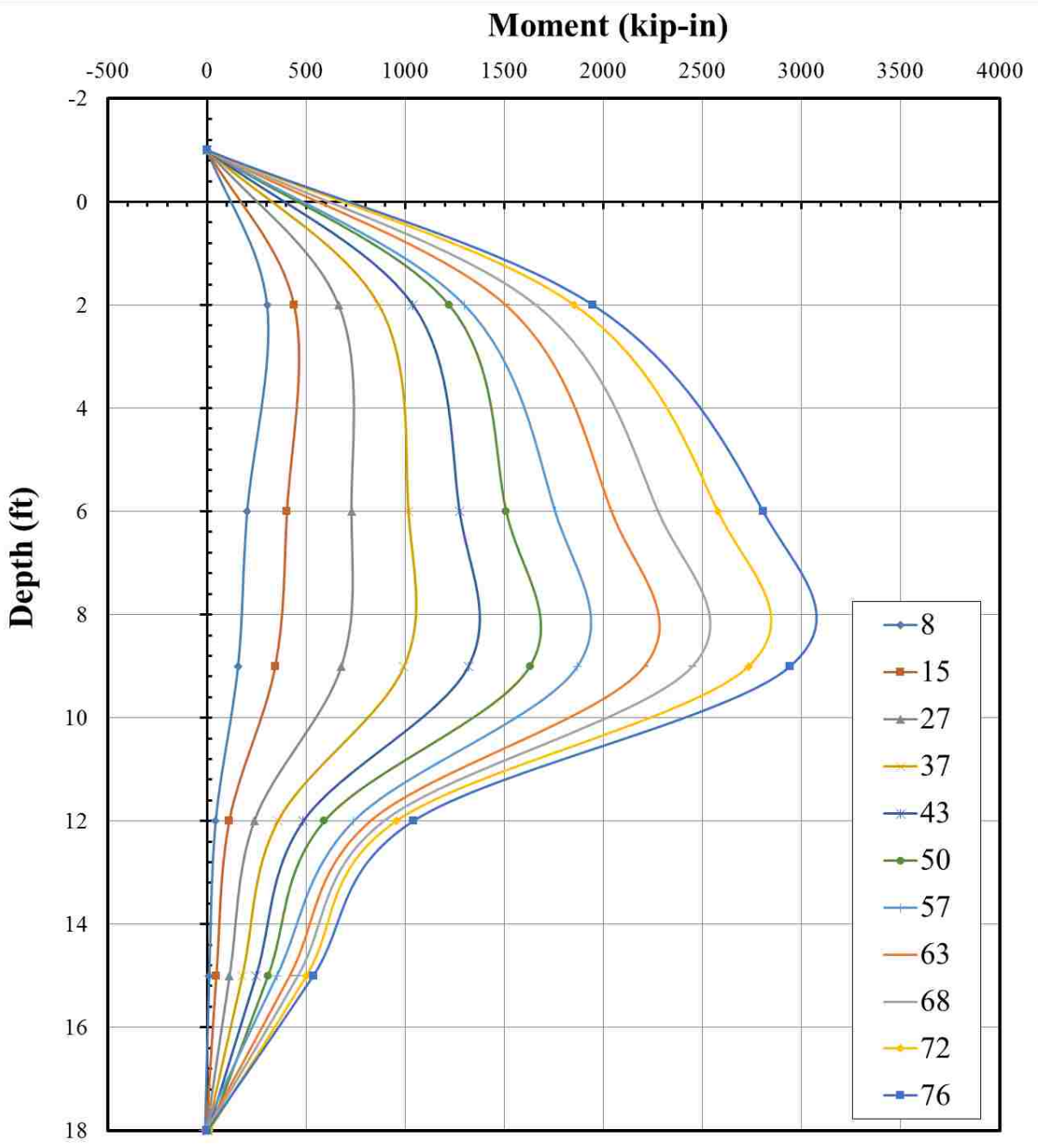

Figure A-10: Moment vs. Depth Curves for a Round Pile in a CMS with Sand Infill at Various Load States

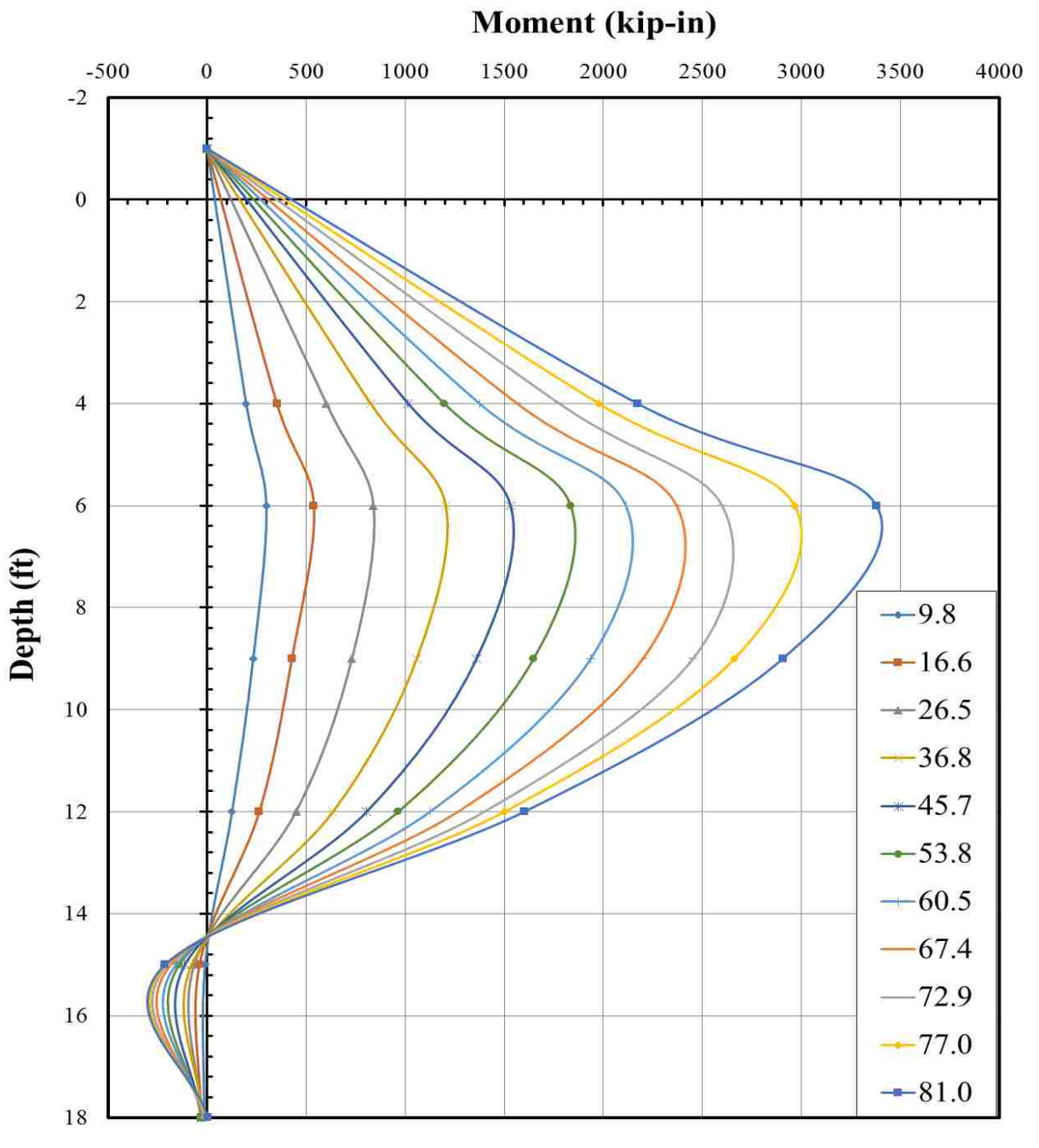

Figure A-11: Moment vs. Depth Curves for a Round Pile in a CMS with Gravel Infill at Various Load States

A.4 Deflection with Distance from Pile for all Loads

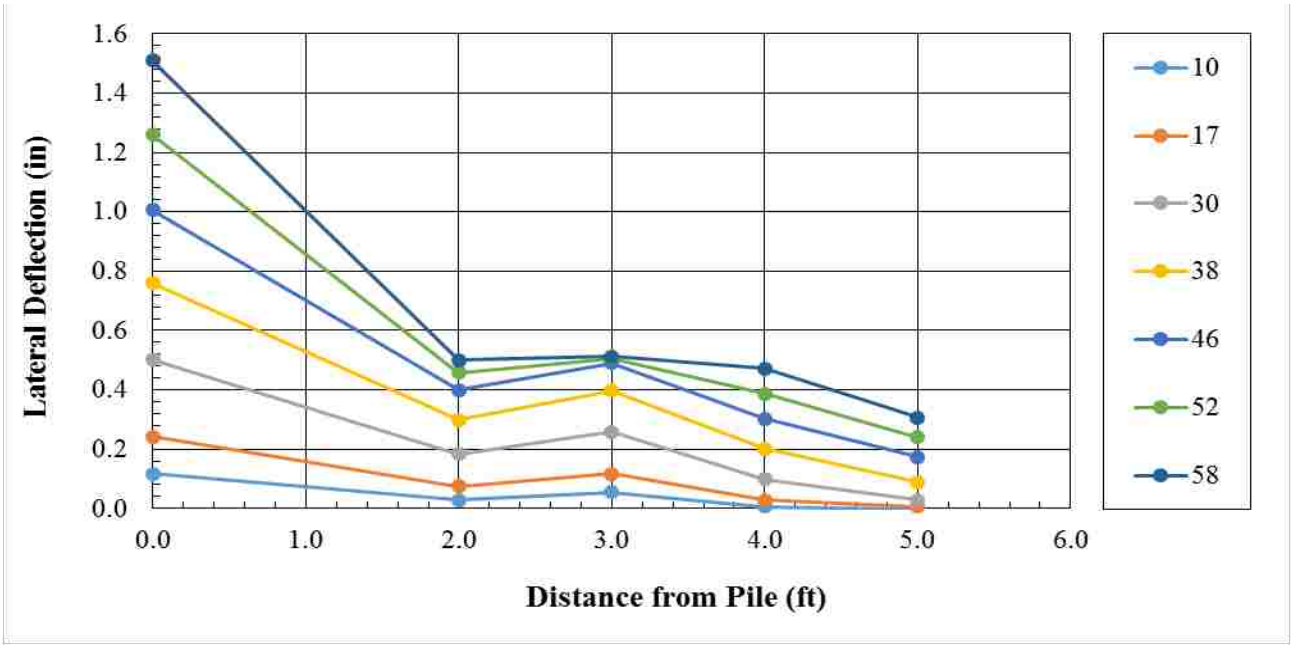

Figure A-12: Lateral Deflection with Distance from a Round Pile at Various Load States

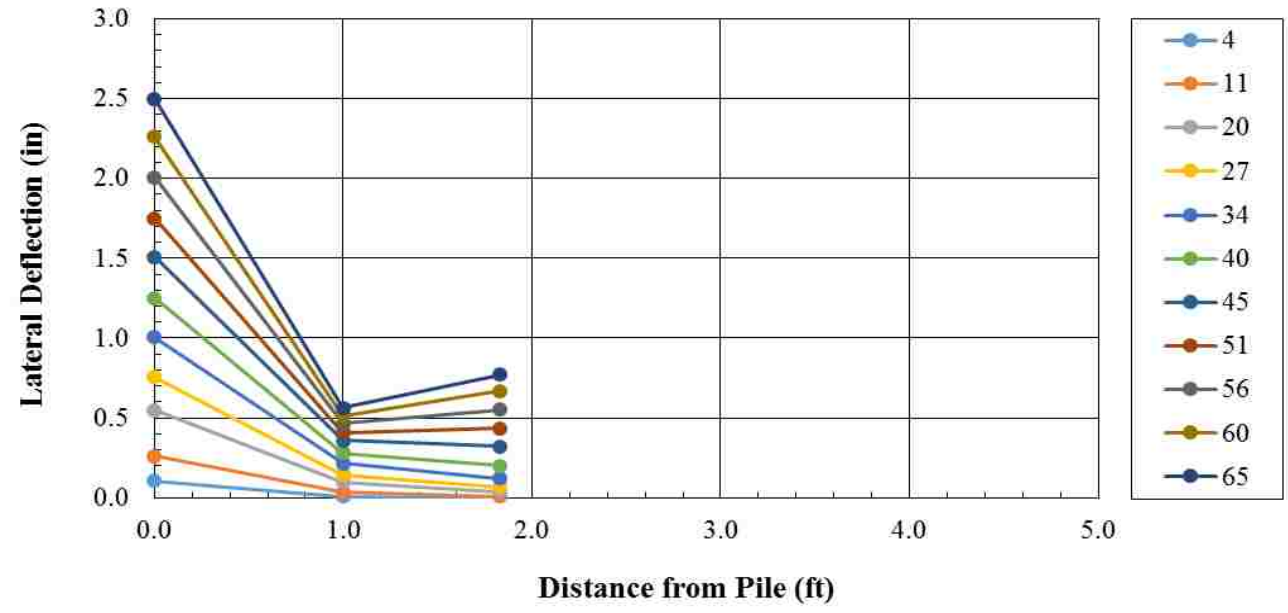

Figure A-13: Lateral Deflection with Distance from a Round (1) Pile in an HDPE Sleeve at Various Load States

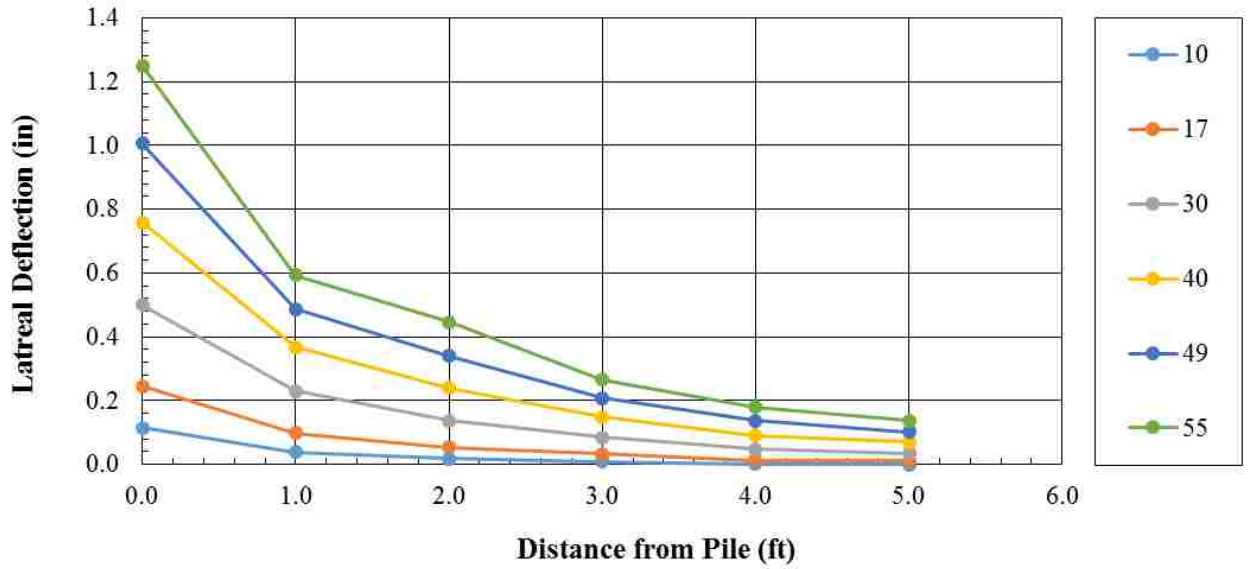

Figure A-14: Lateral Deflection with Distance from a Round (2) Pile in an HDPE Sleeve at Various Load States

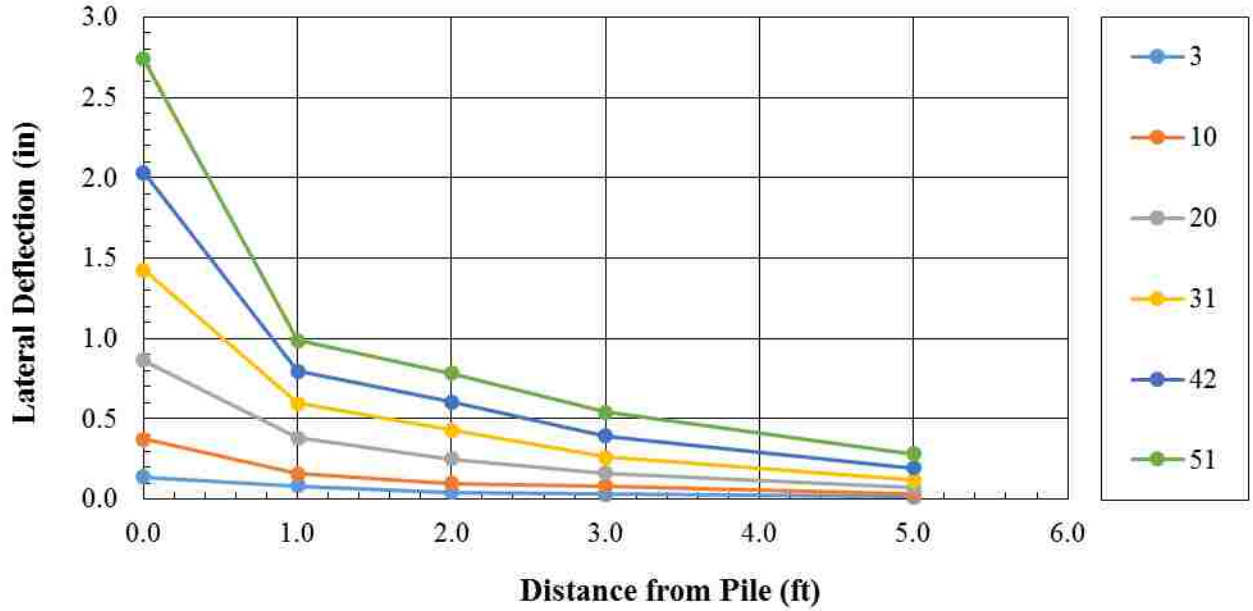

Figure A-15: Lateral Deflection with Distance from an H Pile at Various Load States

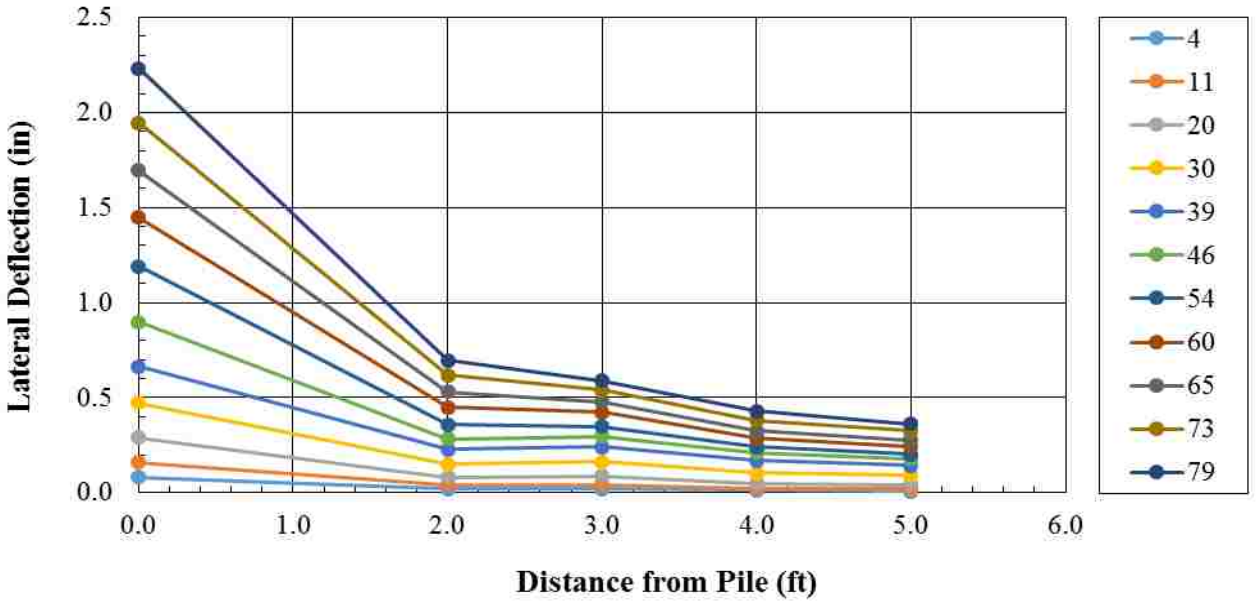

Figure A-16: Lateral Deflection with Distance from the Square (1) Pile at Various Load States

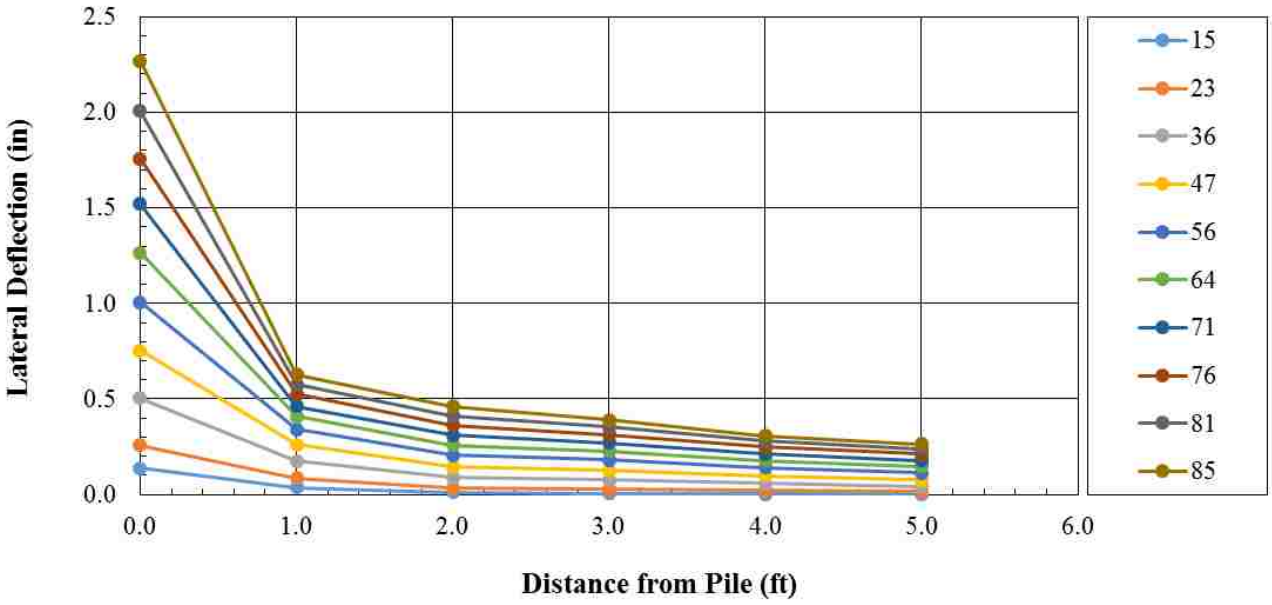

Figure A-17: Lateral Deflection with Distance from the Square (2) Pile at Various Load States

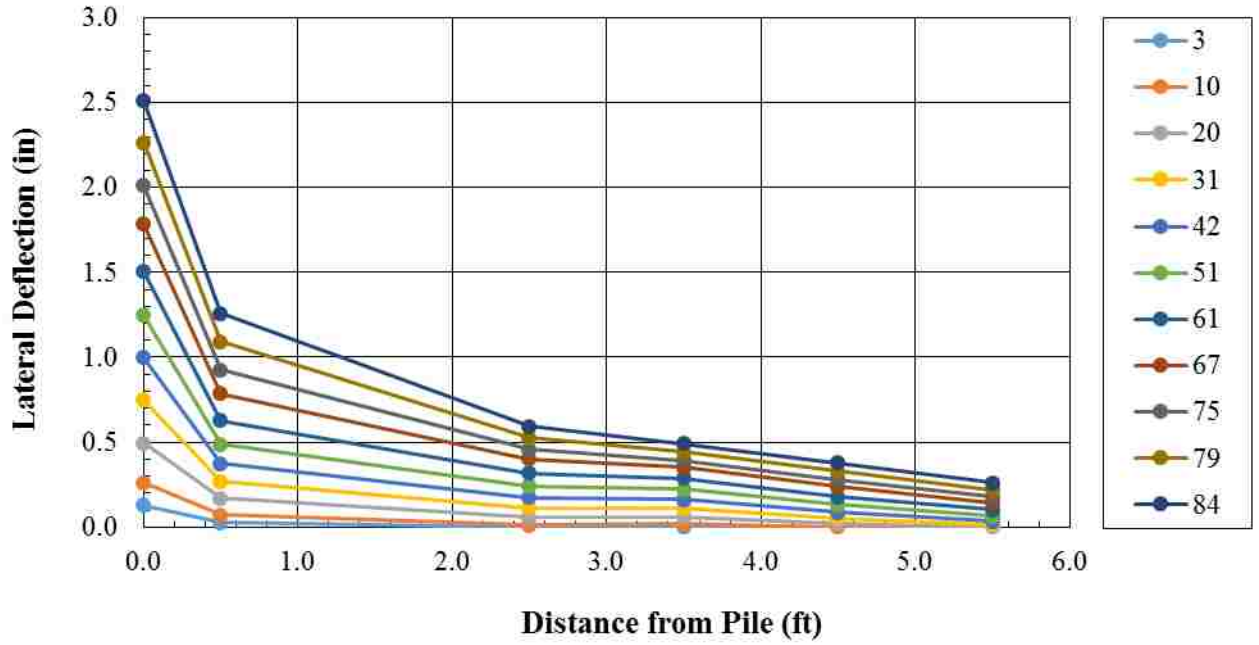

Figure A-18: Lateral Deflection with Distance from a Round Pile in a CMS with Sand Infill at Various Load States

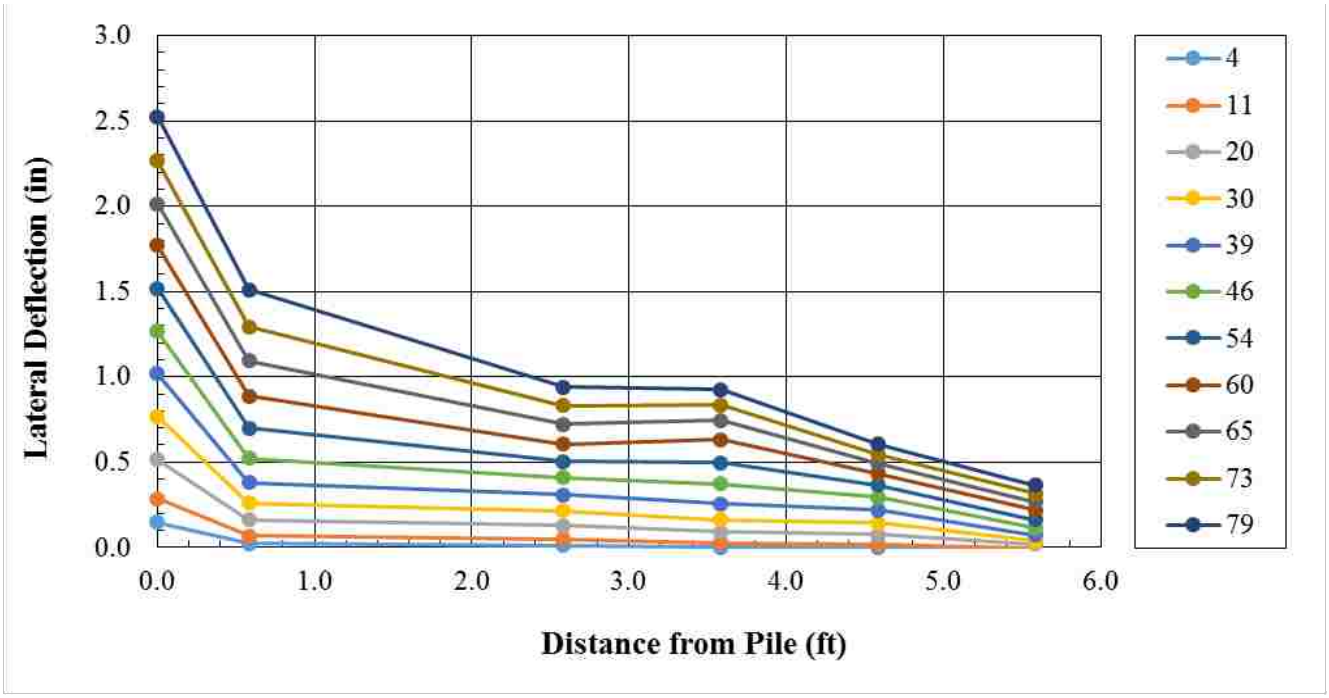

Figure A-19: Lateral Deflection with Distance from a Round Pile in a CMS with Gravel Infill at Various Load States

A.5 Heave with Distance from Pile for all Loads

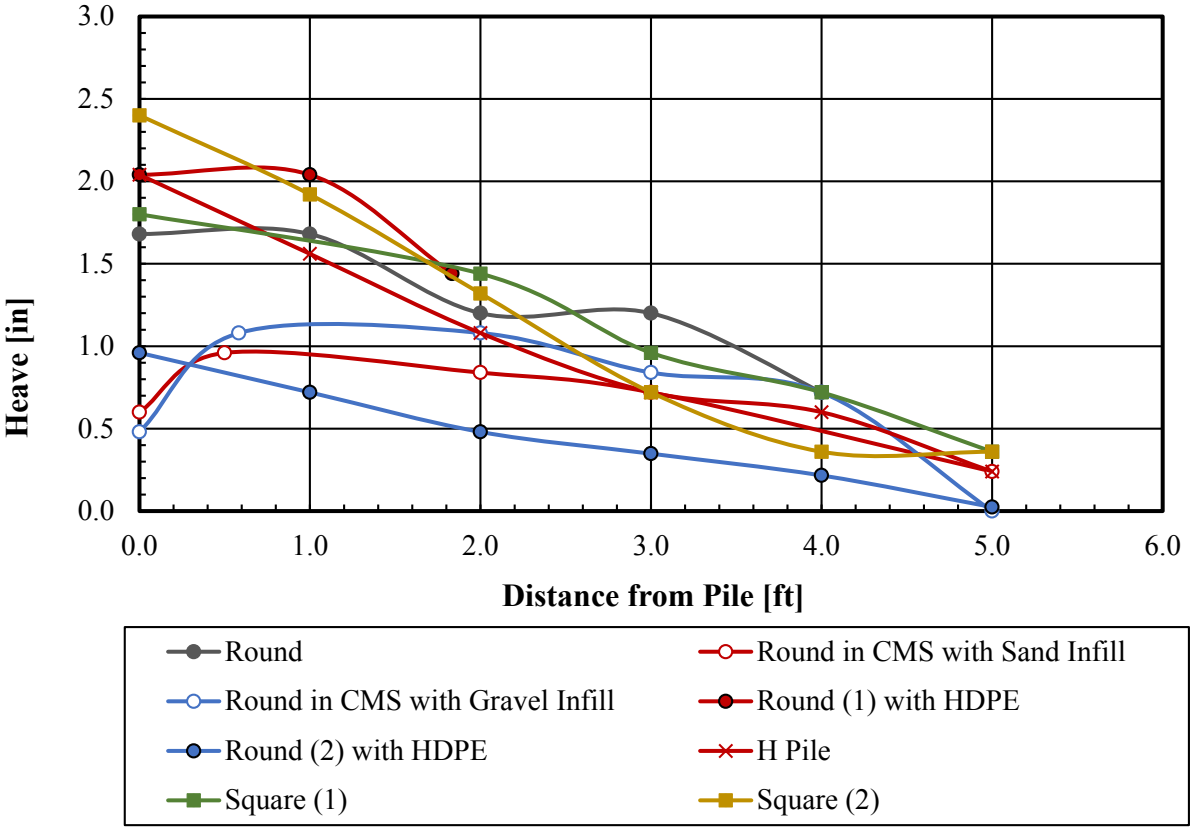

Figure A-20: Heave with Distance from Pile face for all Pile Types

APPENDIX B. API METHOD FOR CALCULATING LATERAL RESISTANCE IN COHESIONLESS SAND ABOVE THE WATER TABLE

1. List the soil and pile parameters

γ' =	0.075	pci	α =	22.5	
φ' =	45	degrees	β =	67.5	
b =	12.75	in	K_p =	5.8	
k =	395	psi	K_0 =	0.4	
			K_A =	0.17	

2. Obtain coefficients C_1, C_2, C_3

C_1 = 7.3

C_2 = 5.7

C_3 = 211.4

*extrapolated from C curves

3. Compute the Ultimate soil resistance p_u.

x = 16 in

p_{us} = 227.1

p_{ud} = 3244.6

p_u = 227.1

4. Compute coefficient A

A = 2.00

5. Compute p for different y values.

if y = 1.33 inch, k = 394.713 pci (from Figure 3-32)

p = 453 lb/in

APPENDIX C. REESE AND VAN IMPE EQUIVALENT DIAMETER

Square Dimensions		
w =	12	in
d =	12	in
φ =	45	deg
$\frac{2}{3}\varphi$ =	30	deg
γ' =	7.6E-05	k/in^2
K =	1.00	

H Dimensions		
w =	12.2	in
d =	12.1	in
C_1 =	7.3	
C_2 =	5.7	
C_3 =	211.4	

$$b_{eq} = w\left[\frac{P_{uc}+2\left(d-\frac{w}{2}\right)f_z}{P_{uc}}\right]$$

$$f_z = K_z \gamma_z \tan(\phi_z)$$

$$P_{us} = (C_1 x + C_2 b)\gamma' x$$

$$P_{ud} = C_3 b \gamma' x$$

			Square				H			
x (ft)	x (in)	f_z (k/in^2)	P_{us} (k/in)	P_{ud} (k/in)	P_{uc} (k/in)	b_{eq} (in)	P_{us} (k/in)	P_{ud} (k/in)	P_{uc} (k/in)	b_{eq} (in)
1	12	0.001	0.14	2.31	0.14	12.5	0.14	2.35	0.14	12.7
2	24	0.001	0.44	4.63	0.44	12.3	0.44	4.70	0.44	12.5
3	36	0.002	0.90	6.94	0.90	12.3	0.91	7.06	0.91	12.5
4	48	0.002	1.52	9.25	1.52	12.2	1.53	9.41	1.53	12.4
5	60	0.003	2.30	11.57	2.30	12.2	2.31	11.76	2.31	12.4
6	72	0.003	3.24	13.88	3.24	12.1	3.25	14.11	3.25	12.3
7	84	0.004	4.34	16.19	4.34	12.1	4.35	16.46	4.35	12.3
8	96	0.004	5.60	18.51	5.60	12.1	5.61	18.81	5.61	12.3
9	108	0.005	7.01	20.82	7.01	12.1	7.02	21.17	7.02	12.3
10	120	0.005	8.59	23.13	8.59	12.1	8.60	23.52	8.60	12.3
11	132	0.006	10.33	25.45	10.3	12.1	10.34	25.87	10.34	12.3
12	144	0.006	12.22	27.76	12.2	12.1	12.24	28.22	12.24	12.3
13	156	0.007	14.28	30.07	14.3	12.1	14.29	30.57	14.29	12.3
14	168	0.007	16.49	32.38	16.5	12.1	16.51	32.92	16.51	12.3
15	180	0.008	18.87	34.70	18.9	12.1	18.88	35.28	18.88	12.3
16	192	0.008	21.40	37.01	21.4	12.1	21.42	37.63	21.42	12.3
17	204	0.009	24.09	39.32	24.1	12.1	24.11	39.98	24.11	12.3
18	216	0.009	26.94	41.64	26.9	12.1	26.96	42.33	26.96	12.3
19	228	0.010	29.96	43.95	30.0	12.0	29.98	44.68	29.98	12.2
20	240	0.011	33.13	46.26	33.1	12.0	33.15	47.03	33.15	12.2
					Avg =	**12.3**			**Avg =**	**12.5**

APPENDIX D. BRIAUD AND SMITH F-Y/Q-Y MECHANISM

k =	1.0	API
γ =	7.6E-05	kip/in^3
ϕ =	45	deg
δ =	30	deg
Depth (z) =	1	ft

Pile Shape Properties

	SF (F_f)	SF (Q)	D
Square	1.76	1	12
Round	0.79	0.75	12.75

$$F = k\gamma z tan(\delta) D(SF)$$

	Round			Square		
y	P	F_f	Q	F_f	Q	P
in	kip/in	kip/in	kip/in	kip/in	kip/in	kip/in
0.00	0.00	0.000	0.00	0.000	0.00	0.0000
0.02	0.10	0.001	0.10	0.002	0.13	0.1363
0.04	0.20	0.002	0.19	0.005	0.26	0.2629
0.07	0.28	0.003	0.27	0.007	0.37	0.3724
0.09	0.34	0.005	0.34	0.010	0.45	0.4617
0.11	0.40	0.005	0.39	0.011	0.52	0.5307
0.13	0.43	0.005	0.43	0.011	0.57	0.5818
0.15	0.46	0.005	0.46	0.011	0.61	0.6187
0.17	0.48	0.005	0.48	0.011	0.63	0.6449
0.20	0.49	0.005	0.49	0.011	0.65	0.6631
0.22	0.50	0.005	0.50	0.011	0.66	0.6757
0.24	0.51	0.005	0.50	0.011	0.67	0.6844
0.26	0.51	0.005	0.51	0.011	0.68	0.6903
0.28	0.52	0.005	0.51	0.011	0.68	0.6943
0.30	0.52	0.005	0.51	0.011	0.69	0.6970
0.33	0.52	0.005	0.52	0.011	0.69	0.6989
0.35	0.52	0.005	0.52	0.011	0.69	0.7001

k =	1.0	API
γ =	7.6E-05	kip/in^3
ϕ =	45	deg
δ =	30	deg
Depth (z) =	1	ft

Pile Shape Properties

	SF (F_f)	SF (Q)	D
Round	0.79	0.75	12.75
H	1.76	1	12.1

$$F = k\gamma z tan(\delta) D(SF)$$

	Round			H		
y in	P kip/in	F_f kip/in	Q kip/in	F_f kip/in	Q kip/in	P kip/in
0.00	0.00	0.000	0.00	0.000	0.00	0.0000
0.01	0.06	0.001	0.06	0.002	0.08	0.0851
0.03	0.12	0.001	0.12	0.003	0.16	0.1640
0.04	0.17	0.002	0.17	0.005	0.23	0.2324
0.05	0.21	0.003	0.21	0.006	0.28	0.2881
0.07	0.25	0.004	0.24	0.008	0.32	0.3314
0.08	0.27	0.004	0.27	0.009	0.35	0.3638
0.10	0.29	0.005	0.28	0.011	0.38	0.3874
0.11	0.30	0.005	0.29	0.011	0.39	0.4039
0.12	0.31	0.005	0.30	0.011	0.40	0.4153
0.14	0.31	0.005	0.31	0.011	0.41	0.4232
0.15	0.32	0.005	0.31	0.011	0.42	0.4286
0.16	0.32	0.005	0.32	0.011	0.42	0.4323
0.18	0.32	0.005	0.32	0.011	0.42	0.4348
0.19	0.32	0.005	0.32	0.011	0.43	0.4365
0.20	0.33	0.005	0.32	0.011	0.43	0.4376
0.22	0.33	0.005	0.32	0.011	0.43	0.4384